Advancing Oncolytic Virotherapy: The Role of Chemical Sensitizers in Enhancing Viral Oncolysis in Resistant Cancers

By

Akram Alwithenani, MSc

A Thesis Submitted to the Faculty of Medicine
in Partial Fulfillment of the Requirements for the Degree of
Doctor of Philosophy in Microbiology and Immunology

in the
University of Ottawa
Department of Biochemistry, Microbiology, and Immunology
Faculty of Medicine

Supervisor: Dr. Jean-Simon Diallo, PhD

Abstract

Oncolytic virotherapy, leveraging viruses to target cancer selectively, has shown promise with the FDA-approved oncolytic herpes simplex virus-1 (HSV-1) for melanoma treatment. However, the efficacy of oncolytic viruses (OVs) varies across cancer types, highlighting the need for strategies to sensitize resistant tumors. This thesis investigates the potential of Dimethyl fumarate (DMF), its analog Tepilamide Fumarate (TPF), and novel synthetic small molecules identified from a high-throughput screen to enhance OV effectiveness in cancer therapy.

DMF, approved for multiple sclerosis and psoriasis, and TPF, under trial for psoriasis, were evaluated for their ability to boost HSV-1 and vesicular stomatitis virus (VSVΔ51) activity against cancer cells. Our findings reveal that pre-treatment with DMF or TPF significantly increases HSV-1 and VSVΔ51 replication in various cancer cell lines, including melanoma, and improves viral oncolysis. Notably, both DMF and TPF enhance OV infection in mouse-derived tumor cores and human tumor samples, while TPF exhibits a remarkable capacity to heighten VSVΔ51 infection and cell killing, outperforming DMF in vitro. Both compounds achieve these effects by downregulating the interferon (IFN) pathway, rendering cancer cells more susceptible to viral infection. Additionally, we demonstrate the ability of DMF and TPF to boost gene therapy vectors' transduction efficiency, which points to the broader utility of these drugs in gene therapy.

Further exploration through a high-throughput screen identified several small molecules that sensitize human renal carcinoma cells to HSV-1 and VSVΔ51, highlighting potential new avenues for overcoming tumor resistance to OVs. These compounds enhance viral replication

and oncolysis, presenting a promising path for future oncolytic virotherapy research and development.

The synergistic potential of combining approved therapies like DMF with OVs, the promising effects of TPF, and newly identified small molecule sensitizers underscore the feasibility of enhancing OV efficacy in resistant cancers. This study not only broadens our understanding of how small molecules can potentiate oncolytic virotherapy but also sets the stage for clinical evaluation and the development of more effective, personalized cancer treatment strategies. Collectively, these findings advocate for further investigation into DMF, TPF, and other sensitizing compounds to unlock their full therapeutic potential in oncolytic virotherapy.

Acknowledgements

At the outset, I am deeply grateful to God for bestowing upon me the resilience and determination necessary to navigate through the challenges and triumphs of this profound journey.

I owe a profound debt of gratitude to my supervisor, Dr. Jean-Simon Diallo, for his unwavering support, invaluable guidance, and for the privilege of being part of his research team. His encouragement has been a cornerstone of my academic pursuit.

My sincere appreciation also goes to Dr. Rozanne Arulanandam for her invaluable mentorship and insights, which have significantly shaped my Ph.D. experience.

I extend my gratitude to all members of the Diallo Lab for their support and camaraderie, and to my supervisory committee members, Drs. Ian Lorimer, Robin Parks, and Tommy Alain, for their constructive feedback and sage advice.

A special thank you is extended to the government of Saudi Arabia for their generous financial support and scholarships, enabling my studies in Canada.

To my parents, brothers and sisters, whose endless support and encouragement have been my foundation, I am forever grateful. Your faith in me has been a source of constant motivation.

To my beloved wife, Aetezaz, words cannot fully express my gratitude for your sacrifice, love, and unwavering support. Your willingness to stand by me, sacrificing your own comforts and aspirations, has been the bedrock of my ability to pursue and complete my Ph.D. journey. Your strength, patience, and encouragement have been my guiding light through the highs and lows of this endeavor.

The birth of our children, Raad and Deema, during this period has been a source of unparalleled joy and motivation, enriching this journey in ways I could never have imagined.

To everyone who has played a part in this journey, your support and contributions have been invaluable. Thank you from the bottom of my heart.

Table of Contents

Abstract ..... *ii*

Acknowledgements ..... *iv*

Table of Contents ..... *v*

List of abbreviation ..... *vii*

List of Tables ..... *ix*

List of Figures ..... *x*

Chapter 1: Introduction *1*

1.1. Cancer **1**

1.2. Cancer therapeutics **3**

1.3. Oncolytic viruses (OVs) as promising cancer therapy **4**

1.4. Oncolytic HSV-1 ..... **6**

1.5. Oncolytic VSV **9**

1.6. OVs as monotherapy: challenges and solutions **10**

1.7. Pharmacological approach to improve OV efficacy. **12**

1.8. NF-κB pathway **13**

1.9. NF-κB inhibitors **14**

1.10. DMF: Mechanism of action **14**

1.11. Tepilamide fumarate as potential oncolytic viral enhancer **18**

1.12. High throughput screening to enhance virotherapy. **18**

1.13. Rationale and hypothesis **21**

1.13.1. Central Hypothesis: 21

1.13.2. Rationale and Linkage of Research Objectives: 21

Chapter 2: Unlocking the Potential of Dimethyl Fumarate: Enhancing Oncolytic HSV-1 Efficacy for Wider Cancer Applications *23*

2.1 Abstract **24**

2.2 Introduction **25**

2.3 Results **28**

2.3.1 Dimethyl fumarate sensitizes cancer cells to HSV-1 infection. 28

2.3.2 Dimethyl Fumarate enhances HSV-1 viral infection in a various of ex vivo tumor models. 32

2.3.3 FMAEs promote HSV-1 infection. 36

2.3.4 DMF suppresses the antiviral response....39
2.3.5 DMF enhances the therapeutic effectiveness of oncolytic HSV.n212....42
2.3.6 Effects of HSV-1 / DMF combination therapy on tumor immune profile....46
2.4 Discussion....49
2.5 Materials and methods....53
Chapter 3: Tepilamide Fumarate as a Novel Potentiator of Virus-Based Therapy....61
3.1. Abstract....62
3.2. Introduction....63
3.3. Results....65
3.3.1. TPF Enhances Susceptibility of Cancer Cells to VSVΔ51 infection....65
3.3.2. TPF enhances VSVΔ51 and HSV-1 infection in cancer cells compared to DMF....69
3.3.1 TPF potentiates Infectivity of VSVΔ51 in Human and Murine Tumor Explants....73
3.3.4. TPF inhibits the type-I IFN response and NF-κB to Amplify VSVΔ51 Oncolytic Potency....77
3.3.5. TPF Amplifies Transduction Efficiency Across Multiple Viral Vectors....81
3.4. Discussion....89
3.5. Materials and Methods....92
Chapter 4: High Throughput Screen Approach Identifies Several Novel Synthetic Compounds with the ability to Potentiate Oncolytic Virus Therapy....99
4.1. Abstract....100
4.2. Introduction....101
4.3. Results....103
4.4. Discussion....135
4.5. Materials and Methods....138
Chapter 5: Concluding Remarks....142
Contribution of collaborators....148
Chapter 6: References....150
Appendix A Chapter 2: Supplemental information....160
Appendix B: Chapter 3 Supplemental Information....174
Appendix C: Curriculum Vitae....184

List of abbreviation

DMF	Dimethyl fumarate
TPF	Tepilamide fumarate
MMF	Monomethyl fumarate
FAE	Fumaric acid esters
DEM	Diethyl maleate
DEF	Diethyl fumarate.
DMM	Dimethyl maleate
FA	Fumaric acid
FMAEs	Fumaric and maleic acid esters
VSe	Viral sensitizer
OV	Oncolytic virus
HSV-1	Herpes simplex virus-1
VSV	Vesicular stomatitis virus
T-VEC	Talimogene laherparepvec
Ad5	Adenovirus type 5
Lenti	Lentivirus
AAV2	Adeno-associated virus type 2
GFP	Green fluorescent protein
FLuc	Firefly luciferase
MOI	Multiplicity of infection
GM-CSF	Granulocyte-macrophage colony stimulating factor.

HTS	High-throughput screen
IFN	Interferon
IFN-β	Interferon beta
IL	Interleukin
JAK	Janus-associated kinase
IKK	inhibitor of NF-κB kinase
STAT	Signal transducer and activator of transcription
IRF	Interferon response factor
ISG	IFN-stimulated genes
NF-κB	Nuclear factor kappa-beta
CD	Cluster of differentiation
DNA	Deoxyribonucleic acid
mRNA	Messenger RNA
ELISA	enzyme-linked immunosorbent assay
PD-1	Programmed cell death protein 1
PD-L1	Programmed cell death protein ligand 1
qPCR	Quantitative real-time polymerase chain reaction
RNA	Ribonucleic acid
DMEM	Dulbecco's Modified Eagle's Medium
FBS	Fetal bovine serum
ICP0	Infected cell protein 0
HVEM	Herpesvirus entry mediator

List of Tables

Table 4.1. GPF fold change of VSVΔ51 compounds 108
Table 4.2 Viability and Viral Sensitizer Score of VSVΔ51compounds 109
Table 4.3. GPF fold change of HSV.n212 compounds.....110
Table 4.4. Viability and Viral Sensitizer Score of HSV.n212 111

Table S2.1. Synergistic Effect of DMF + HSV.n212 in CT26.wt Model.....163
Table S3.1. Clinical characteristics of patients-derived tumor specimens used in the study. 181
Table S3.2. List of cell lines used in this study.....182
Table S3.3. List of primers used in this study.....183

List of Figures

Fig. 2.1 DMF sensitizes human and murine tumor types to HSV-1 31

Fig. 2.2 DMF enhances the replication of HSV.n212 in ex vivo tumor tissues and patient-derived explants.....35

Fig. 2.3 FMAEs promote infection by HSV.n212.....38

Fig. 2.4 DMF increases HSV.n212 infection via IFN-1 inhibition 41

Fig. 2.5 DMF improves HSV.n212 therapeutic efficacy in murine in vivo tumor models 45

Fig. 2.6 FACS analysis of combination treatment in CT26.wt model 48

Fig. 3.1 Tepilamide Fumarate demonstrates remarkable viral sensitizing capabilities.....68

Fig. 3.2 TPF demonstrates a superior effect in enhancing OV infection within cancer cells 72

Fig. 3.3 Tepilamide Fumarate promotes VSVΔ51 infection in ex vivo models 76

Fig. 3.4 Tepilamide Fumarate promotes VSVΔ51 infection via IFN-1 inhibition.....80

Fig. 3.5 The impact of TPF in transduction of lentivirus 84

Fig. 3.6 The impact of TPF in transduction of Ad5-GFP.....86

Fig. 3.7 The impact of TPF in transduction of AAV-2 88

Fig. 4.1 High throughput screening processes diagram.....105

Fig. 4.2 Identification of several synthetic compounds that boost oncolytic VSVΔ51...114

Fig. 4.3 Identification of several synthetic compounds that boost oncolytic HSVn.212. 117

Fig. 4.4 Clustering analysis of VSVΔ51, HSV.n212 and mutual hits.....122

Fig. 4.5 Validation of AAHTS-V2 compound on 786-0 cells.....126

Fig. 4.6 Validation of AAHTS-H2 compound on 786-0 cells.....129

Fig. 4.7 Assessing the impact of AAHTS-V2 on murine colon carcinoma 131

Fig. 4.8 AAHTS-V2 promotes VSVΔ51 infection in ex vivo models. 134

Fig. S2.1 DMF enhances GFP of HSV.n212 in Several cancer cell lines 162
Fig. S2.2 DMF enhances HSVd810.....165
Fig. S2.3 DMF enhances HSVγ34.5 and HSVG47Δ.....167
Fig. S2.4 DMF promotes HSV.n212 infection in S180 and CT2A tumour cores 169
Fig. S2.5 HSV.n212 dose optimization in vivo 171
Fig. S2.6 DMF administered intratumorally improved survival compared to gavage 173

Fig. S3.1 The impact of DMF, MMF on 786-0 cells.....176
Fig. S3.2 TPF promotes VSVΔ51 infection in several murine cancer cells.....178
Fig. S3.3 TPF decrease activation of STAT1 and STAT2 180

Chapter 1: Introduction

1.1. Cancer

Cancer is a significant contributor to premature mortality globally. Recent epidemiological data suggest that approximately 40% of the Canadian population will be diagnosed with cancer during their lifetimes, with an estimated 25% succumbing to the disease. Forecasts for the year 2023 predict that Canada will witness 239,100 new cancer cases and approximately 86,700 cancer-related deaths [1]. These statistics not only highlight the significant morbidity and mortality associated with cancer in Canada but also underscore the urgent need for continued research in oncology, advancements in therapeutic interventions, and comprehensive public health strategies aimed at cancer prevention and early detection [1].

Cancer can be identified by the buildup of genetic mutations and the absence of normal cellular regulatory processes [2]. Understanding the etiology of cancer is crucial for mitigating its occurrence and devising effective therapeutic interventions. The etiology of cancer has been defined by a multifactorial nature, involving a complex interplay of various factors. These factors include genetic predisposition, environmental exposures such as tobacco smoke, radiation, and chemical carcinogens, lifestyle factors such as diet, physical activity, and viral infections such as Human papillomavirus. Each of these factors plays a significant role in the initiation of cancer [3].

Cancer development is characterized by a gradual and sequential transformation of healthy cells into malignant ones. The process encompasses three key stages: initiation, during which DNA damage or mutations arise; promotion, characterized by the clonal proliferation of aberrant cells; and progression, distinguished by the infiltration into neighboring tissues and

the potential for metastasis to distant organs. Furthermore, tumors manifest identifiable biological characteristics, including unregulated proliferation, angiogenesis (generating new blood vessels), infiltration into adjacent tissues, and spread to distant locations. The aforementioned attributes contribute to the inherently aggressive behavior of cancer and its ability to escape therapeutic interventions [4].

Cancer is characterized by several key hallmarks that distinguish malignant cells from normal cells. These include sustaining proliferative signaling, where cancer cells continuously signal themselves to divide uncontrollably, and evading growth suppressors by bypassing mechanisms that inhibit cell growth, such as tumor suppressor genes like p53 and Rb. Cancer cells also resist apoptosis, the programmed cell death that normally eliminates damaged cells, enabling them to survive longer than normal cells. They achieve replicative immortality by maintaining the length of their telomeres through the activation of the enzyme telomerase, allowing them to divide indefinitely. Additionally, cancer cells induce angiogenesis, the formation of new blood vessels, to supply the tumor with nutrients and oxygen essential for its growth and survival. They also activate invasion and metastasis, acquiring the ability to invade surrounding tissues and spread to distant organs, forming secondary tumors [5].

Beyond these primary hallmarks, cancer cells often deregulate cellular energetics, frequently relying on glycolysis for energy production even in the presence of oxygen, known as the Warburg effect. They also avoid immune destruction, evading detection and elimination by the body's immune system. These processes are facilitated by enabling characteristics such as genome instability and mutation, which increase the rate of genetic changes and promote tumor diversity and adaptability. Tumor-promoting inflammation, often chronic, further supports cancer development and progression by providing bioactive molecules that aid in

tumor growth. Understanding these hallmarks and characteristics is crucial for developing targeted therapies that address the specific mechanisms underlying cancer growth and survival [3].

1.2. Cancer therapeutics

Cancer treatment modalities commonly encompass surgical intervention, chemotherapy, immunotherapy, or a combination of these approaches. In the case of localized tumors, surgical resection is frequently the initial therapeutic preference. Although conventional treatments like chemotherapy and radiation therapy demonstrate effectiveness, they are frequently associated with substantial adverse effects, including off-target toxicities [5].

Immunotherapy represents an innovative strategy in the field of cancer therapy, which leverages the inherent capabilities of the human immune system to identify, selectively attack, and eradicate malignant cells. In contrast to conventional cancer therapies that specifically target tumors or their genetic material, immunotherapy aims to augment the innate defense systems of the human body, thereby empowering it to combat cancer with greater efficacy [3]. This therapeutic strategy has transformed cancer care and provides new hope for patients facing various malignancies. Immune cells have inbuilt "checkpoints" that govern their functionality to prevent exaggerated immune reactions. Cancer cells can exploit these checkpoints in order to escape detection [6]. Checkpoint inhibitors, highlighted by Pembrolizumab (Keytruda) and Nivolumab (Opdivo), impede these checkpoints, thereby enabling immune cells, particularly T cells, to identify and combat malignant cells [7]. Various drugs and therapies are designed to modulate the immune system, enhancing its responsiveness to cancer. These include interferons, interleukins (IL), and other immune-stimulating agents [8].

1.3. Oncolytic viruses (OVs) as promising cancer therapy

Oncolytic virotherapy is well-recognized as a type of immunotherapy. Oncolytic virotherapy involves using genetically modified or naturally occurring viruses to specifically target and eradicate cancerous cells, while minimizing harm to normal, healthy cells. The therapy modality induces direct cytotoxicity in cancer cells, but also elicits an immune-mediated antitumor response by stimulating the patient's immune system [9].

For over a century, scientists have explored the use of viruses as potential tools to combat cancer [10]. Due to bioengineering technology, researchers can now genetically modify various viruses to specifically target and destroy tumor cells. With the advancement of knowledge regarding mechanisms of OV activity, such as their capacity to stimulate endogenous antineoplastic immune responses and modulate the tumor microenvironment, the discipline of virotherapy has experienced significant growth [11].

OV's interaction with tumor cells leads to immunogenic cell death, an important factor in stimulating the immune response. Those viruses play a crucial role in activating and recruiting various immune cells. They achieve this by releasing soluble antigens and danger signals, which serve as potent immune stimulants. Notably, oncolytic viruses bolster both the innate and adaptive immune responses. In the innate immune response, they recruit immature dendritic cells and innate lymphoid cells. Simultaneously, they promote the recruitment of T cells to stimulate the adaptive immune response. This orchestrated immune response is integral to the overall effectiveness of oncolytic viruses in cancer therapy [12].

Both DNA and RNA viruses have been integral to the development of oncolytic virotherapy, each bringing its own set of advantages. DNA viruses offer distinct advantages for various applications, including gene therapy and oncolytic agents. Their spacious genome allows for

the incorporation of substantial eukaryotic transgenes without compromising replication efficiency. This unique feature expands the scope of potential therapeutic interventions, enabling the delivery of large genetic payloads to enhance therapeutic activity and immune modulation [13]. Furthermore, DNA viruses are equipped with high-fidelity DNA polymerases, which are important in maintaining the integrity of their genomes. This high fidelity ensures that the viral genome remains intact during replication, minimizing the risk of detrimental mutations and preserving the genetic information required for therapeutic effects. Additionally, DNA viruses exhibit minimal, if any, nuclear integration, reducing the potential for disruption of host cell functions and genomic stability. These advantages collectively position DNA viruses as versatile and efficient vectors for diverse biomedical applications [14].

On the other hand, RNA viruses offer distinct advantages. Their smaller size relative to DNA viruses allows them to effectively penetrate the blood-brain barrier, enabling precise targeting of tumors within the central nervous system [15]. However, it's important to note that RNA viruses do have a limitation in their genome size, which constrains their ability to accommodate large transgenes. Despite this limitation, their suitability for systemic delivery is heightened by the relatively low pre-existing immunity to certain RNA viruses in humans [16]. This characteristic allows them to be a promising option for systemic delivery, particularly during the initial phase before antiviral immunity is induced.

1.4. Oncolytic HSV-1

HSV-1 are neurotropic viruses belonging to the herpesviridae family. Each virus is composed of an icosahedral capsid core, an amorphous tegument, and an envelope covered with viral glycoproteins. The length of the HSV-1 genome is approximately 152 kilobases (kb) structured with two unique regions: the unique long (UL) and unique short (US), each bordered by inverted repeats (RL and RS). These genomes encode for around 84 distinct gene products [17].

HSV-1, belonging to the Herpesviridae family within the Alphaherpesvirinae subfamily, commences its entry into the host cell by binding to heparan sulfate proteoglycans via glycoproteins B and C. This initial interaction is followed by a more stable attachment when glycoprotein D binds to specific cellular receptors, including nectin-1, integrins, and Herpesvirus entry mediator (HVEM). The virus can then enter the host cell either through pH-independent fusion with the plasma membrane or via endocytosis. Once inside, the nucleocapsid is transported along microtubules to the nucleus, where the viral DNA is introduced through the nuclear pore complex, assisted by importin β. The tegument protein VP16 recruits host transcription factors to initiate immediate-early gene transcription by host RNA polymerase II [17,18].

HSV's replication is a precisely timed process, initiating with the expression of immediate-early genes such as infected cell protein 0 (ICP0), ICP4, ICP22, ICP27, and ICP47. These genes facilitate the viral takeover of the host cell machinery and prepare for viral DNA synthesis. Early genes, which encode for the viral DNA polymerase and other replication machinery, follow, employing a rolling circle mechanism for DNA replication. Subsequently, late genes are expressed, providing structural components for new virions [17].

Post-replication, viral DNA is encapsulated into nucleocapsids, which bud at the nuclear membrane to acquire a primary envelope that is lost upon fusion with the trans-Golgi network. Mature virions then gain their final envelope embedded with multiple glycoproteins and lipid bilayers from trans-Golgi membranes and are ultimately released from the cell through exocytosis, ready to infect new cells. This finely orchestrated cycle ensures HSV's propagation and highlights its potential as a vector in gene therapy applications due to its capacity to deliver genetic material efficiently into host cells [18].

The first generation of oncolytic HSV-1 was genetically engineered to selectively target and proliferate within rapidly dividing cancer cells. This specificity was achieved by deleting key viral genes—namely thymidine kinase (TK) and ICP6—from the HSV-1 genome, thereby conferring a replication advantage in transformed cells that exhibit high mitotic activity [19–21].

Subsequent endeavors to refine HSV-1 for oncolytic therapy focused on enhancing its safety profile, particularly for the treatment of brain tumors. To this end, the neurovirulence gene ICP34.5, also designated as RL1, was deleted from the viral genome. Concurrently, the ICP6 gene was disrupted via the insertion of a lacZ gene, resulting in the creation of the G207 HSV-1 strain. This modified virus underwent evaluation in a Phase I clinical trial involving patients with glioma and was found to be safe and well-tolerated following intracerebral administration [22,23].

In an effort to enhance the antitumor immune response elicited by the G207 HSV-1, Todo et al. advanced the virus's design by deleting the gene encoding ICP47, which is responsible for inhibiting antigen peptide presentation. This modification gave rise to the HSV-1 G47Δ

variant. In a comparative study utilizing both xenograft and syngeneic murine tumor models, HSV-1 G47Δ demonstrated superior efficacy compared to its predecessor, G207 [24].

G47Δ is showing promise in clinical trials. In glioblastoma patients, G47Δ demonstrated safety and a notable 1-year survival rate of 84.2% in a phase 2 trial [25]. These results have led to its conditional and time-limited approval in Japan for glioma treatment, pending further studies. Another notable example is Talimogene laherparepvec (T-VEC), an HSV-1 -based oncolytic virus, which garnered FDA approval in 2015 for treating melanoma [26,27]. The genetic modifications of TVEC paralleled that of HSV-1 G47Δ, involving the deletion of ICP34.5 and ICP47 genes. Additionally, the human granulocyte-macrophage colony-stimulating factor (GM-CSF) gene was inserted to augment dendritic cell recruitment and activation, enhancing antigen presentation following the lysis of tumor cells [28].

Another important HSV-1 mutant is HSV-null ICP0. Several studies have shown the ability of HSV-1 that have non-functional ICP0, to function as oncolytic virus in cancer cells. For instance, It was shown that HSV-1 with mutations in the immediate early gene ICP0, which encodes a protein responsible for overcoming aspects of the host IFN response (supressing IRF-3 and IRF-7), has oncolytic properties [29]. HSV.n212 and HSV-d810 are HSV-1 ICP0 null viruses. Both HSV.n212 and HSV-d810 result in non-functional of ICP0, which encodes a protein responsible for overcoming aspects of the host IFN response [30]. The only difference being that HSV-d810 has an 810 amino acid deletion in ICP0 while HSV-n212 is a point mutation in the coding sequence resulting in a frameshift in ICP0. Several studies have shown the anti-tumor activities of ICP0 null HSV-1 in different murine cancer models [29–33].

1.5. Oncolytic VSV

Vesicular Stomatitis Virus (VSV), is a single-stranded RNA virus from the Rhabdoviridae family and Vesiculovirus genus, characterized by its nonsegmented structure. This virus forms bullet-shaped particles, roughly 75 nm wide and 180 nm long.

VSV has an 11kb genome featuring five genes, each responsible for a specific protein. These include the nucleocapsid (N) protein, which attaches to viral RNA, and the phosphoprotein (P) and large (L) protein, which together comprise the RNA-dependent RNA polymerase (RdRp) essential for virus replication and transcription. Additionally, the matrix (M) protein blocks RNA movement from the nucleus and facilitates viral budding, whereas the glycoprotein (G) plays a key role in cellular entry by latching onto low-density lipoprotein (LDL) receptors on host cells [34].

VSV's life cycle commences with the virus attaching to LDL receptors and being internalized into cells via endocytosis. Inside the cell, the virus releases its RNA core, and the RdRp begins transcribing leader RNA and multiple mRNAs. The replication involves creating a complete RNA genome that acts as a blueprint for further replication. The N protein immediately coats both genome copies, but only the negative-sense genome is incorporated into new virions. VSV replicates swiftly, with each infected cell releasing up to thousands of new virions, highlighting its potential as an effective agent in oncolytic virus therapy [31].

The wild type of VSV has a natural ability to weaken the interferon response from infected cells, which can make the virus risky for use as a therapeutic agent in cancer treatment. To address this issue, Stojdl et al. modified VSV to increase its sensitivity to interferon signals. They achieved this by removing methionine at the 51 positions in the M gene, which is known

to block the export of host mRNA from the nucleus, including antiviral response genes. This modification resulted in the creation of a new virus, VSVΔ51, which is both oncolytic and more targeted towards cancer cells that have varying levels of defects in their antiviral defense pathways: an immune escape mechanism. VSVΔ51 has since become widely utilized in preclinical studies in the field of virotherapy [35].

1.6. OVs as monotherapy: challenges and solutions

Using oncolytic viruses as a monotherapy in cancer treatment presents several significant challenges that need to be addressed to enhance their therapeutic efficacy. One of the primary hurdles is the complex nature of the extracellular matrix (ECM) in solid tumors, which forms a dense barrier impeding viral penetration and spread. Additionally, OVs face a robust antiviral response from the host's immune system, which can quickly identify and eliminate these viruses before they can effectively target and destroy cancer cells. Furthermore, the innate immune response, particularly the rapid deployment of various immune cells and cytokines upon OV infection, can further complicate the therapeutic response by limiting viral replication and spread. These challenges highlight the need for advanced strategies to improve the effectiveness of OVs as a standalone treatment in oncology [36].

OV therapy in tumors initiates a rapid immune response, creating an antiviral environment. This response includes the production of interferons (IFNs), antiviral cytokines induced by pathogen-associated molecular patterns (PAMPs) detected by pattern recognition receptors (PRRs). IFNs, mainly type I IFNs like IFN-α and IFN-β, are produced in response to OV infection. While they serve as a natural defense mechanism against viral infections, they can also impede OV therapy by limiting viral replication and spread within the tumor. For instance, studies have shown that oncolytic virus infection leads to increased levels of IFNs, which can

restrict the virus's ability to lyse tumor cells and reduce its overall efficacy [37,38]. Interestingly, many tumor cells exhibit resistance to the antiviral effects of IFNs due to the dysfunction of key pathways such as PKR and p53. This resistance allows OVs to replicate in tumor cells more effectively than in normal cells [15]. However, the cellular innate immune response, albeit often impaired in cancer cells, can still hinder the effectiveness of OV therapy. OVs have been observed to trigger different innate and adaptive immune responses. Immune cells play a vital role in response to oncolytic virus therapy, triggered by the production of IFNs and IFN-inducible chemokines. Key players in this immune orchestra include macrophages and dendritic cells (DCs), which upon activation by the virus, release a range of antiviral and pro-inflammatory cytokines. These cytokines are instrumental in recruiting and activating a diverse array of immune cells such as additional macrophages, natural killer (NK) cells, neutrophils, and cytotoxic T lymphocytes (CTLs), contributing significantly to the clearance of the virus but also tumor cells [39]. The depletion of certain immune cells like macrophages or neutrophils has been shown to increase viral spread within tumors, underscoring their vital role in viral containment [40]. However, the recruitment and activation of NK cells and T-cells, which target and destroy virally infected and uninfected tumor cells, underscores the complexity of the immune response elicited by OV therapy [41]. This multifaceted immune interaction is a double-edged sword, offering both challenges and opportunities in enhancing the efficacy of OVs as a cancer treatment modality.

1.7. Pharmacological approach to improve OV efficacy.

The initial belief that defective innate immunity in cancer contributes to the tumor-selectivity of oncolytic viruses has evolved with the understanding that antiviral defenses remain functional in many tumors, countering OV replication and spread [42]. This realization has driven research towards identifying or combining drugs that target the cellular innate immune response in cancer cells to enhance OV therapy. Numerous small molecules have been discovered by our group and others that significantly boost OV spread and oncolytic activity in tumors, primarily by transiently disrupting innate antiviral signaling pathways [43–47]

A key focus of these efforts is targeting the type I interferon pathway, which plays a central role in mediating innate antiviral immunity. Type I IFNs are produced in response to virus detection by various pattern recognition receptors, leading to activation of transcription factors like Interferon response factor (IRF)3/7, Nuclear factor kappa-beta (NF-κB), and AP-1 [48]. These IFNs are secreted and function in an autocrine or paracrine manner to also activate the Janus associated kinase (JAK)/ Signal transducer and activator of transcription (STAT) pathway, resulting in the up-regulation of numerous IFN-stimulated genes (ISGs) with direct antiviral effects [49].

It is also crucial to recognize that type I IFNs and other antiviral cytokines are vital for the systemic activation of cells in both the innate and adaptive immune responses. These cytokines are critical not only for antiviral defenses but also for antitumor immune control. Consequently, targeting the type I IFN pathway has become a strategic approach in OV research, aimed at overcoming the innate immune barriers in cancer cells to improve the efficacy of OV therapies [50]. For example, JAK inhibitors have emerged as a promising tool in enhancing the efficacy of oncolytic virus therapies against cancer. By inhibiting JAKs,

clinically approved inhibitors like ruxolitinib can decrease both IFN-induced and pre-existing ISG expression, thereby dampening the antiviral response. While initially used for treating myelofibrosis, ruxolitinib has shown potential in boosting OV activity in various cancer types [51].

Ruxolitinib has been effective in enhancing OV activity in malignant peripheral nerve sheath tumors (MPNSTs) in combination with oncolytic VSVΔ51 and in resistant head and neck and pancreatic ductal adenocarcinoma cells in combination with VSVΔ51 [52].

1.8. NF-κB pathway

NF-κB inhibitors have been identified as potential agents to improve the efficacy of oncolytic virus therapy in cancer. NF-κB, a crucial transcription factor, is activated in response to viral infections and controls the expression of type I IFN, particularly IFNβ, and a subset of interferon-stimulated genes (ISGs). Its frequent deregulation in cancer makes it an attractive target for selectively enhancing OV spread in resistant tumors [53].

The NF-κB pathway is a crucial signaling pathway in cells that regulates the immune response, cell proliferation, apoptosis, and other vital cellular processes. It plays a key role in the body's defense against infections and stress.

In the inactive state, NF-κB is sequestered in the cytoplasm by inhibitory proteins known as IκBs. When cells are stimulated by various signals such as stress, cytokines, free radicals, ultraviolet irradiation, or bacterial or viral antigens, the IκB proteins are phosphorylated by the IκB kinase (IKK) complex. This phosphorylation marks IκBs for proteasomal degradation. With the degradation of IκBs, NF-κB is freed and translocate to the nucleus where it binds to specific DNA sequences to regulate the transcription of target genes. These genes are involved in inflammation, immune response, cell survival, and other critical cellular functions.

The NF-κB pathway is tightly regulated and its chronic activation has been linked to various diseases, including cancer, chronic inflammation, and autoimmune disorders. As such, this pathway is a target for therapeutic interventions in these diseases [53].

1.9. NF-κB inhibitors

TPCA-1, an inhibitor of both IκB kinase (IKK) and JAK 1, has shown promise in improving the in vitro spread of oncolytic HSV and oncolytic (VSVΔ51) [54]. This enhancement in viral growth is linked to a decrease in the expression of antiviral ISGs [55]. Although there are numerous NF-κB inhibitors reported in preclinical studies, their clinical development has been unsuccessful, with few approved for medical use [56].

Triptolide, a diterpenoid compound extracted from the Tripterygium wilfordii plant, acts as an inhibitor of NF-κB and impacts IRF-3 signaling pathways. A study has demonstrated that Triptolide inhibits the production of type I interferon and interferon-stimulated genes, facilitating the propagation of the oncolytic virus VSVΔ51 both in laboratory settings and in live animal xenograft models [57].

1.10. DMF: Mechanism of action

DMF has emerged as a versatile therapeutic agent with a broad spectrum of action, impacting multiple crucial biological pathways. Primarily known for treating multiple sclerosis and psoriasis, DMF gained FDA and European Medicines Agency approval in 2013 for managing relapsing-remitting multiple sclerosis under the brand name Tecfidera [58]. DMF, characterized by its α,β-unsaturated carboxylic acid ester structure, is known for its strong electrophilic nature, enabling it to swiftly engage in reactions with nucleophilic agents via Michael addition. Following its oral intake, DMF is presumed to undergo rapid conversion by intestinal esterase enzymes, resulting in the formation of its active metabolite, monomethyl

fumarate [59]. Its role extends to inhibiting the NF-κB pathway, key in regulating immune responses, inflammation, and cell survival. This inhibition results in reduced proinflammatory cytokine production, impacting inflammation and enhancing the efficacy of oncolytic virus therapies.

DMF inhibits the NF-κB pathway through a unique mechanism involving its reactive nature with specific protein components. As a thiol-reactive electrophile, DMF targets cysteine residues on proteins, notably affecting the IκB Kinase (IKK) complex responsible for activating NF-κB. This interaction disrupts the usual phosphorylation and degradation of IκB proteins, which normally release NF-κB to translocate to the nucleus. By hindering this process, DMF effectively prevents NF-κB from entering the nucleus and binding to DNA, thereby reducing the transcription of various pro-inflammatory genes that NF-κB typically regulates [60,61]. This is primarily achieved through the covalent modification of the RelA/p65 subunit of NF-κB at the cysteine 38 residue [62]. This modification prevents the nuclear translocation of RelA/p65, a critical step required for NF-κB to exert its effects in the cell nucleus, such as the transcription of genes involved in inflammation and cell survival/death. Of relevance, these genes include those encoding cytokines and chemokines, crucial for inflammatory and immune responses such as IL6, IL1B, and CCL5. Particularly significant in cancer cells, where NF-κB often has a role in promoting growth and survival, DMF's inhibition of this pathway can lead to suppressed tumor growth and metastasis. Overall, the ability of DMF to modulate the NF-κB pathway underscores its potential as a therapeutic agent with anti-inflammatory and anticancer properties. Furthermore, DMF has shown potential in anti-inflammatory and cytoprotective activities. At low concentrations, it activates the NRF2 pathway, known as the "Master redox switch," which is crucial for cellular defense.

DMF disrupts NRF2's inactivation by KEAP1, leading to enhanced transcription of antioxidant and anti-inflammatory enzymes [63,64]. This action boosts the production of antioxidants like glutathione (GSH) and reduces oxidative stress and inflammation. However, at higher concentrations, DMF modulates cellular redox signaling and inhibits the NRF2/DJ-1 axis, inducing pro-oxidative and cytotoxic effects in cancer cells. This dual role in both activating and inhibiting NRF2 highlights DMF's complex impact on cellular physiology [65]. DMF's interaction with GSH is also noteworthy. It forms conjugates with GSH, altering its availability and impacting cellular responses to oxidative stress [66]. This effect varies between cell types; in non-tumorigenic cells, DMF can increase GSH levels, while in cancer cells, it can reduce GSH and increase ROS, leading to cell death [65]. These multifaceted actions of DMF underline its potential as a powerful tool in both anti-inflammatory and anticancer therapies.

Numerous studies have demonstrated the anticancer effects of DMF in a variety of cancers. In melanoma, DMF has demonstrated effectiveness in both cells and animal models. It inhibits the proliferation of melanoma cells, causes cell cycle arrest, and induces apoptosis [67]. Additionally, DMF targets the NF-κB pathway, essential for cancer progression, thus reducing melanoma cell invasion and metastasis by inhibiting matrix metalloproteinases [68]. These results underline DMF's potential as a therapeutic agent for melanoma. In breast cancer, DMF has been shown to effectively impair the growth of breast cancer cells and significantly reduce tumor growth in animal models[62].

In cervical cancer cells, DMF demonstrated antiproliferative effects by inhibiting cell growth in a concentration-dependent manner. It induced cell cycle arrest at the G0/G1 phase and triggered apoptosis, as shown by the activation of caspase-3 and PARP. DMF also caused a

loss of mitochondrial membrane potential, increased reactive oxygen species (ROS) levels, and decreased glutathione levels, indicating its impact on the cells' redox systems [69].

A number of studies have shown the impact of DMF on colorectal cancer. The first study demonstrated that DMF induces cell death in several colon cancer cell lines, including HT29, Caco-2, SW480, and CT26. This effect is associated with decreased nuclear translocation of NRF2, a decrease in DJ-1 levels, and a reduction in downstream targets of NRF2, such as HO-1[65]. In a chemically induced colorectal cancer model, DMF prevented common cancer-related symptoms like weight loss, colon shortening, and rectal prolapse, and it reduced chronic inflammation associated with colorectal cancer. [65]. A study by Xie et al. explored DMF's antiproliferative activity and gene expression changes in colon cancer cell lines. They found that DMF inhibits cell proliferation and induces necroptosis — an inflammatory form of cell death — in these cancer cells. This effect is achieved through GSH depletion, increased ROS production, and activation of the MAPKs pathway, occurring in a time- and dose-dependent manner in various colon cancer cell lines [70].

Our group has shown that DMF improves the infection efficiency of oncolytic viruses in cancer cell lines and human tumor biopsies. The ability of DMF to enhance viral infection leads to better therapeutic outcomes in resistant tumor models, including syngeneic and xenograft models. This is attributed to its ability to block the nuclear translocation of NF-κB, a transcription factor that plays a role in the immune response against viral infections as explained above [45].

1.11. Tepilamide fumarate as potential oncolytic viral enhancer

Tepilamide fumarate, also known as PPC-06, is a pro-drug of monomethyl fumarate (MMF) and belongs to the fumaric acid esters (FAE) class of drugs. Developed as an oral treatment option, it targets moderate-to-severe plaque psoriasis. This extended-release tablet is designed for absorption throughout the gastrointestinal tract and is rapidly hydrolyzed to release MMF as its active component. Unpublished Phase I data suggest that PPC-06 provides more efficient and sustained MMF exposure compared to currently marketed DMF formulations [71].

The structure of Tepilamide fumarate is more complex than that of DMF, primarily because it contains a tertiary amine. This feature adds an additional dimension to the compound, potentially influencing its basicity and interactions within biological systems, which is of particular interest for pharmacological applications.

1.12. High throughput screening to enhance virotherapy.

High throughput screening (HTS) has been previously established as a sophisticated methodological approach to identify new molecular entities or genetic perturbations that can overcome cancer cell resistance to oncolytic virus therapy [72,73]. By subjecting OV-infected cancer cells to a variety of experimental pressures, including pharmacological agents, genome editing techniques, and gene expression manipulations, these screens endeavor to uncover previously unrecognized interactions between tumor cells and OVs. The strategic application of such pressures facilitates the identification of molecular targets within the cancer cells that, when modulated, may enhance cellular susceptibility to OV-mediated lysis. Consequently, insights derived from screens are instrumental in guiding the development of more efficacious OVs and identifying novel therapeutic targets and modalities. This, in turn, contributes to the optimization of OV therapy, potentially leading to improved treatment outcomes for cancer

patients. Through an unbiased (as much as feasible) perturbation and measurement of the interactions between cancer cells and OVs, screens offer a promising avenue for advancing the field of oncolytic virotherapy.

Our lab developed the first high-throughput screening method to discover compounds capable of boosting VSVΔ51 replication. This approach facilitated the screening of vast chemical libraries, encompassing both drugs with established functions and synthetic compounds with unidentified targets. Vorinostat served as a positive control in this screen. The term “viral sensitizer” emerged from this work, identifying 15 compounds that surpassed Vorinostat's effectiveness. Among these, the leading compound, Viral Sensitizer 1 (VSe1), a chlorinated furanone derivative, showed promise by significantly enhancing VSVΔ51 proliferation up to 1000-fold in cancer cells and tumor explants, without affecting normal cells and tissues. Despite its potent in vitro effects, VSe1's clinical application is limited due to poor serum stability and pharmacokinetics [73].

This screening also identified microtubule destabilizers, notably colchicine, which significantly enhance VSVΔ51-mediated oncolysis. Colchicine, commonly used for treating gouty arthritis, demonstrated synergistic, cancer-selective killing both in vitro and in various mouse tumor models when used in conjunction with oncolytic rhabdoviruses. These agents facilitate oncolysis by reducing type I IFN translation and promoting the secretion of virally induced cytokines, thereby increasing bystander killing [44]

Another example uncovered from HTS from our group includes Pevonedistat, a NEDD8-activating enzyme inhibitor, which enhances the effectiveness of VSVD51 oncolytic virotherapy by sensitizing cancer cells to viral infection. It achieves this by inhibiting key

antiviral defenses in tumor cells, specifically through blocking the type 1 interferon response and NF-kB nuclear translocation. This combined approach improves tumor cell death and therapeutic outcomes in resistant cancer models, showing potential for clinical application in human cancers [38].

High-throughput screening, whether it involves functional genomics or pharmacological agents, stands as an exceptionally useful strategy. It enables the acquisition of vast amounts of information critical for enhancing oncolytic virotherapy.

1.13. Rationale and hypothesis

1.13.1. Central Hypothesis:

The therapeutic efficacy of oncolytic viruses, specifically HSV-1 and VSVΔ51, can be significantly enhanced in cancer treatment through strategic combinations with known/approved anti-inflammatory agents or novel compounds identified by pharmaceutical screens.

1.13.2. Rationale and Linkage of Research Objectives:

A - Improving Oncolytic HSV-1 with DMF in preclinical cancer models:

Rationale: Dimethyl fumarate, a clinically approved agent known for its anti-inflammatory and immunomodulatory properties, may augment the oncolytic activity of HSV-1. Its combination with HSV-1 could potentially modulate the tumor microenvironment, enhancing the virus's therapeutic efficacy.

Linkage: This project establishes the foundation for combining oncolytic viruses with approved anti-inflammatory agents, setting the stage for further exploration of similar strategies.

B - Enhancing Oncolytic VSVΔ51 and HSV-1 with Tepilamide Fumarate:

Rationale: Tepilamide fumarate, an anti-inflammatory agent currently in clinical trials for psoriasis, could synergistically enhance the oncolytic effects of VSVΔ51 and HSV-1,

potentially improving their therapeutic index in cancer treatment. Given that Tepilamide fumarate is a pro-drug of MMF and shares aspects of DMF's structure, we hypothesize that Tepilamide fumarate may possess anticancer properties and could potentially play a role in oncolytic virotherapy.

Linkage: Building upon the first project, this objective explores the combination of oncolytic viruses with another anti-inflammatory agent, broadening the scope of potential therapeutic combinations.

C - High-Throughput Screening for Novel Drugs to enhance virotherapy:

Rationale: Identifying novel pharmacological agents that can synergize with oncolytic viruses is crucial for developing more effective cancer therapies. High-throughput screening offers a methodical approach to discovering such candidates.

Linkage: This project complements the first two by providing a systematic method for finding new drugs that can be tested in combination with oncolytic viruses, potentially leading to more effective cancer treatments.

Chapter 2: Unlocking the Potential of Dimethyl Fumarate: Enhancing Oncolytic HSV-1 Efficacy for Wider Cancer Applications

Akram Alwithenani[1,2,3], Zaid Taha[1,2], Max Thomson[1], Andrew Chen[1], Boaz Wong[1,2], Rozanne Arulanandam[1], Jean-Simon Diallo[1,2]

[1]Centre for Cancer Therapeutics, Ottawa Hospital Research Institute, Ottawa, Ontario, K1H 8L6, Canada.

[2]Department of Biochemistry, Microbiology, and Immunology, Faculty of Medicine, University of Ottawa, Ontario, K1H 8M5, Canada

[3]Department of Clinical Laboratory Science, Faculty of Applied Medical Science, Umm Al-Qura University, Makkah, Saudi Arabia

Keywords: HSV-1, DMF, Cancer, Cancer therapeutics, Human specimens, Fumarate esters

Published on December 18, 2023, in Frontiers in Immunology

2.1 Abstract

Immunotherapy and specifically oncolytic virotherapy has emerged as a promising option for cancer patients, with oncolytic herpes simplex virus-1 (HSV-1) expressing granulocyte macrophage colony stimulating factor being the first OV to be approved by the FDA for treatment of melanoma. However, not all cancers are sensitive and responsive to oncolytic viruses. Our group has demonstrated that fumaric and maleic acid esters (FMAEs) are very effective in sensitizing cancer cells to OV infection. Of note, these FMAEs include dimethyl fumarate (DMF, also known as Tecfidera®), an approved treatment for multiple sclerosis and psoriasis. This study aimed to assess the efficacy of DMF in combination with oncolytic HSV-1 in preclinical cancer models. We demonstrate herewith that pre-treatment with DMF or other FMAEs leads to a significant increase in viral growth of oHSV-1 in several cancer cell lines, including melanoma, while decreasing cell viability. Additionally, DMF was able to enhance *ex vivo* HSV-1 infection of mouse-derived tumor cores as well as human patient tumour samples but not normal tissue. We further reveal that the increased viral spread and oncolysis of the combination therapy occurs via inhibition of type I IFN production and response. Finally, we demonstrate that DMF in combination with HSV-1 can improve therapeutic outcomes in aggressive syngeneic murine cancer models. In sum, this study demonstrates the synergistic potential of two approved therapies for clinical evaluation in cancer patients.

2.2 Introduction

Oncolytic virus (OV) therapy is a promising new option for cancer treatment. OVs represent a class of therapeutically useful viruses that preferentially infect and kill cancer cells while leaving normal cells relatively unharmed [74,75]. This tumor tropism is derived from the aberration of anti-viral responses commonly found within tumor cells. Enhanced virus growth and reduced viral clearance is typically observed in innate immunity-compromised, transformed cells [76].

Several kinds of OVs have been described with the potential to eradicate tumors, leading to long term anti-tumor immunity. In the last decade, oncolytic Herpes Simplex Virus has made its way to the clinic to treat advanced melanoma (unresectable stage IIIB to IV) [26]. The first FDA-approved OV called T-VEC or Imlygic® is based on an engineered version of HSV-1 devoid of γ34.5. In June 2021 another genetically engineered OV based on HSV-1 (G47Δ), DELYTACT® received conditional and time-limited approval for the treatment of malignant gliomas in Japan [25]. Both HSVG47Δ and HSV.γ34.5 have the ICP34.5 gene deleted to provide more selective tumor replication [28]. These strains have been shown to induce tumor regression and prolong survival significantly in different animal models of cancers such as glioma, melanoma and ovarian cancer [77,78]. Furthermore, it has been shown that HSV-1 with mutations (HSV.n212) or deletions (HSV.d810) in the immediate early gene ICP0, which encodes a protein responsible for overcoming aspects of the host IFN response (suppressing IRF-3 and IRF-7), has oncolytic properties [29].

Unfortunately, not all cancers are sensitive and responsive to oncolytic virotherapy. Numerous studies have shown that a subset of cancer patients are resistant to OV treatment due to various mechanisms, including a functional type I interferon pathway and an immunosuppressive

tumour microenvironment (TME) [79]. Several strategies to overcome the resistance and maximize the therapeutic efficacy of OV treatment have been under investigation [43,47]. One promising strategy to increase the impact of the OV is to administer pharmacological drugs that facilitate OV infection of cancer cells but not normal cells. Multiple promising drug classes have been discovered to this end [38,52,57,80]. These drugs can transiently decrease the type I IFN response to allow OVs to gain a foothold and propagate within the tumour [73]. One of the drugs previously described to promote effectiveness of oncolytic virotherapy is Dimethyl Fumarate. DMF is an approved drug for psoriasis taken as an oral therapy, and since 2013 DMF has also been approved for relapsing multiple sclerosis [81]. In the context of cancer treatment, DMF has demonstrated anti-tumor properties by reducing tumor growth and metastasis [82,83]. Specifically, DMF was shown to suppress the nuclear factor kappa B (NFκB) pathway and induce oxidative stress through cellular Reactive oxygen species (ROS); resulting in tumor regression [70]. DMF has also been reported to suppress cell proliferation in multiple breast cancer cell lines via inhibition of NFκB activity [84]. In addition, DMF was shown to sensitize tumors to chemotherapy [85], as NFκB regulates several genes that are involved in chemotherapy resistance. In a previous study published by our group [45], it was shown that DMF effectively enhanced the spread and oncolysis of Vesicular Stomatitis Virus (VSVΔ51) across a range of resistant cancer cell lines, including human clinical specimens. The combination of DMF and VSVΔ51 demonstrated significant efficacy in various immune-competent cancer model such as murine colon carcinoma (CT26.wt). Notably, DMF's capacity to augment viral spread can be attributed to its capability in suppressing type I interferon (IFN).

Drawing on DMF's established effectiveness in cancer therapy, its clinical availability and its successful combination with oncolytic VSVΔ51[45], as well as the clinical progress of oncolytic HSV, the amalgamation of these modalities emerges as a compelling therapeutic strategy. DMF's demonstrated potential to suppress tumour growth, combined with oncolytic HSV's tumor-selective replication and cytotoxicity, presents an opportunity for a multifaceted approach with enhanced therapeutic impact. The objective of this study is to demonstrate the preclinical feasibility of employing DMF in conjunction with oncolytic HSV-1, both in vitro and in vivo settings. In the current study, our investigation exploited ICP0 null HSV-1 strains, denoted as HSV.n212 and HSVd810, alongside ICP34.5-deficient HSV-1 strains, specifically HSV.γ34.5 and HSVG47Δ.

2.3 Results

2.3.1 Dimethyl fumarate sensitizes cancer cells to HSV-1 infection.

The main objective of our study was to evaluate the potential applicability of DMF to HSV-1-based oncolytic virus platforms. Consequently, we first investigated the effects of DMF on HSV-1 replication in various murine and human cancer cell lines. As a starting point, human renal 786-0 carcinoma cells, which are typically resistant to oncolytic virus infection, underwent a pre-treatment phase of 4 hours with DMF as per previous studies [45]. Subsequently, these cells were infected with HSV.n212 that was genetically modified to express green fluorescent protein, at a low multiplicity of infection (MOI), as shown in (Figure 2.1A). An increase in fluorescence upon pretreatment with DMF and infection with HSV.n212 was observed in 786-0 cells as well as in murine CT26.wt colon carcinoma cells which are HSV-resistant at baseline and syngeneic in Balb/c mice (Figure 2.1A). In addition, fluorescent microscopy confirmed increased HSV.n212-GFP transgene expression in murine CT26.wt, CT2A glioma, S180 sarcoma and human 786-0 cells as shown in (Figure S2.1A & S2.1B). Subsequently, the viral sensitizing potential of DMF in impacting HSV.n212 viral titers was evaluated in several cancer subtypes including breast (murine 4T1), colon (murine CT26.wt, human HT29), glioma (murine CT2A), sarcoma (murine S180), renal (human 786-0) and melanoma (patient derived OHRI-13) where we observed a significant increase compared to HSV.n212 alone (Figure 2.1B&C). This viral enhancing effect was also observed when DMF was administered concurrently with the virus as well as with post-treatment times as long as 8 hours as shown in (Figure 2.1D). In addition, we conducted assessments with various strains of HSV-1 to ascertain the generalizability of DMF's impact across diverse oncolytic mutants. Our findings revealed a consistent increase in titer of other strains of HSV including

HSV.G47Δ, HSV.d810 and HSV.γ34.5 within distinct cancer models, as shown in (Figure S2.2&2.3), affirming the broad applicability of DMF's efficacy across oncolytic HSV-1 strains. Furthermore, we looked into the ability of DMF to potentiate HSV-1 infectivity by comparing multi-step to single-step growth curves. Similar to what we observed with VSVΔ51, DMF was able to strongly improve HSV.n212 when infected at a low MOI of 0.01, but not at a high MOI of 1 through quantification of titer by plaque assay as illustrated in (Figure 2.1E&F). This suggests that DMF promotes viral spread to increase its growth, but not through increasing the rate of HSV-1 replication or viral entry. To further assess the oncolytic impacts of HSV.n212 in the presence of DMF, we pretreated cancer cells with DMF before infection with HSV.n212, and cell viability was assessed 72 hours after infection. Combined treatment with DMF and HSV.n212 resulted in a significant (25-50%) decrease in cell viability in human 786-0 as well as several other human and murine cell lines (Figure 2.1G). To confirm the synergetic effect of the combination therapy, an analysis of non-constant combinations was conducted, focusing on the interaction between HSV.n212 and DMF compared to their respective monotherapies. This analysis is detailed in (Table S2.1), which presents the Combination Index Score (CSI) consistently between 0.7-0.8 in CT26.wt cells, confirming a synergistic interaction.

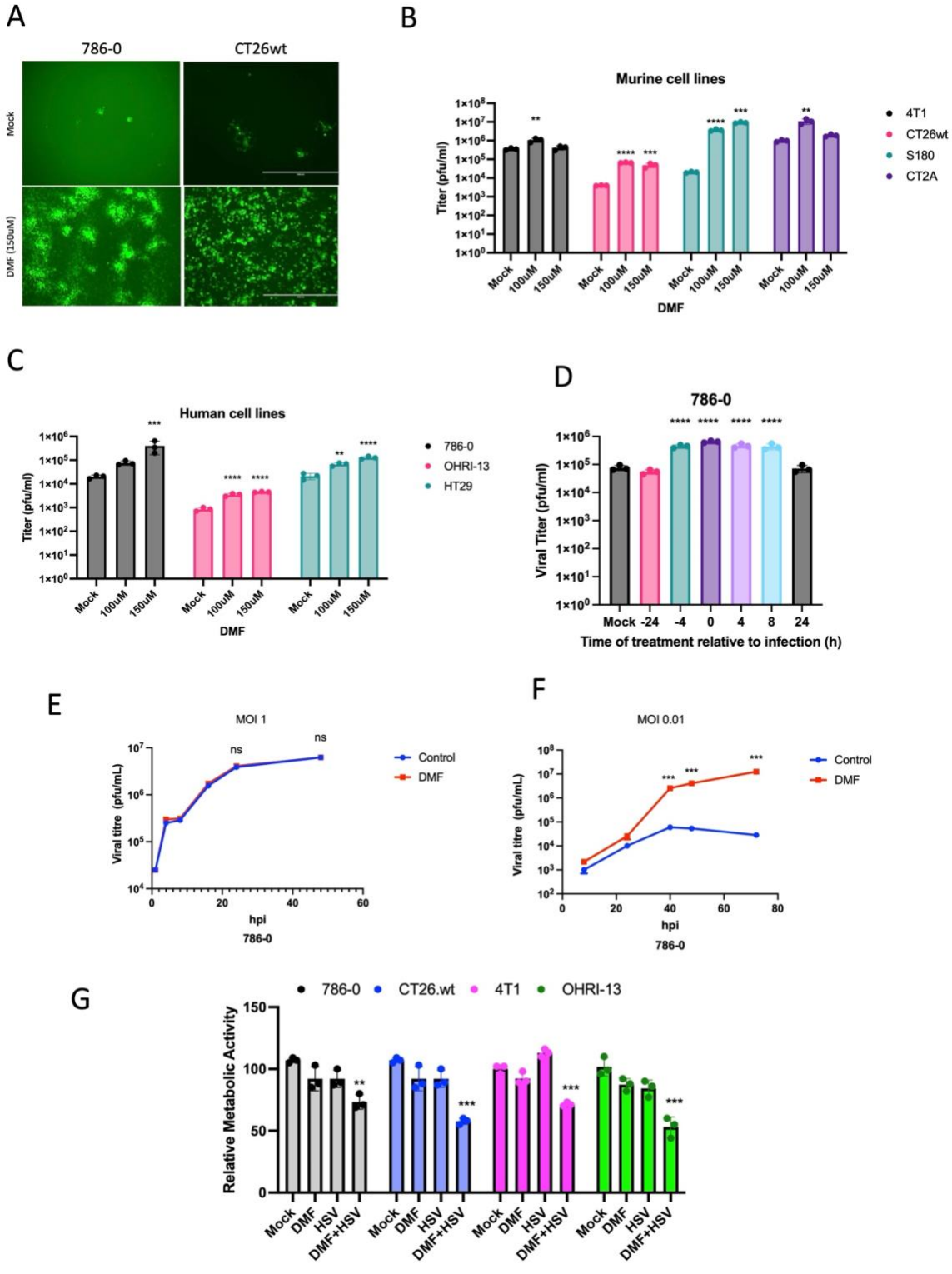
A
786-0
CT26wt
Mock
DMF (150uM)
B
Murine cell lines
Titer (pfu/ml)
Mock
100uM
150uM
DMF
4T1
CT26wt
S180
CT2A
C
Human cell lines
Titer (pfu/ml)
DMF
786-0
OHRI-13
HT29
D
786-0
Viral Titer (pfu/ml)
Mock -24 -4 0 4 8 24
Time of treatment relative to infection (h)
E
MOI 1
Viral titre (pfu/mL)
hpi
786-0
Control
DMF
ns
F
MOI 0.01
Viral titre (pfu/mL)
hpi
786-0
Control
DMF
G
786-0 CT26.wt 4T1 OHRI-13
Relative Metabolic Activity
Mock
DMF
HSV
DMF+HSV

Figure 2.1: DMF sensitizes human and murine tumor types to HSV-1.

(**A-C**) Various human and murine cell lines were pre-treated with DMF (100, and 150uM), then infected with HSV.n212 (MOI 0.01). Forty-eight hours after infection, fluorescence images were taken from the infected cancer cells, as shown in (A) infectious viral particles were quantified by plaque assay as shown in B&C (N=3 mean ± SEM; one-way ANOVA with Dunnett's multiple comparisons test compared to Mock for each cell line). **(D)** 786-0 cells were treated with 150 μM of DMF at various times before or after infection with HSV.n212 (MOI: 0.01) or untreated. Samples were collected 48 hours after infection and tittered by plaque assay (N=3 mean ± SEM; one-way ANOVA with Dunnett's multiple comparisons test compared to Mock for each cell line). (**E&F)** Multistep (MOI, 0.01) and single-step (MOI, 3) growth curves. 786-0 cells were pretreated with DMF and infected with HSV.n212 at an MOI of 0.01, or 3; samples were tittered by plaque assay (n = 3; mean ± SD; two-tailed t-test). **(G)** 786-0 and other cancer cell lines indicated were pre-treated with DMF with different concentrations for 4 hours and then infected with HSV.n212 at an MOI of (0.01). Seventy-two to ninety-six hours post-infection cytotoxicity was assessed by incubating samples with Resazurin metabolic dye for 150 minutes at 37C before measuring fluorescence (530nm excitation, 590 nm emission). Values were normalized to that of untreated control (N=3 mean ± SEM; *P < 0.05, ***P < 0.001; one-way ANOVA with Dunnett's multiple comparisons test compared to Mock for each cell line).

2.3.2 Dimethyl Fumarate enhances HSV-1 viral infection in a various of ex vivo tumor models.

The inherent selectivity of oncolytic virotherapy towards cancer tissues is one of its advantages over conventional therapies. Therefore, the effect of DMF on oncolytic HSV-1 selective infectivity was evaluated to confirm that DMF does not enhance the replication of the virus in normal tissues. Tumour cores from mice subcutaneously implanted with CT26.wt murine colon cancer cells, as well as cores from normal tissues such as brain, spleen, muscle, and lung, were collected and subsequently infected with HSV.n212 in the presence or absence of DMF (150 μM). (Figure 2.2A) shows representative fluorescence images of cores that were pretreated with DMF prior to HSV.n212 infection. Images and corresponding viral titers (Figure 2.2B) show a clear enhancement of HSV.n212 following pretreatment with DMF in CT26.wt cores. In sharp contrast, no enhancement of HSV.n212 was observed in normal brain tissues and other normal tissues, indicating that the selectivity of the virus towards the tumour is still maintained regardless of DMF pretreatment. Furthermore, similar results were observed in cores obtained for S180 and CT2A tumours, as shown in (Figure S2.4). When we tested our combination strategy in primary human ex vivo clinical samples, DMF increased HSV.n212 infection across a large variety of tumour types, including breast, lung, and ovarian, as demonstrated by viral plaque assay and fluorescence microscopy (Figure 2.2C-E). In an ovarian cancer sample, DMF increased the viral titer by over 14-fold. Of 6 human cancer specimens tested, only a melanoma sample was found to be non-responsive to DMF even though baseline infection / viral titer was similar across all samples. Together, these results

demonstrate that DMF's ability to increase HSV.n212 viral infectivity is selective and applicable across different types of human and murine tumours.

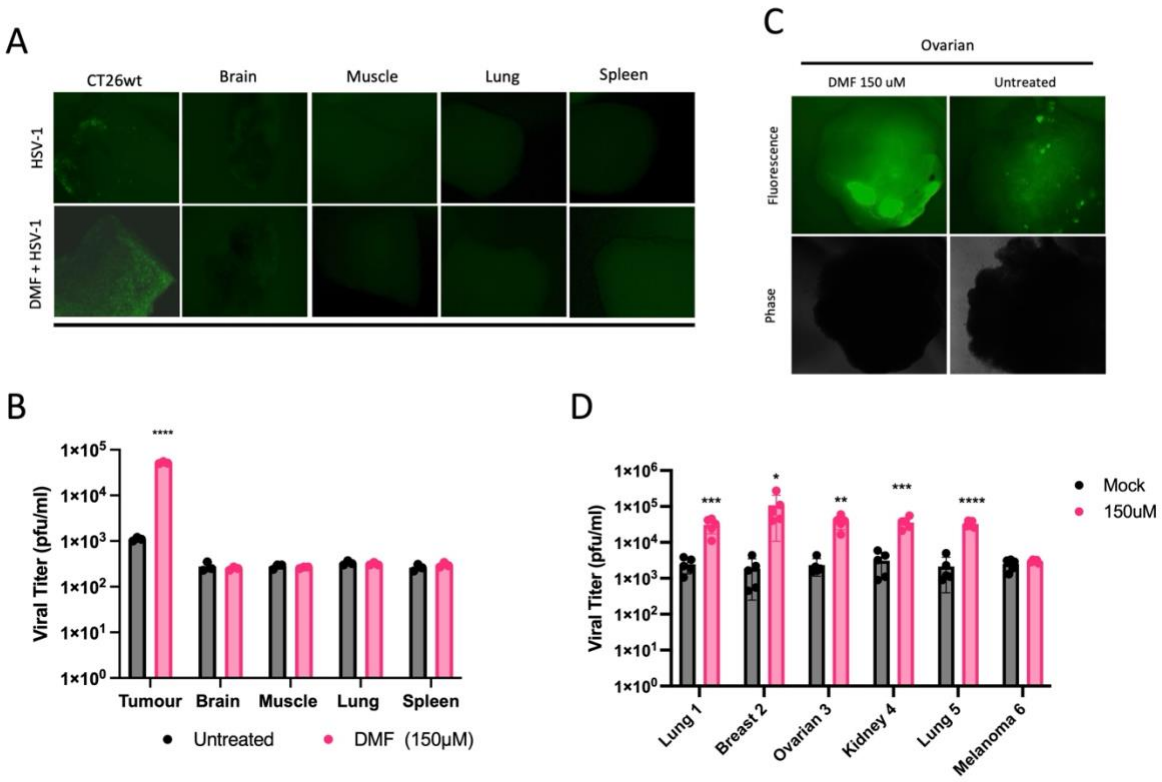

E

Specimen	ID	Age	Biological sex	Pathology report
Ovarian	GTC 323	65	F	Metastatic serous carcinoma, consistent with Mullerian primary
Breast	GTC 109	72	F	Breast carcinoma with ER postive and HER2 negative
Lung	GTC 185	76	M	Squamous cell carcinoma; areas of tumour necrosis are noted.
Kidney	GTC 418	66	M	Renal cell carcinoma
Lung	GTC 419	74	M	Large cell nueroendocrine carcinoma
Skin	GTC 425	84	F	Metastatic Melanoma, single nodule measuring 1 cm.

Figure 2.2. DMF enhances the replication of HSV.n212 in ex vivo tumor tissues and patient-derived explants.

(A-B) CT26.wt (murine colon carcinoma) tumors were grown in BALB/c mice until they reached a volume of 1500mm^3. Tissues were collected, cored, and treated for four hours with DMF at indicated concentrations prior to infection with 3x10^{10} plaque-forming units of HSV.n212. To monitor viral infection, GFP images were captured, and supernatants were collected at 72 hpi. Representative GFP images are shown for tumor and normal tissues as in B. Infectious viral particles were quantified by standard plaque assay (B) (n>5, mean ± SD; ns = no significance, *P< 0.05, ****P<0.0001 by two-tailed t-test).. (**C-D)** Clinical human samples were obtained and cored. Cores were treated with DMF (150μM) for 4 hours, then infected with HSV.n212 (3 x 10^4 pfu/core). At 72hpi, representative fluorescent images were obtained. Infectious viral particles were quantified by standard plaque assay (n>5; ns = no significance, *P< ****P<0.0001 by two-tailed t-test). **(E)** A table presents clinical characteristics of patient-derived tumour specimens used in this study

2.3.3 FMAEs promote HSV-1 infection.

Apart from DMF, a number of fumaric and maleic acid esters (FMAEs) exhibit properties that reduce inflammation and regulate the immune response. In light of this, we investigated whether other FMAEs and their cis- and trans-isomers (maleic acid esters) had an impact HSV.n212 infection of cancer cells, comparable to what was previously shown with VSVΔ51 [45]. Indeed, dimethyl maleate (DMM), diethyl maleate (DEM), and diethyl fumarate (DEF) pretreatment led to strong HSV.n212 infection and oncolysis within 786-0 cells in vitro (Figure 2.3A-B). Additionally, MMF, the biologically active metabolite of DMF, did enhance HSV.n212 as shown in (Figure 2.3A-B). While some enhancement in HSV.n212 spread and titer (Figures 2.3A and 3B) was observed when pre-treating 786-0 with fumaric acid (FA), a compound that does not easily traverse the cell membrane, this did not reach statistical significance. Collectively, our findings suggest that the use of DMF and other FMAEs, characterized by their high bioavailability, can significantly enhance the growth of HSV-1 in 786-0 cells.

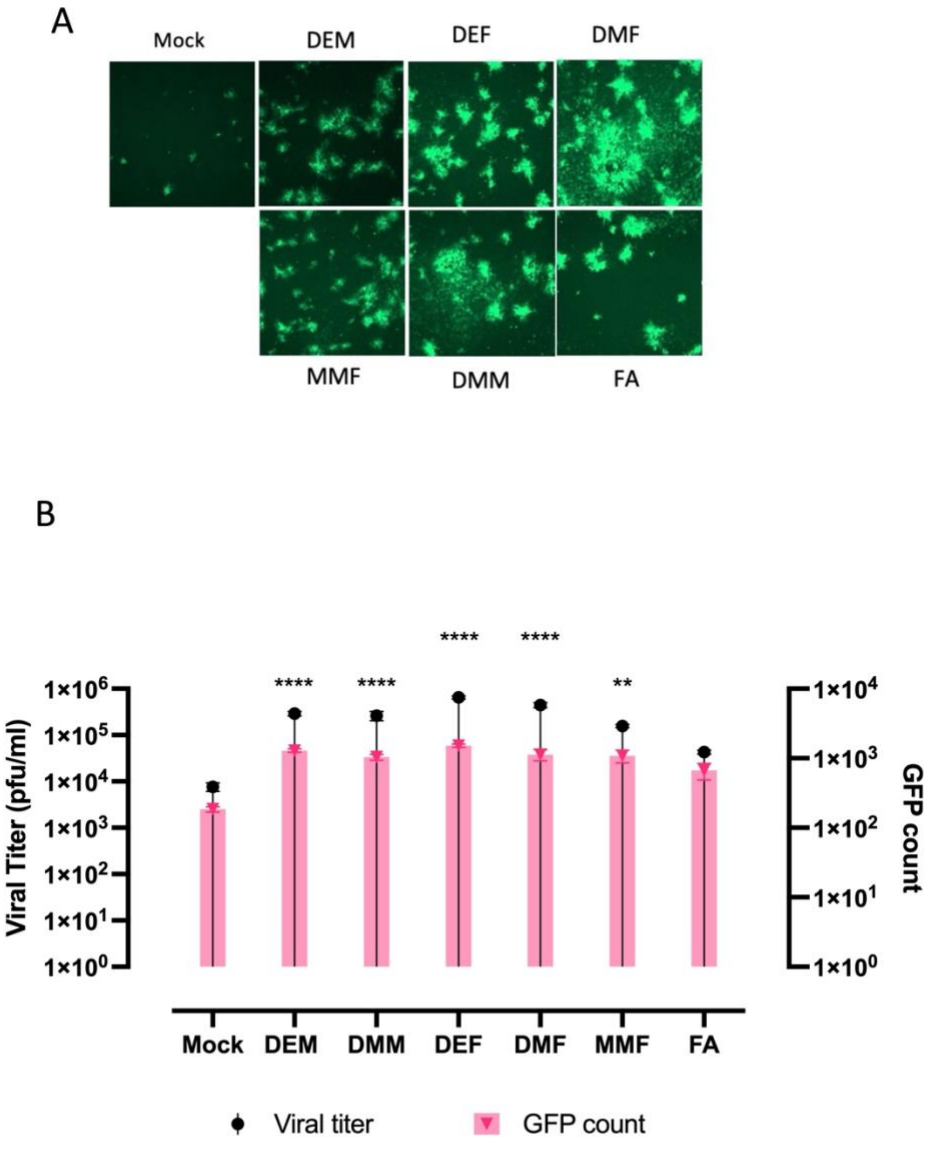
A
Mock
DEM
DEF
DMF
MMF
DMM
FA
B
Viral Titer (pfu/ml)
1×10^6
1×10^5
1×10^4
1×10^3
1×10^2
1×10^1
1×10^0
GFP count
1×10^4
1×10^3
1×10^2
1×10^1
1×10^0
****
****
****
****
**
Mock
DEM
DMM
DEF
DMF
MMF
FA
Viral titer
GFP count

Figure 2.3: FMAEs promote infection by HSV.n212

786-0 cells were pretreated with various FMAEs and analogs for 4 hours and subsequently infected with oncolytic HSV.n212 expressing GFP at **(A)** an MOI of 0.01. Seventy-two hours after infection, we obtained fluorescence images of the infected 786-0 cells. **(B)** Corresponding viral titers were determined from supernatants 72 hours after infection. (N=3 mean ± SEM; *P < 0.05, ***P < 0.001; one-way ANOVA with Dunnett's multiple comparisons test compared to Mock).

2.3.4 DMF suppresses the antiviral response.

To further assess if DMF treatment suppresses innate immunity induced by oncolytic HSV-1 as previously observed in the context of VSVΔ51 [45], IFN-β and downstream interferon-stimulating genes (ISGs) were investigated at the mRNA level. 786-0 cells were pretreated with either mock or DMF (150 μM) and four hours later infected with HSV.n212, or mock infected. 24 hour later, RNA was collected, converted to cDNA and qRT-PCR was performed. All genes, including IFN-β, MX2, IFITM1, and IL6, were significantly suppressed with the combination treatment in comparison with HSV.n212 alone as shown in (Figure 2.4A). This suggests that DMF increases HSV.n212 infection via IFN-1 inhibition analogous to what was previously observed with oncolytic VSVΔ51. Quantification of IFN-β secretion by enzyme-linked immunosorbent assay (ELISA) followed a similar trend as shown in (Figure 2.4B).

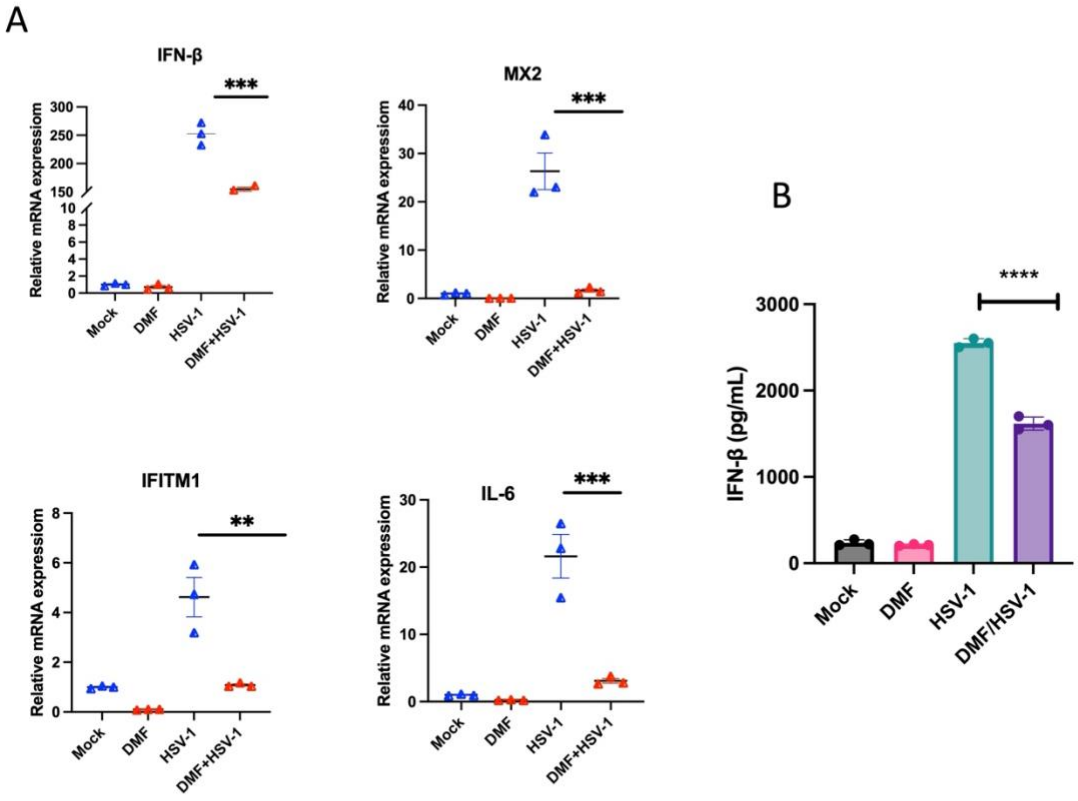
A
IFN-β
***
Relative mRNA expressiom
300
250
200
150
10
8
6
4
2
0
Mock
DMF
HSV-1
DMF+HSV-1
MX2
***
Relative mRNA expressiom
40
30
20
10
0
Mock
DMF
HSV-1
DMF+HSV-1
IFITM1
**
Relative mRNA expressiom
8
6
4
2
0
Mock
DMF
HSV-1
DMF+HSV-1
IL-6
***
Relative mRNA expressiom
30
20
10
0
Mock
DMF
HSV-1
DMF+HSV-1
B
****
IFN-β (pg/mL)
3000
2000
1000
0
Mock
DMF
HSV-1
DMF/HSV-1

Figure 2.4: DMF increases HSV.n212 infection via IFN-1 inhibition.

(A) 786-0 were pretreated with Mock or DMF (150uM) for 4h, after which time cells were washed and infected with HSV-1 MOI 0.1 or mock infected. 24 hour later, RNA was collected, converted to cDNA and qRT-PCR was performed. Cut off for y axis in IFN-β graph was 150. Data represented the normalized fold change. (B) 786-0 cells were treated as in (A) and at 36 hours post-infection, supernatants were collected and assayed by ELISA for IFN-β levels (N=3 mean ± SEM; **P < 0.01, ***P < 0.001; one-way ANOVA with Tukey's multiple comparisons test).

2.3.5 DMF enhances the therapeutic effectiveness of oncolytic HSV.n212.

Given that DMF is a clinically approved drug, and it broadly and robustly enhances the growth and activity of oncolytic HSV-1 in several human and murine cancer cells with conversely limited effects on normal tissues, we next evaluated the potential therapeutic benefit of combining DMF with oncolytic HSV-1 in vivo. The primary aim of the first experiment was to determine the optimal dosage of HSV.n212 that would have a significant effect on the progression of tumours. We administered HSV.n212 intratumorally up to six times in the CT26.wt model. We saw that infection with HSV.n212 administered either three or six times resulted in regression of the tumours as compared to the monotherapy at lower frequencies or with PBS treatment. A survival study of this experiment shows that CT26.wt-bearing mice having received HSV.n212 either 3x or 6x had significantly prolonged survival compared to PBS (HSV-1 3x: $P = 0.019$ vs. PBS group; HSV-1 6x: $P = 0.013$ vs. PBS group) (Figure S2.5). We next sought to determine the most effective route of administration for DMF. DMF has received approval from the U.S. Food and Drug Administration (FDA) for oral administration to patients with multiple sclerosis, which is convenient, but which may not sufficiently reach the tumor. Conversely, administration through intratumoral injection can be more effective by directly impacting the tumour microenvironment, offering opportunities for co-administration as HSV-1 is currently approved for applications where the virus is administered intra-tumourally.

The CT26.wt model was used to assess the efficacy of oral and intratumoral (i.t) routes of delivery of DMF in achieving tumour control in combination with HSV-1. In our study, we had four distinct groups, including DMSO, HSV.n212 alone, DMF (i.t.)/HSV.n212, and DMF

(gavage)/HSV.n212. CT26.wt tumour-bearing mice received DMF either intratumorally or by oral gavage (200mg/kg). Five hours later, a bolus of 25µL PBS containing 1 x 10^8 pfu of HSV.n212 was injected intratumorally. This treatment was repeated two more times, with a one-day interval between each treatment. While both routes of administration led to delayed tumor progression in combination with HSV.n212, delivering DMF and HSV i.t. had the most robust effect, leading to some long-lasting remissions (approximately 10%) as shown in (Figure S2.6).

Having established that intratumoral administration of DMF over gavage results in better survival rates in combination with i.t. HSV.n212, our subsequent objective was to more robustly investigate the efficacy of DMF (intratumoral) in combination with HSV.n212 compared to other monotherapies, including HSV.n212, DMF, and DMSO. Treatments were tested in two different murine models of cancer: CT26.wt colon and 4T1 breast carcinoma. Mice given the combination therapy after tumours reached ~100mm^3 in size three times every other day (days 0, 2 and 4) showed a significant regression in tumor progression when compared to monotherapies in both the CT26.wt and 4T1 model. When looking at survival data in these models, the combination therapy significantly prolonged survival compared with either monotherapy (combination therapy compared to DMSO alone P = 0.001; HSV.n212 alone: P = 0.006, DMF alone: p = 0.03) (Figure 2.5A). In the more aggressive 4T1 model, the DMF/HSV.n212 combination significantly increased survival in comparison to all other conditions (combination therapy compared to DMSO alone P = 0.001; HSV.n212 alone: P = 0.01, DMF alone: p = 0.02) (Figure 2.5B). These results demonstrate that the combination of DMF and HSV.n212 therapy results in a greater therapeutic benefit compared to placebo or monotherapy in two different mouse models of cancer.

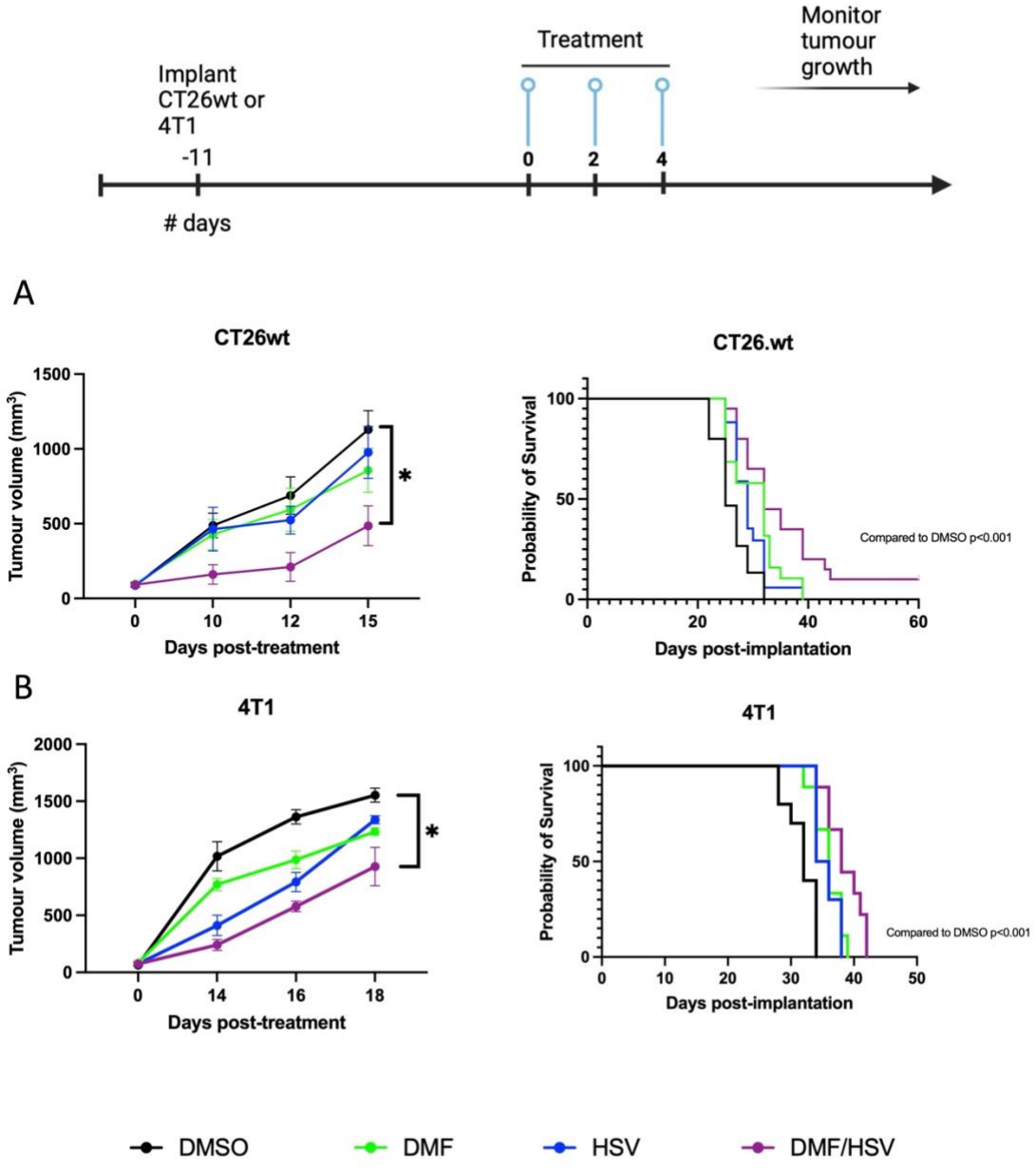
Implant
CT26wt or
4T1
-11
days
Treatment
0
2
4
Monitor
tumour
growth
A
CT26wt
Tumour volume (mm³)
1500
1000
500
0
0
10
12
15
Days post-treatment
*
CT26.wt
Probability of Survival
100
50
0
0
20
40
60
Days post-implantation
Compared to DMSO p<0.001
B
4T1
Tumour volume (mm³)
2000
1500
1000
500
0
0
14
16
18
Days post-treatment
*
4T1
Probability of Survival
100
50
0
0
10
20
30
40
50
Days post-implantation
Compared to DMSO p<0.001
DMSO
DMF
HSV
DMF/HSV

Figure 2.5: DMF improves HSV.n212 therapeutic efficacy in murine in vivo tumor models.

BALB/c nude mice were implanted with 3×10^5 CT26.wt cells or 5×10^5 4T1 cells. Upon reaching ~ 100mm3, mice were treated three times every other day with the regimen of 200 mg/kg DMF or DMSO (intratumorally) followed by HSV.n212 (1E8 pfu) or PBS (intratumorally) 5 hours later. Tumor volumes were monitored every 2-3 days ($n > 15$, mean ± SEM; *$P<0.05$, **$P<0.01$ by one-way ANOVA). Mice were culled when tumor volumes reached 1500mm3 for survival analysis. Kaplan-Meier curves were plotted and compared using the log-rank (Mantel-Cox) test (CT26.wt: DMSO = 15, DMF = 19 HSV.n212 = 18, combo = 20; 4T1: DMSO = 10 DMF = 9, HSV.n212 = 10, combo = 9).

2.3.6 Effects of HSV-1 / DMF combination therapy on tumor immune profile.

In order to provide a more comprehensive understanding of the immune response subsequent to therapy in the CT26.wt cancer model, mice were subjected to euthanasia on days 5 and 14 subsequent to the first administration of the treatment dosage (as per i.t dosing regimen described above). Tumours, tumour-draining lymph nodes (TdLN), and spleens were collected for the purpose of assessing cell-mediated immune responses. We detected an increase in the CD3+ population inside the tumour compartment of mice treated with the combination regimen compared to all other groups by day 14; however, this did not reach statistical significance comparing to individual groups in post-hoc tests (ANOVA p=0.09, Figure 2.6A). Notably, there was no concurrent increase detected in the CD4 and CD8 at any time point, suggesting this could be attributable to a rise in double-negative T-cells (Figure 2.6B). Notably, we also observed elevated expression levels of PD-L1 on the CD45- population which are predominantly CT26.wt cells as shown in (Figure 2.6C).

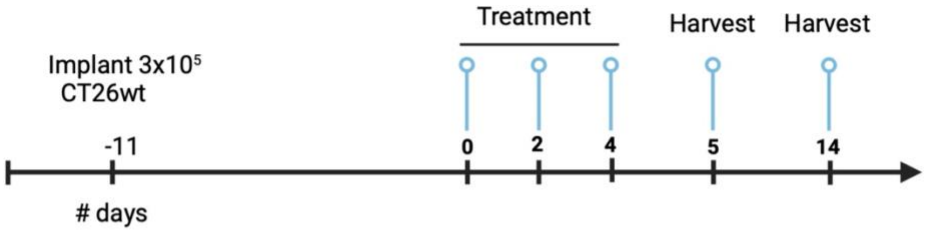
Treatment
Harvest
Harvest
Implant 3x10^5
CT26wt
-11
0
2
4
5
14
days

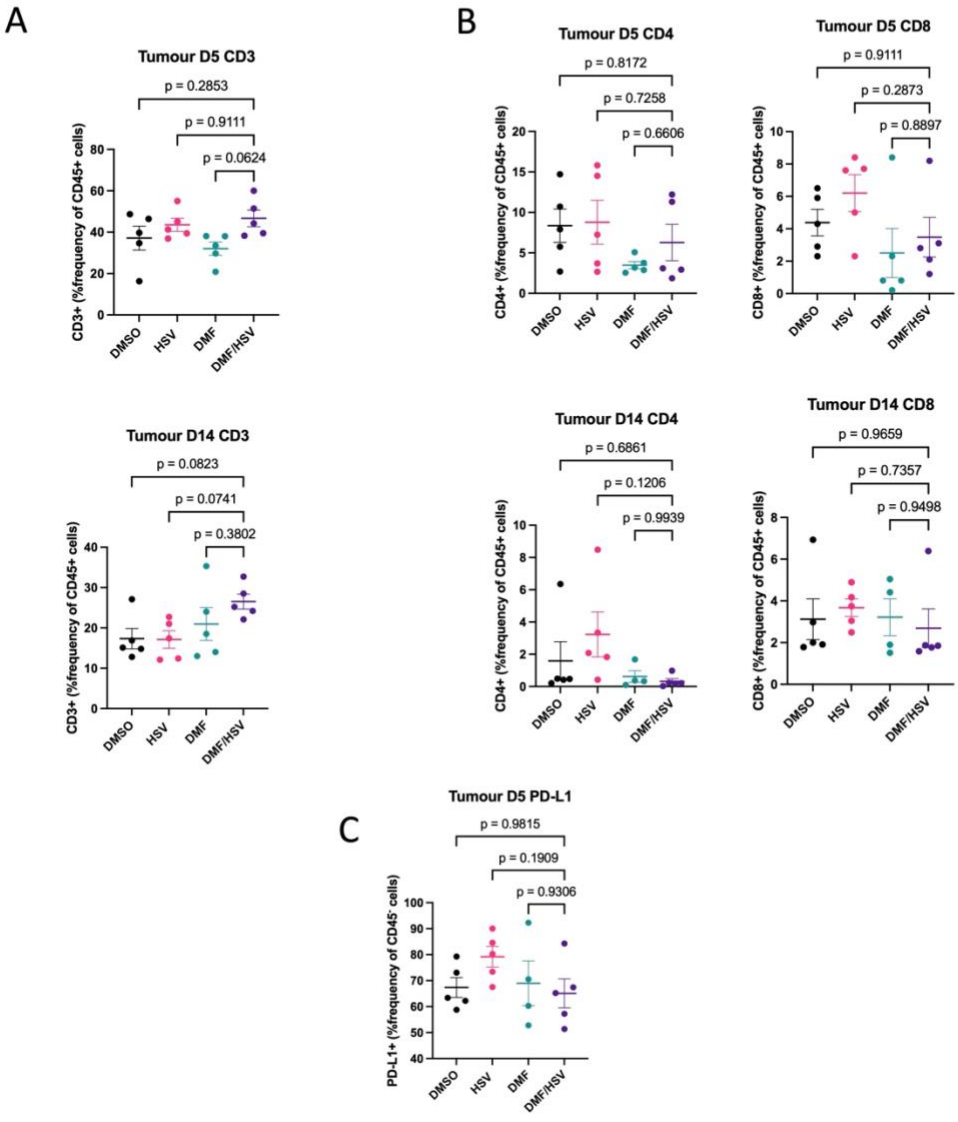
A
Tumour D5 CD3
p = 0.2853
p = 0.9111
p = 0.0624
CD3+ (%frequency of CD45+ cells)
DMSO
HSV
DMF
DMF/HSV
Tumour D14 CD3
p = 0.0823
p = 0.0741
p = 0.3802
B
Tumour D5 CD4
p = 0.8172
p = 0.7258
p = 0.6606
CD4+ (%frequency of CD45+ cells)
Tumour D5 CD8
p = 0.9111
p = 0.2873
p = 0.8897
CD8+ (%frequency of CD45+ cells)
Tumour D14 CD4
p = 0.6861
p = 0.1206
p = 0.9939
Tumour D14 CD8
p = 0.9659
p = 0.7357
p = 0.9498
C
Tumour D5 PD-L1
p = 0.9815
p = 0.1909
p = 0.9306
PD-L1+ (%frequency of CD45+ cells)

Figure 2.6: FACS analysis of combination treatment in CT26.wt model.

BALB/c mice were implanted with 3×10^5 CT26.wt cells. Upon reaching ~ 100mm3 mice were treated three times every other day with the regimen of 200 mg/kg DMF or DMSO 5 h later (intratumorally) followed by HSV.n212 ($1E^8$ pfu) or PBS (intratumorally). On day 5 and 14 post-treatment, mice were sacrificed, and tumors, spleen and lymph nodes harvested, cells were dissociated and stained with fluorochrome-conjugated anti-mouse antibodies, and multicolor FACS was performed. (A) Tumour-infiltration in total CD45+CD3+ T-cell populations (B) Tumour-infiltration total CD45+ CD4+ and CD8+ T-cell populations on day 5 and 14 post treatment. (C) PD-L1+ in CD45- population within tumour microenvironment. (N=5 mean ± SEM; one-way ANOVA with Tukey's multiple comparisons test).

2.4 Discussion

The obstacle presented by the resistance of tumours to oncolytic virotherapy is a well-recognized problem that hampers the achievement of clinical efficacy. Several research groups including ours have dedicated efforts towards developing strategies involving small molecules to enhance the susceptibility of tumors to oncolytic virus infection [47]. DMF arises as a versatile therapeutic candidate in the field of oncology due to its multifaceted characteristics, which include potent anti-tumor properties, immunomodulatory capabilities, and FDA-approved status [86]. A recent study conducted by our team has demonstrated that DMF can improve the effectiveness of VSVΔ51 in a variety of preclinical models [45]. Despite the commercial failure of Imlygic, HSV-1 remains a leading candidate in the OV field and holds much promise in the field of cancer therapy due to its ease of genetic manipulation, its ability to specifically target and eliminate cancer cells, and induce immune responses against tumours. Additionally, HSV-1 continues to stand as the only platform that has successfully transitioned into clinical use in North America, Europe and most recently Japan [26]. In this study, we examined the effects of DMF and various FMAEs on oncolytic HSV-1 in the context of cancer.

In the present investigation, our findings demonstrate that the utilization of the clinically approved DMF leads to a notable augmentation of HSV-1 propagation, evident through increased expression of virally encoded green fluorescent protein (GFP) across a variety of HSV-1 mutant strains (Figure 2.1A, S2.2 &3). This results in enhanced viral output, as well as significantly enhanced oncolytic effects within multiple human and murine cancer cell lines

(Figure 2.1 B, C, G). In addition to DMF, several FMAEs demonstrated a consistent effect on HSV.n212, resulting in an increase in both GFP expression and viral titers in 786-0 cells (Figure 2.3). Importantly, these outcomes align closely with our prior observations involving VSVΔ51 [45].

DMF exerts inhibitory effects on the cellular response to type I IFN by, in part, reducing IFN production through the modulation of NFκB [87]. Additionally, DMF hinders the activation of signal transducer and activator of transcription 1 (STAT1) following IFN stimulation. Indeed, as we observed in the context of oncolytic VSVΔ51, a significant decrease in the expression of interferon stimulating genes was observed following DMF treatment and HSV.n212 infection (Figure 2.4).

In this study, we also optimized an intratumoral HSV.n212 dosage regimen in a subcutaneous CT26.wt murine tumour model. We found that administration of three- and six-times HSV.n212 every other day similarly reduced tumour growth compared to lower frequency regimens (Figure S2.5). Consequently, we proceeded with the three-dose infection regimen.

Given the current practice of oral DMF delivery in MS patients, we investigated whether gavage DMF could match intratumoral injection, which was used in our previous study with VSVΔ51. While DMF administered by gavage led to a delay in tumour growth, intratumoral DMF delivery surpassed gavage in tumour management in combination with HSV.n212 (Figure S2.6). Several preclinical studies have used oral DMF as a monotherapy for cancer

with favourable findings [67,88]. However, these studies used frequent and lengthy dosing strategies, at lower concentrations, which may explain the difference in results.

We chose the CT26.wt model as a starting point to evaluate the combination of HSV-1 and DMF in this study owing to its relative resistance to OVs in vivo, and in vitro and ex vivo responsiveness to DMF with respect to enhancing OV spread. As predicted, the combination of DMF and HSV.n212 resulted in a significant delay in tumour growth, surpassing the effect of either monotherapy (Figure 2.5). While neither monotherapy led to long-term tumor control, the combination strategy demonstrated a 10% cure rate within the CT26.wt model, aligning with prior findings reported with oncolytic VSVΔ51 (cure rate of 20%) [45]. We also evaluated the combination therapy in a more aggressive 4T1 model. In this case, the combination therapy significantly extended survival and reduced tumour growth but did not lead to long term cures.

The compelling findings reported in our study of the combination of DMF with oncolytic HSV-1 in two different tumour murine models underscore the potential of this strategy as a therapeutic avenue.

While further dose optimization experiments will be required, the current study suggests that a combinatory approach involving the administration of DMF intratumorally ahead of HSV.n212 (5h apart), administered a total of three times every other day can be effective for tumor control. Nevertheless, it is apparent that additional efforts are required to enhance the effectiveness of this therapy. Thus, we examined the treatment's immunological effects in CT26.wt to determine if they were linked to tumour control. There was an increase in CD3

cell counts was found in response to the combined therapy (Figure 2.6A); however, there was no concurrent rise in the populations of CD4 and CD8 cells. This suggests an increase in double-negative T-cells, however further studies will be needed to determine whether these are beneficial or not to tumour control, as these have been reported to either play a pro or anti-tumor role depending on the context and tumor microenvironment [89]. The anti-inflammatory effects of DMF are well-known which might overall dampen lymphocyte responses despite greater infiltration of CD3+ cells [90]. While outside the scope of the current study, this suggests that a potential avenue for exploration entails the use of oncolytic HSV-1 candidates that have been genetically modified to express therapeutic genes capable of stimulating immunological responses. Based on our current findings, strategies that could capitalize on the infiltration of double-negative T-cells or conversely enhance CD4+/CD8+ recruitment to the tumor may be beneficial, as may be strategies to dampen the (Programmed cell death protein 1) PD-1-1/ Programmed cell death protein ligand 1 (PD-L1) axis.

Moreover, it is noteworthy that the CT26.wt model exhibits a notable expression of PD-L1 in CD45- populations (tumor cells) (Figure 2.6C). In this particular situation, it is plausible that the effectiveness of the combination approach could be enhanced by integrating an immune checkpoint inhibitor that specifically targets PD-L1, hence amplifying immune responses.

In short, this work shows that the clinically approved DMF increases HSV-1 propagation in several human and murine cancer cell lines. In the immune competent murine CT26.wt colon cancer and 4T1 breast cancer models, we showed that the DMF-HSV-1 combination therapy significantly reduced tumour growth more than respective monotherapies. Altogether, our findings suggest that combination approaches using DMF and engineered HSV-1 that can maximize anti-tumor immune response warrant further testing.

2.5 Materials and methods

Cell lines

OHRI-MEL-13 (primary human melanoma cells) was obtained as a generous gift from Dr. Carolina Ilkow of the Ottawa Hospital Research Institute (Ottawa, Canada) [91].

All other cell lines used in this study including 786-0 (human renal cell adenocarcinoma), HT29 (human colon carcinoma), 4T1 (mouse breast carcinoma), CT26.wt (mouse colon carcinoma), S-180 (mouse sarcoma), CT2A (mouse glioma), Vero (African Green Monkey Kidney, CCL81). Cells were obtained from the American Type Culture Collection (ATCC) and maintained in Dulbecco's modified Eagle's medium (DMEM, HyClone, Waltham, Massachusetts, or Corning, Manassas, Virginia), supplemented with 1% penicillin-streptomycin (Gibco) and 10% fetal bovine serum (FBS; VWR, Mississauga, Ontario).

All cells were incubated at 37 °C in a 5% CO2 humidified incubator and routinely tested for mycoplasma contamination by Hoechst staining and PCR (Diamed, Mississauga, Ontario, Catalog # ABMG238).

Viruses, purification, and quantification

ICP0-Null HSV including (HSV.n212) expressing GFP and (HSV.d810) expressing GFP was obtained as a generous gift from Dr. Karen Mossman of McMaster University (Hamilton, Canada). HSV titers were determined by a standard plaque assay on Vero cells according to a previously published protocol (14). Herpes simplex virus gamma 47 delta (HSV-G47Δ) has deletions in the g34.5 and a47 genes, and the inactivating insertion of LacZ into ICP6 was obtained as a generous gift from Dr. Samuel Rabkin of Harvard University. HSV titers were determined by a standard plaque assay on Vero cells according to a previously published protocol [92]. The oncolytic HSV.n212 and HSVG47Δ were grown and tittered on Vero cells.

Briefly, HSV was added at multiplicity of infection (MOI) of 0.05 to 95% confluent Vero cells in roller bottles in a total volume of 25 ml of complete DMEM. Infected Vero cells were incubated at 37 °C with 5% CO2 for 48-72 h or when reach ~90% CPE (cell syncytia) was observed. Supernatants and cells were collected. Supernatants were pelleted at 25,000 RPM for 2 hours. Cells were frozen and thawed twice, then pelleted at 1200 RPM for 10 minutes to clear cell debris. The virus contained within the cleared supernatant was combined with the pellets of the first supernatant and purified using a 36% sucrose gradient.

Plaque assay

Vero cells were used to titer HSV infected samples. Briefly, all infectious samples were serially diluted then transferred into monolayer of Vero cells. After an incubation of 60 mins, an overlay of CMC: DMEM were added for 72 hours. For visualization of plaques, a 0.5 % Crystal Violet solution were added to the wells.

Viral growth curves

786-0 were cultured overnight to reach in a confluency next day. Subsequently, the cells were infected with HSV-1 at two different MOI: 0.01, utilized for multi-step growth curve analysis, and 1.0, for single-step growth curve analysis. MOI 1.0-infected cells underwent a 60-minute incubation, followed by a washing step and media replenishment. The cells were then maintained for up to 72 hours post-infection (hpi), with 200 µl of supernatant collected and stored at -80°C at specific time intervals: 0, 4, 8, 12, 24, 32, and 48 hpi. Viral titers in the collected samples were subsequently quantified using plaque assays, following established procedures [92].

Drugs

Dimethyl fumarate (DMF) (Sigma-Aldrich) was resuspended in 100% DMSO to 100mM and further diluted at indicated dilutions before use in all in-vitro experiments. For in-vivo experiments, DMF was dissolved in 100% DMSO or 0.8% methyl cellulose at 50mg/mL diluted at indicated dilutions before use.

Monomethyl fumarate (MMF), Diethyl fumarate (DEF), Dimethyl maleate (DMM), Diethyl maleate (DEM) and Fumaric acid (FA) were all obtained from (Sigma-Aldrich) and all resuspended in 100% DMSO to 100mM and further diluted at indicated dilutions before use in all in-vitro experiments.

Cell viability assay

The assessment of cellular metabolic activity was conducted through the use of Resazurin (metabolic dye) (Millipore Sigma, cat. SI03200) according to the manufacturer's protocol. 10% of resazurin were added to all samples for 1-2 hours, depending on the cell line. Using the BioTek Microplate Reader (BioTek, Winooski, VT, USA) and Gen5 2.07 software. Fluorescence was measured at 590 nm upon excitation at 530 nm. Readings were expressed relative to the average of the uninfected, mock treated condition.

IFN-β ELISA

786-0 cells were first treated with DMF at 150uM for a duration of 4 hours then infected with HSV at an MOI of 0.1. The 786-0 cell supernatant, obtained 24 hours post-infection following treatment and infection, underwent assessment for the concentration of human IFN-β. This quantification was conducted using the Human IFN Beta ELISA Kit (PBL Assay Science, cat. 41410), adhering to the guidelines provided by the manufacturer. Absorbance readings were taken using BioTek Cytation C10 Confocal Imaging Reader.

Quantitative real-time PCR.

786-0 cells were first treated and then infected as described. After 24 hours, the RNA from the lysed cells was homogenized with the QIAshredder (Qiagen, cat. 79656) and extracted with the QIAGEN Rneasy kit (Qiagen, cat. 74106) following the manufacturer's protocol. The RNA was quantified using a NanoDropTM One Microvolume UV-Vis Spectrophotometer (Thermo Fisher Scientific, Rockford, IL). RevertAid First Strand cDNA Synthesis Kit was used to convert 1 ug of RNA to cDNA. The real-time PCRs were carried out on a 7500 Fast Real-Time PCR system (Applied Biosystems) using the Applied Biosystems PowerUp SYBR Green Master Mix (ThermoFisher Scientific) following the manufacturer's protocol. The Pfaffl method was used to calculate gene expression.

In vivo mouse tumor models

All experiments were conducted following the University of Ottawa Animal Care and Veterinary Service guidelines for animal care under protocols OHRI-2264 and OHRI-2265.

Dose escalation study.

BALB/c mice that were 6 weeks old and obtained from Charles River Laboratories were implanted subcutaneously with syngeneic CT26.wt colon carcinoma cells in the right flank using 100μL PBS. Once the tumours reached a volume of approximately 100 mm^3 after 11 days, the mice received injections of HSV (1×10^8 pfu) directly intratumorally, either once, twice, thrice, or six times. Tumor size was monitored every other day using an electronic caliper, and their volumes were calculated using the formula $(\text{length} \times \text{width}^2)/2$. The mice were euthanized when tumour volumes exceeded 1500 mm^3.

Route of administration study

BALB/c mice that were 6-8 weeks old and obtained from Charles River Laboratories were implanted subcutaneously with syngeneic CT26.wt colon carcinoma cells in the right flank using 100µL PBS. Once the tumors reached a volume of approximately 100mm^3 after 11 days, mice were injected either intratumorally or given DMF by oral gavage (200mg/kg). Five hours later, a bolus of 25µL PBS containing 1 x 10^8 pfu of HSV.n212 was injected intratumorally. This treatment was repeated two more times, with a one-day interval between each treatment.

CT26.wt Model

BALB/c mice that were 6-8 weeks old and obtained from Charles River Laboratories were implanted subcutaneously with syngeneic CT26.wt colon carcinoma cells in the right flank using 100µL PBS. Once the tumours reached a volume of approximately 100mm^3 after 11 days, mice were injected intratumorally with either DMF (200mg/kg) or vehicle alone. Five hours later, a bolus of 25µL PBS containing 1 x 10^8 pfu of HSV.n212, or PBS alone, was injected intratumorally. This treatment was repeated two more times, with a one-day interval between each treatment.

4T1 Model

BALB/c mice that were 6 weeks old and obtained from Charles River Laboratories were implanted subcutaneously with 5 x 10^5 4T1 syngeneic 4T1 mammary carcinoma cells in 100µL PBS in their right flanks. After 9 days, when the tumor volumes reached about 100mm3, DMF (200mg/kg) or vehicle alone was injected intratumorally. Five hours later, a bolus of 25µL PBS containing 1 x 10^8 pfu of HSV.n212, or PBS alone, was injected intratumorally. This treatment was repeated two more times, one day apart.

Mice were randomized to different treatment groups based on tumor size prior to the first treatment. For survival studies, mice were end pointed when tumor volumes exceeded 1500mm^3 or when they showed significant respiratory distress from lung metastases.

Human and Murine Ex Vivo Tumor Models

To initiate the study, BALB/c mice were implanted with 3 x 10^5 CT26.wt colon carcinoma cells subcutaneously. Once tumor volumes reached 1500 mm^3, the mice were euthanized, and relevant tissues were extracted. For human tissue samples, tumor samples were collected from patients who had given informed consent and followed the Declaration of Helsinki guidelines during surgical resection. Collection of human tissue/fluid for this study was made possible by the Global Tissue Consent and Collection Program at the Ottawa Hospital Research Institute. The tissue collection program was approved by OHSN-REB under the protocol OHSN REB 20180079-01H. All tissues were processed fresh; sliced into 2mm sections and circular cores of 2mm diameter were extracted using a punch biopsy tool. These cores were then kept in a humidified incubator at 37°C and 5% CO2 in DMEM supplemented with 10% serum, 30mM HEPES, 1% (v/v) penicillin-streptomycin and 0.25 mg/L amphotericin B. The cores were treated with DMF for four hours and then infected with HSV.n212 at 3 x 10^4 pfu/core. After 72 hours post-infection, fluorescence images were captured using the EVOS Live Cell Imaging System (Thermo Fisher) and cores were homogenized with a TissueLyser II (Qiagen) prior to titering.

Immune profiling

Tissue processing

The tumours were dissociated utilizing the Miltenyi mouse tumour dissociation kit (Miltenyi Biotec, CA, USA, Cat. # 130-096-730) in conjunction with the gentleMACS Octo Dissociator

(Miltenyi Biotec, Cat. # 130-096427). The spleens and tumor-draining lymph node (TdLN) (ipsilateral axillary, inguinal, cervical) were obtained and subjected to dissociation by mechanically crushing the organs through a 70 µm strainer, utilizing the plunger of a 3 mL syringe. The erythrocyte lysis of all dissociated spleens was performed using ACK buffer (Gibco, Cat. # A1049201). The cell suspensions were counted, and a total of 2 x 10^6 cells were reconstituted in 200 µl of FACS buffer (0.5% BSA-PBS) before being transferred to round-bottom 96-well plates for the purpose of staining.

Flow cytometry

Following the aforementioned tissue processing protocol, the cells were exposed to staining using the fixable viability dye FVS510 (BD Biosciences, NJ, USA, Cat. #564406) at a dilution of 1:1000 in phosphate-buffered saline (PBS) for a duration of 30 minutes at the room temperature. The cells underwent a washing process and were subsequently subjected to incubation with anti-CD16/32 (1:100, BD Biosciences, Cat. # 553141) in a solution of 0.5% BSA-PBS for a duration of 30 minutes at a temperature of 40°C. This step was performed in order to prevent non-specific antibody binding to Fc receptors. The cells were subsequently subjected to staining using a specific subset of antibodies against the following targets: CD45-BV786 (1:1000, BD Biosciences, Cat. # 564225), CD3-AlexaFluor 700 (1:100, BD Biosciences, Cat. # 561805), CD4-V450 (1:1000, BD Biosciences, Cat. # 560468), CD8aPE-CF594 (1:100, BD Biosciences, Cat. # 562283), CD25-PE (1:100, Thermo Scientific, Cat. # 12-0251-82), CD69-BV605 (1:100, BD Biosciences, Cat. #563290), CD44-APC (1:100, BD Biosciences, Cat. #563058), CD62L-FITC (1:100, BD Biosciences, Cat. #553150), PD1-APC (1:100, BD Biosciences, Cat. # 562671), CD127-PE-Cy7 (1:100, BD Biosciences, Cat. # 560733), CD49b-BUV395 (1:100, BD Biosciences, Cat. # 553857), CD11b-APC-Cy7 (1:200,

BD Biosciences, Cat. #553312), CD11c-PE (1:100, BD Biosciences, 553802), CD86-APC-R700 (1:100, BD Biosciences, Cat. # 565479), IA/IE-BV605 (1:200, BD Biosciences, Cat. # 563413), CD19 (1:100, BD Biosciences, Cat. # 553785), F4/80-BUV605 (1:100, BioLegend, CA, USA, Cat. #123118). The PD-L1-APC-Cy7 antibody (BioLegend, Cat. # 124313) was used at a dilution of 1:100. The cells were subsequently rinsed and reconstituted in a solution containing 1% paraformaldehyde (PFA) in phosphate-buffered saline (PBS). The acquisition of samples was conducted using the BD LSRFortessa™ instrument in the Flow Cytometry and Cell Sorting core facility of the Ottawa Hospital Research Institute. The data underwent analysis using FlowJo v10.8 software. Unstained controls and fluorescence-minus-one (FMO) controls were made concurrently. Compensation was performed using Ultracomp eBeads (Thermo Scientific, Cat. # 01-2222-42), which are single-stained beads were used for compensation.

Statistics

GraphPad Prism were used in all graphs and statistical tests. Individual statistical tests were detailed in figure legends. Two-tailed unpaired Student's t-test was used when means of two groups were compared. One-way ANOVA with Dunnett's or Tukey's multiple correction test were used when means of more than two groups were compared. Analysis of in vivo survival data was performed by the Kaplan-Meier method followed by log-rank test. Biological replicates are indicated by a number n, and error calculated as the standard error of the mean (SEM) For all analyses, *$p < 0.05$, **$p < 0.01$, ***$p < 0.001$, ****$p < 0.0001$; n.s. = not significant.

Chapter 3: Tepilamide Fumarate as a Novel Potentiator of Virus-Based Therapy

Akram Alwithenani[1, 2, 3], Rozanne Arulanandam[1], Boaz Wong[1, 2], Marcus M. Spinelli[1], Victoria H. Gilchrist[1,4], Tommy Alain[1,4], Jean-Simon Diallo[1,2]

[1]Centre for Cancer Therapeutics, Ottawa Hospital Research Institute, Ottawa, Ontario, K1H 8L6, Canada.

[2]Department of Biochemistry, Microbiology, and Immunology, Faculty of Medicine, University of Ottawa, Ontario, K1H 8M5, Canada

[3]Department of Clinical Laboratory Science, Faculty of Applied Medical Science, Umm Al-Qura University, Makkah, Saudi Arabia

[4]Children's Hospital of Eastern Ontario Research Institute, Apoptosis Research Center, Ottawa, ON, Canada

Key words: Cancer therapeutics, Tepilamide fumarate, VSVΔ51, Viral vectors, Gene therapy

This chapter is published in Viruses in June 2024

3.1. Abstract

Oncolytic virotherapy, using viruses such as vesicular stomatitis virus (VSVΔ51) and Herpes Simplex Virus-1 (HSV-1) to selectively attack cancer cells, faces challenges such as cellular resistance mediated by the interferon (IFN) response. Dimethyl Fumarate (DMF) is used in the treatment of multiple sclerosis and psoriasis and is recognized for its anti-cancer properties and has been shown to enhance both VSVΔ51 and HSV-1 oncolytic activity. Tepilamide Fumarate (TPF) is a DMF analog currently undergoing clinical trials for the treatment of moderate-to-severe plaque psoriasis. The aim of this study was to evaluate the potential of TPF in enhancing the effectiveness of oncolytic viruses. In vitro, TPF treatment rendered 786-0 carcinoma cells more susceptible to VSVΔ51 infection, leading to increased viral replication. It outperformed DMF in both increasing viral infection and increasing killing of these resistant cancer cells and other cancer cell lines tested. Ex vivo studies demonstrated TPF's selective boosting of oncolytic virus infection in cancer cells without affecting healthy tissues. Effectiveness was notably high in pancreatic and ovarian tumor samples. Our study further indicates that TPF can downregulate the IFN pathway, through a similar mechanism to DMF, making resistant cancer cells more vulnerable to viral infection. Furthermore, TPF's impact on gene therapy was assessed, revealing its ability to enhance the transduction efficiency of vectors such as lentivirus, adenovirus type 5, and adeno-associated virus type 2 across various cell lines. This data underscore TPF's potential role in not only oncolytic virotherapy but also in the broader application of gene therapy. Collectively, these findings position TPF as a promising agent in oncolytic virotherapy, warranting further exploration for its therapeutic potential.

3.2. Introduction

Oncolytic viruses (OVs) are specialized therapeutic agents designed to selectively infect and destroy cancer cells, leaving healthy tissues unharmed [36,93]. These agents, through their multifaceted therapeutic mechanisms, not only directly induce lysis of malignant cells but also potentiate antitumor immune responses and target the tumor vasculature [94], thereby comprehensively impeding tumor progression. A notable example is Talimogene laherparepvec (T-VEC), a Herpes Simplex Virus (HSV-1) -based oncolytic virus, which garnered FDA approval in 2015 for treating melanoma [26,27]. Other HSV-1 based oncolytic viruses like G47Δ are showing promise in clinical trials. In glioblastoma patients, G47Δ demonstrated safety and a notable 1-year survival rate of 84.2% in a phase 2 trial [25]. These results have led to its conditional and time-limited approval in Japan for glioma treatment, pending further studies.

Oncolytic virotherapy, while promising, encounters significant hurdles, particularly the resistance of cancer cells to viral infection, among other challenges. This resistance is frequently attributed to the host immune response and in part type I interferon (IFN) signaling [95]. Typically, cancer cells show a lack of interferon (IFN) reactivity as part of their neoplastic evolution; however IFN signaling signatures can be observed in some tumor types and may be linked to OV resistance [79,96]. The IFN pathway which is induced among others by viral infection can activate a series of antiviral genes that effectively suppress viral replication. This innate immune mechanism, designed to protect cells from viruses, poses a challenge in oncolytic virotherapy, as it can significantly reduce the ability of therapeutic viruses to infect and destroy cancer cells. Overcoming this resistance is one key focus in the

development of more effective oncolytic viral therapies. To tackle the challenge of cancer cell resistance in oncolytic virotherapy, our team and others have tested the strategic use of selected pharmacological agents in conjunction with OVs. These strategies mostly aim to temporarily dampen the cancer cells' IFN-related antiviral defenses, enhancing effectiveness of oncolytic virotherapy. Multiple small molecules have been identified through high-throughput screening and rational approaches [38,44,73,80,97]. Many of these molecules target the IFN pathway and its downstream regulated genes, leading to increased viral titers and enhanced effectiveness in killing tumor cells. One notable example is Dimethyl Fumarate (DMF), an FDA-approved drug for multiple sclerosis, which has shown significant potential in enhancing the activity of Vesicular Stomatitis Virus (VSVΔ51) and various oncolytic HSV-1 strains in different cancer cell lines and mouse models[45]. Its effectiveness largely stems from its ability to inhibit the IFN type 1 pathway through preventing the nuclear translocation of NF-κB [38,46].

While DMF is an approved drug, it suffers from some known pharmacological limitations and side effects, which have led to the discovery and development of analogs with potentially more favorable pharmacokinetic and toxicological profiles. In this study, we focus on Tepilamide Fumarate (TPF), one such analog that is currently under investigation in late stage clinical trials for patients with psoriasis [71]. The unexplored potential of TPF in cancer treatment and in combination with OVs presents a significant opportunity to develop improved therapeutic regimens. Our study aimed to assess the anticancer potential of TPF, exploring its ability to enhance the ef-fectiveness of oncolytic viruses and other viral vectors.

3.3. Results

3.3.1. TPF Enhances Susceptibility of Cancer Cells to VSVΔ51 infection.

To delineate the virus-enhancing potential of TPF (Figure 3.1 A), we utilized human renal 786-0 carcinoma cells that are inherently resistant to VSVΔ51 infection as a model system. The 786-0 cells were subjected to pre-treatment with TPF at different concentrations for a duration of four hours. Subsequently, these cells were infected with VSVΔ51 that expresses GFP. Fluorescence microscopy pictures captured 24 h after infection, as depicted in (Figure 3.1 B), revealed that TPF pre-treatment increases VSVΔ51 infection in these cells compared to untreated, infected controls. Similar outcomes were noted when 786-0 cells were pre-treated with other drugs from the fumarate class, including DMF and the active metabolite of TPF and DMF, Monomethyl fumarate (MMF), as demonstrated in (Figure S3.1). A significant increase in viral titer with rising concentrations of TPF in the 786-0 cells was observed (Figure 3.1 C), suggesting a dose-dependent enhancement of viral growth upon treatment. Additionally, TPF was used to pre-treat other cancer cell lines, such as MC38, 4T1, and B16-OVA, and we observed a similar increase in GFP transgene expression following VSVΔ51 infection, as demonstrated in (Figure S3.2). Quantitative PCR analysis confirmed that the expression levels of the VSV M and N genes were significantly increased in the RNA samples. This supports the presence of greater viral loads in cells exposed to TPF compared to the cells that were not treated as shown in (Figure 3.1 D). In addition, we assessed the enhancing impact of TPF on VSVΔ51 infectivity by comparing multi-step and single-step growth curves. Consistent with our previous findings with DMF[45], TPF significantly increased the infectivity of VSVΔ51 at a low MOI of 0.01, compared to a high MOI of 1. This was determined using a high-throughput titration titer quantification method, as shown in (Figure

3.1 E&F). These findings suggest that TPF enhances viral spread, contributing to augmented growth without necessarily affecting the VSVΔ51 replication rate. The spread of the virus was also evaluated using a plaque assay designed to measure plaque size, revealing that TPF significantly increased the area of viral plaques within a monolayer of the 786-0 cells, as determined by Coomassie blue staining as shown in (Figure 3.1 G).

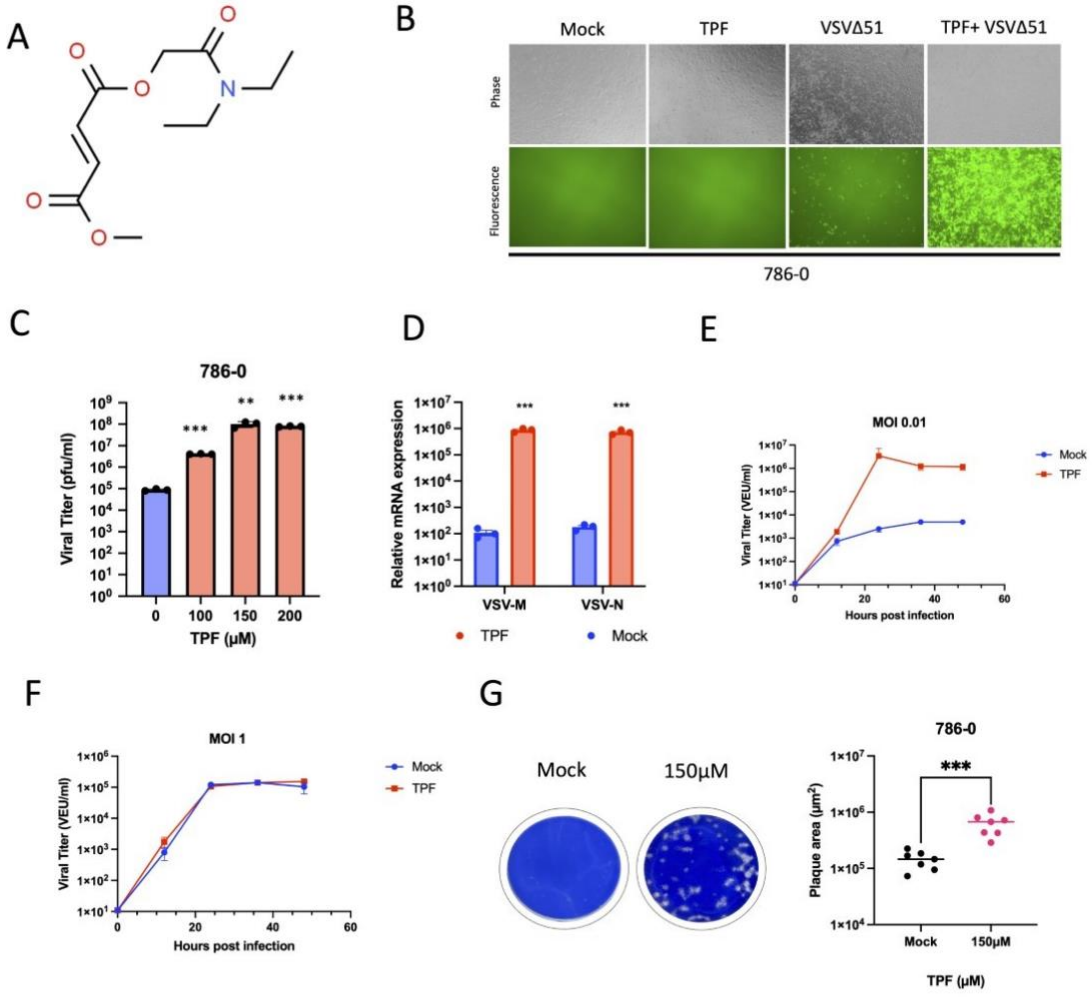
A
B
Mock
TPF
VSVΔ51
TPF+ VSVΔ51
Phase
Fluorescence
786-0
C
786-0
Viral Titer (pfu/ml)
TPF (μM)
D
Relative mRNA expression
VSV-M
VSV-N
TPF
Mock
E
MOI 0.01
Viral Titer (VEU/ml)
Hours post infection
Mock
TPF
F
MOI 1
Viral Titer (VEU/ml)
Hours post infection
Mock
TPF
G
Mock
150μM
786-0
Plaque area (μm²)
Mock
150μM
TPF (μM)

Figure 3.1: Tepilamide Fumarate demonstrates remarkable viral sensitizing capabilities.

(A) The structure of Tepilamide fumarate (TPF). 786-0 cells were pretreated with different doses (0, 100, 150, and 200 μM) of TPF for four hours and then infected with VSVΔ51 expressing GFP (MOI 0.05). (B) GFP images were captured 24 hours post-infection. (C) Samples were quantified for viral titer by standard plaque assay (N=3, mean ± SEM; **P<0.01 ***P<0.001; one-way ANOVA with Dunnett's multiple comparisons test compared to Mock). (D) VSV-M and VSV-N mRNA were quantified by RT-qPCR (n=3, mean ± SD; ***P<0.001 by two-tailed t-test). Multistep (MOI 0.01) and single-step (MOI 1) growth curves were generated. (E & F) 786-0 cells were pretreated with TPF and infected with VSVΔ51 at an MOI of 0.01 or 1, and samples were quantified for viral titer by high throughput method (n=3; mean ± SD; *P<0.05, ***P<0.001; two-tailed t-test). (G) 786-0 cells underwent treatment with TPF at a concentration of 150 μM, followed by infection with VSVΔ51 at an MOI of 0.01. After an incubation period of 1 hour, the cells were overlaid with agarose. At 48 hours post-infection, Coomassie blue staining was performed. The area of randomly selected plaques was then measured (n = 7; mean ± SD), and a two-tailed t-test revealed a highly significant difference (***p < 0.001).

3.3.2. TPF enhances VSVΔ51 and HSV-1 infection in cancer cells compared to DMF.

Given the enhancement of oncolytic activity observed with TPF in conjunction with VSVΔ51 and considering previous studies demonstrating DMF's ability to potentiate VSVΔ51 efficacy[45], our study aimed to conduct a direct comparison between DMF and TPF to determine if one drug exhibits superior effectiveness in vitro. 786-0 cells were pre-treated with TPF or DMF for four hours prior to infection with VSVΔ51-GFP at MOI of 0.05. Subsequent to a 24 h infection period, fluorescence imaging was performed, and GFP expression was quantified as illustrated in (Figure 3.2A). The acquired images and corresponding GFP quantification indicate that both TPF and DMF, at 100 and 150 μM, significantly increase VSVΔ51-GFP associated GFP expression, suggesting an augmentation in viral infectivity in response to compound administration.

Further analysis aimed to evaluate the impact of TPF and DMF on VSVΔ51-mediated oncolysis. Cell viability was measured using the metabolic indicator alamarBlue at 48 h post-treatment, with and without the addition of VSVΔ51 to the TPF or DMF treatment regimens. The results, as depicted in (Figure 3.2C), demonstrate a marked decline in cell viability following the combination therapy, underscoring the compounds' potential to compromise the viability of the VSV-resistant 786-0 cancer cell line. A side-by-side comparison of the TPF-VSVΔ51 and DMF-VSVΔ51 combinations, detailed in (Figure 3.2C), reveals a superior reduction in cell viability by the TPF-VSVΔ51 regimen, particularly at 100μM, suggesting that TPF may exert a more pronounced and potent oncolytic effect in the presence of VSVΔ51 than DMF.

This pattern of reduced cell viability by the TPF-VSVΔ51 combination over the DMF-VSVΔ51 combination was also observed in another cell line, the CT26.wt mouse colon

carcinoma cell line, as shown in (Figure 3.2D–F). These results further support that the TPF-VSVΔ51 combination further improves cancer cell elimination in comparison to the DMF-VSVΔ51 combination.

Resulting viral titers were also quantified, as shown in (Figure 3.2G,H), and revealed a significant increase in viral titers in both 786-0 and CT26.wt cells treated with either the TPF or DMF combination treatments. A slightly greater but statistically significant enhancement in impact on virus titers was observed with TPF-VSVΔ51 compared to DMF- VSVΔ51. To evaluate the effects of TPF in the context of another OV class, HSV.n212 was tested in combination with either TPF or DMF in the 786-0 cells. The results indicate once again a slight superiority of TPF over DMF in enhancing the growth of HSV.n212, as shown in (Figure 3.2I). The data across these figures demonstrate that TPF, especially in combination with VSVΔ51, has a potent ability to augment cancer cell infection and killing across diverse cellular models.

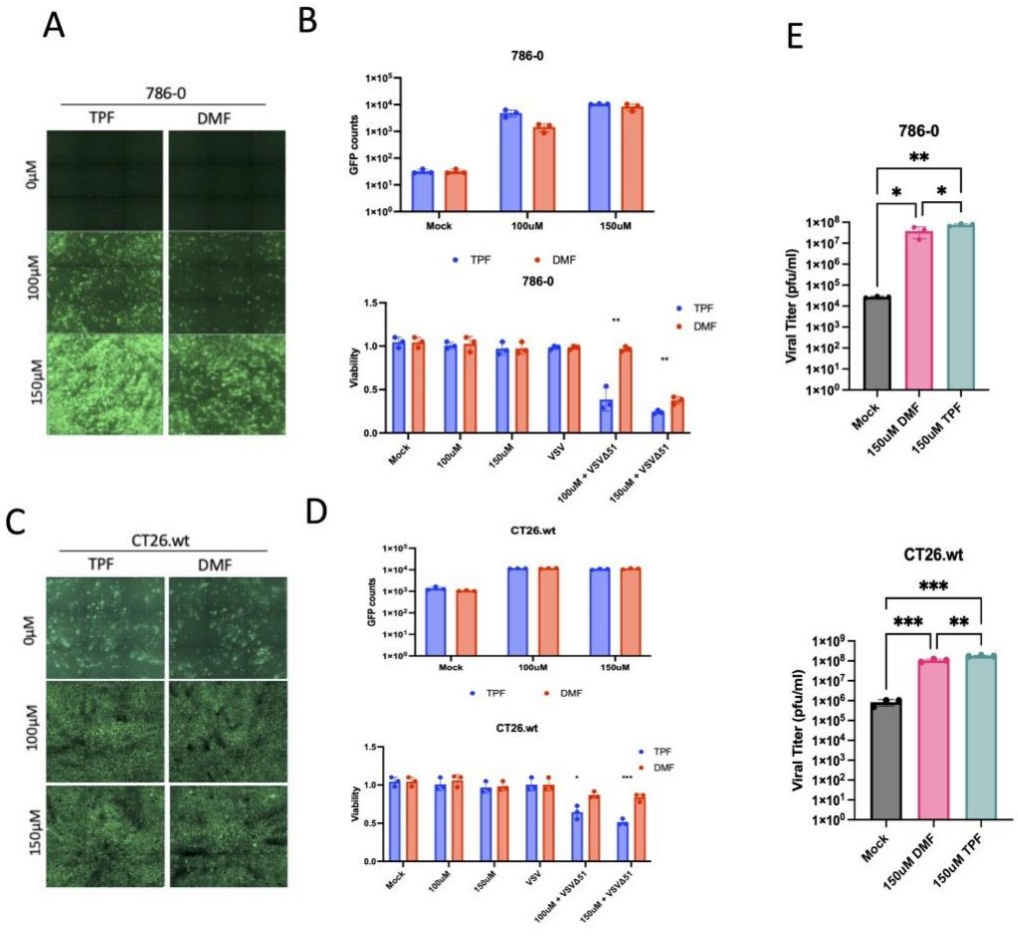
A
786-0
TPF
DMF
0μM
100μM
150μM
B
786-0
GFP counts
Mock
100uM
150uM
TPF
DMF
786-0
Viability
VSV
100uM + VSVΔ51
150uM + VSVΔ51
E
786-0
Viral Titer (pfu/ml)
Mock
150uM DMF
150uM TPF
C
CT26.wt
D
CT26.wt
CT26.wt

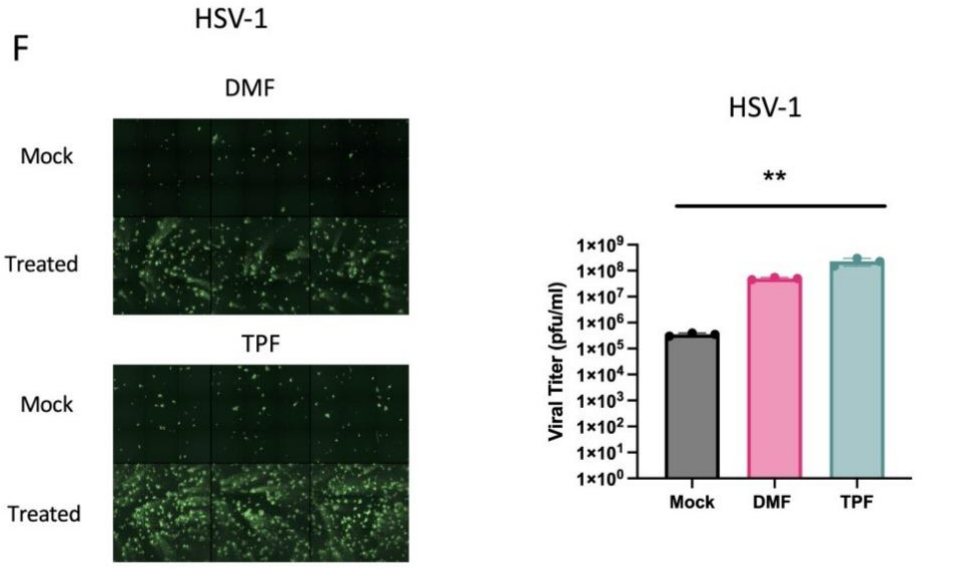
HSV-1
F
DMF
Mock
Treated
TPF
Mock
Treated
HSV-1
**
Viral Titer (pfu/ml)
Mock
DMF
TPF

Figure 3.2: TPF demonstrates a superior effect in enhancing OV infection within cancer cells.

(A & C) 786-0 and CT26.wt cells were first pretreated with TPF and DMF (100μM and 150μM) for a duration of 4 hours then infected with VSVΔ51 at MOI (0.05). 24-hour post infection GFP counts were counted (N=3, mean ± SEM; ***P<0.001; ****P<0.0001; unpaired t test). (B & D) Metabolic viability assay was assessed using Resazurin dye (N=3, mean ± SEM; *P<0.05**, P<0.01, ***P<0.001, ****P<0.0001; unpaired t test. (E) Samples were quantified for viral titer by standard plaque assay (N=3, mean ± SEM; **P<0.01 ***P<0.001; one-way ANOVA with Tukey's multiple comparisons test). (F) 786-0 cells were treated with either TPF or DMF concentration OF 150μM then infected with HSV.n212 expressing GFP (MOI 0.02). Corresponding fluorescent images were taken 48 hours post infection. Supernatants were collected at 72 hours post infection for viral titer quantification by plaque assay (mean ± SD; **P<0.01 by one-way ANOVA).

3.3.1 TPF potentiates Infectivity of VSVΔ51 in Human and Murine Tumor Explants

We next aimed to evaluate the impact of TPF in ex vivo tissues to assess its potential in a more physiologically relevant setting and to assess its tumor selectivity, a feature that has been previously established for DMF [45]. . Briefly, CT26.wt murine colon cancer cells were implanted subcutaneously in mice, and once the tumors had grown to approximately 1500 mm3 these were harvested and cored for in vitro culture using uniform slices from a biopsy punch (Figure 3.3A)[98]. Samples from normal tissues including brain, spleen, and lung, were also similarly harvested. All the cancer and normal tissue samples in culture were then exposed to VSVΔ51, with and without the pre-addition of TPF at a concentration of 150 μM. The resulting fluorescence images and viral titer data in (Figure 3.3B,C) reveal a marked increase in VSVΔ51 infectivity in CT26.wt tumor cores following TPF pre-treatment. Conversely, normal brain and other tissues did not exhibit increased VSVΔ51 levels, demonstrating that the virus's tumor-specific selectivity is preserved despite TPF pre-treatment. Analogous human cancer explant experiments were subsequently performed; wherein consenting patient tumor specimens were obtained from the clinic freshly and were similarly processed. A regimen of TPF pre-treatment followed by VSVΔ51 infection was administered across multiple tumor types, including pancreatic, lung, ovarian, and colon tumors. The results detailed in (Figure 3.3D,E); Table S3.1 indicate a marked variation in TPF's efficacy to potentiate viral infectivity. Notably, one pancreatic tumor explant demonstrated the most substantial response with a fifteen-fold increase in VSVΔ51 output post-TPF pre-treatment. An ovarian tumor also responded substantially, showing a ten-fold enhancement in viral

replication. These findings collectively indicate that TPF selectively enhances the infectivity of VSVΔ51 but with some variation across human and murine tumor explants.

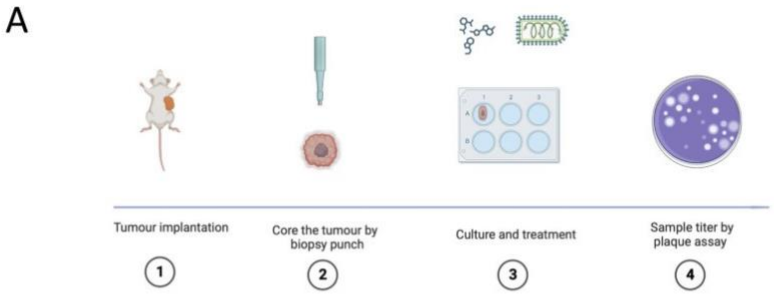
A
Tumour implantation
1
Core the tumour by biopsy punch
2
Culture and treatment
3
Sample titer by plaque assay
4

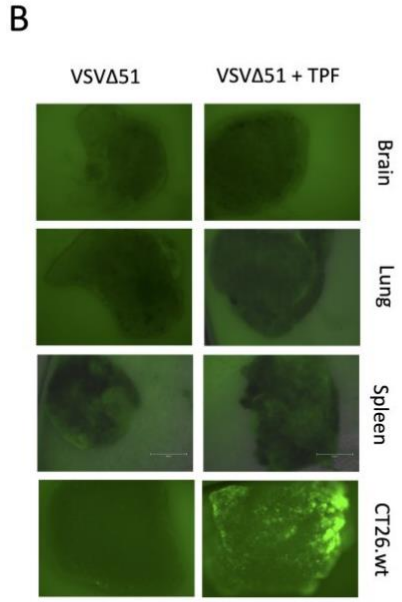
B
VSVΔ51
VSVΔ51 + TPF
Brain
Lung
Spleen
CT26.wt

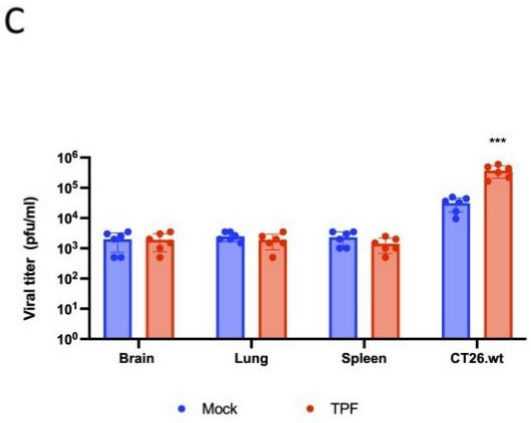
C
Viral titer (pfu/ml)
Brain
Lung
Spleen
CT26.wt
***
Mock
TPF

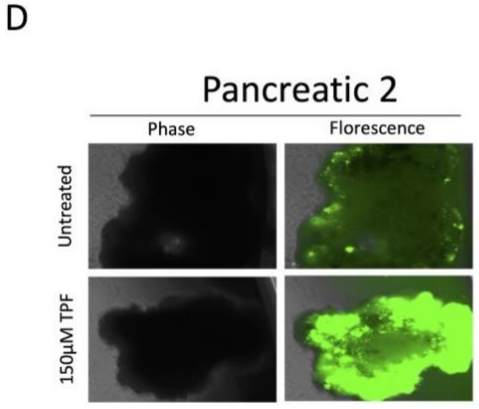
D
Pancreatic 2
Phase
Florescence
Untreated
150μM TPF

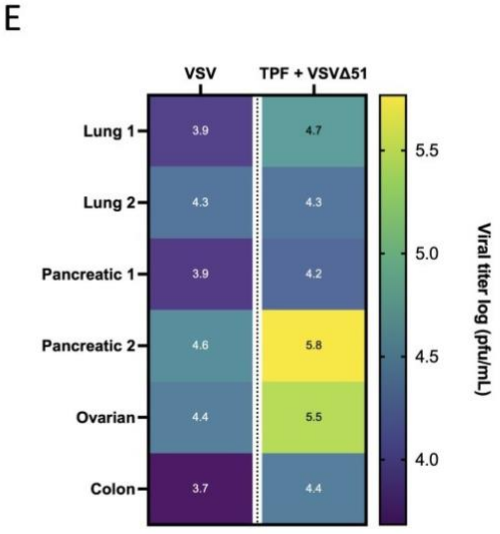
E
VSV
TPF + VSVΔ51
Lung 1
Lung 2
Pancreatic 1
Pancreatic 2
Ovarian
Colon
3.9
4.7
4.3
4.3
3.9
4.2
4.6
5.8
4.4
5.5
3.7
4.4
Viral titer log (pfu/mL)
5.5
5.0
4.5
4.0

Figure 3.3: Tepilamide Fumarate promotes VSVΔ51 infection in ex vivo models.

(A) The schematic diagram illustrates the methodology of the coring experiment. CT26.wt colon tumors were grown in BALB/c mice, once reaching a volume of 1500mm^3. Tissues were collected, cored. Clinical specimens were obtained and cored. Cores were treated with TPF then infected with VSVΔ51 $3x10^4$ (pfu/core). (B & D) Fluorescent images were taken 24h post infection, and (C & E) supernatants were collected at 24 hpi for viral titer quantification by plaque assay ($n>5$, mean ± SD; ***$P<0.001$ by two-tailed t-test).

3.3.4. TPF inhibits the type-I IFN response and NF-κB to Amplify VSVΔ51 Oncolytic Potency

3.3.5. Given the established capacity of DMF to downregulate the interferon (IFN) pathway and interferon-stimulated genes [45], we endeavored to investigate whether TPF exerts comparable modulatory effects on these critical components of the antiviral response.

Utilizing quantitative PCR (qPCR), we measured the transcription levels of key antiviral and pro-inflammatory genes—specifically IFN-β, MX2, IFITM1, IL6, and CCL5—in the 786-0 cells subjected to TPF (150 μM) treatment or vehicle. Following a four-hour incubation, these cells were either infected with VSVΔ51 or left uninfected. Our findings demonstrate that the TPF treatment leads to downregulation of the above antiviral and pro-inflammatory genes as shown in (Figure 3.4A). In addition to qPCR analyses, an enzyme-linked immunosorbent assay (ELISA) was conducted to quantify IFN-β in the supernatant of cell cultures. The results corroborated the qPCR findings, with TPF demonstrating a consistent downregulation of IFN-β secretion as shown in (Figure 3.4B). This further confirms that TPF modulates the antiviral response in 786-0 cells, enhancing their susceptibility to VSVΔ51 infection and underscoring the potential of TPF as a facilitator in oncolytic virus therapy. In line with the suppression of the type I interferon response, TPF treatment led to a reduction in the activation (indicated by phosphorylation) of both STAT1 (signal transducer and activator of transcription 1) and STAT2, observed 24 h post-infection (Figure S3.3). Building on previous studies demonstrating that DMF inhibits the nuclear translocation of the p65 subunit of NF-κB[45], we aimed to evaluate whether TPF exhibits a similar inhibitory effect. Indeed, immunofluorescence staining (Figure 3.4C,D) shows a suppression of TNF-α-stimulated NF-

κB nuclear translocation (p65) in the cells pre-treated with TPF, suggesting that TPF, like DMF, may impede NF-κB signaling in the context of inflammatory stimulation. However, we did note that TPF on its own did lead to elevated NF- κB nuclear translocation, something that has not been previously observed with DMF[45].

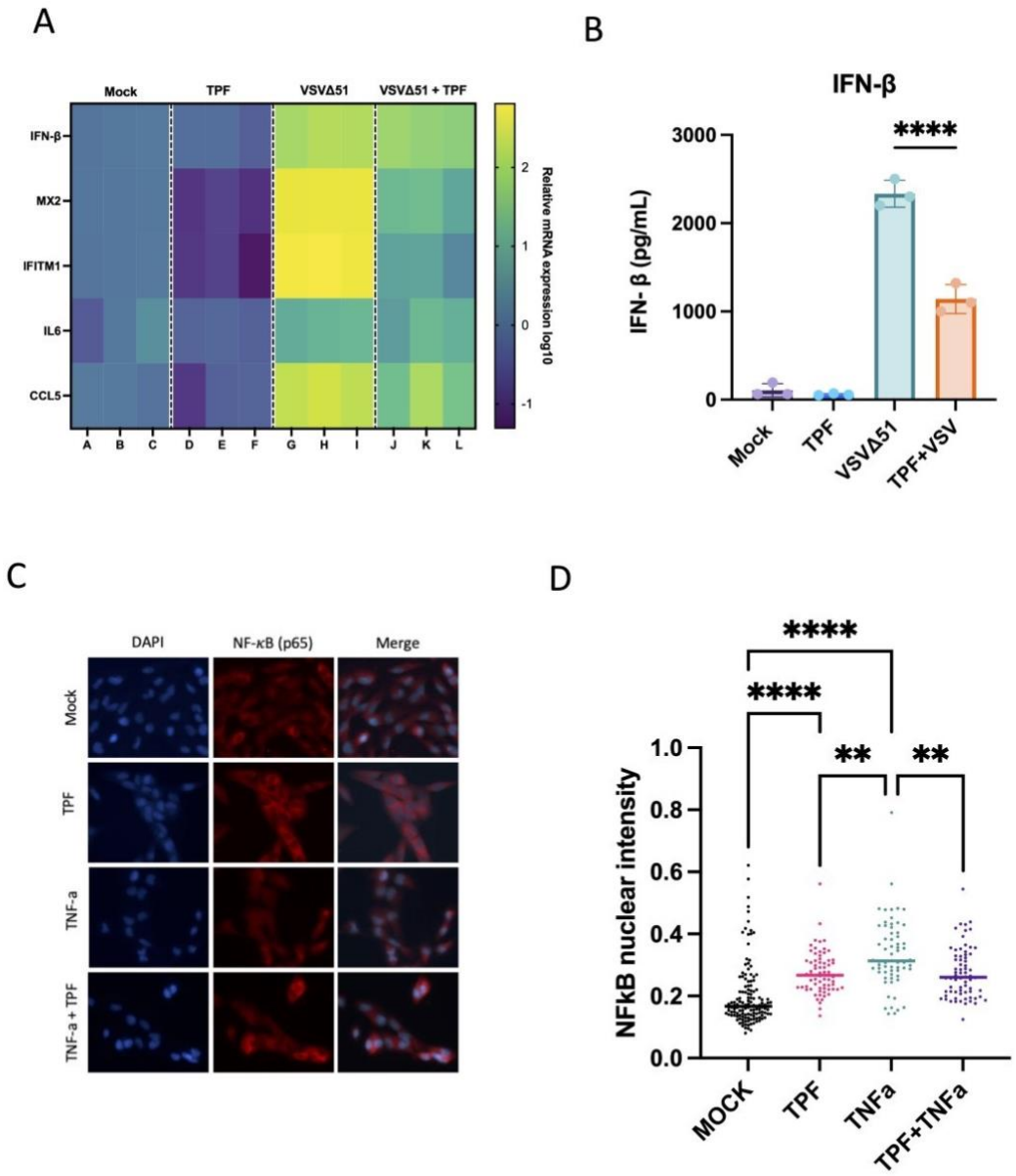
A
Mock
TPF
VSVΔ51
VSVΔ51 + TPF
IFN-β
MX2
IFITM1
IL6
CCL5
A B C D E F G H I J K L
Relative mRNA expression log10
2
1
0
-1
B
IFN-β
****
IFN- β (pg/mL)
3000
2000
1000
0
Mock
TPF
VSVΔ51
TPF+VSV
C
DAPI
NF-κB (p65)
Merge
Mock
TPF
TNF-a
TNF-a + TPF
D
****
****
**
**
NFkB nuclear intensity
1.0
0.8
0.6
0.4
0.2
0.0
MOCK
TPF
TNFa
TPF+TNFa

Figure 3.4: Tepilamide Fumarate promotes VSVΔ51 infection via type 1 IFN inhibition.

(A) 786-0 cells were pretreated for 4 hours with TPF (150μM) then infected with VSVΔ51 (MOI 0.05) 24-hour post infection RNA was extracted and mRNA for indicated genes were quantified by RT-qPCR. (B) Supernatants were taken 24hpi and assayed for IFN-β by ELISA. (N=3, mean ± SEM; ****P<0.0001; one-way ANOVA with Tukey's multiple comparisons test) 786-0 cells were pretreated for 4 hours with TPF (150μM) or TNFa (25ng/ml) for 30 minutes. Cells were fixed and immunostained for NF-κB and nuclei (DAPI). (C) Representative fluorescent images were taken. (D) Nuclear NF-κB intensity was quantified. (n = 3; mean ± SD; **p < 0.01, ****p < 0.0001 one-way ANOVA with Tukey's multiple comparisons test).

3.3.6. TPF Amplifies Transduction Efficiency Across Multiple Viral Vectors

Following the observed enhancement of oncolytic virus activity by TPF, we sought to examine the influence of TPF on other viral vectors, particularly non-replicating vectors used in gene therapy. This included lentivirus, adenovirus type 5 (Ad5), and adeno-associated virus type 2 (AAV2). The aim was to unravel TPF's potential in boosting the transduction efficiency of these vectors, potentially expanding the utility of TPF for other gene therapy techniques.

We initially evaluated the ability of TPF and DMF to enhance the transduction efficiency of lentivirus across a spectrum of cell lines, including MRC5, HT1080, HepG2, A549, and Jurkat. Following a 4 h pre-treatment with a broad, non-toxic dose range of each compound and the transduction of cells with a GFP-expressing lentivirus at MOI 10, our observations revealed that TPF, alongside DMF, exhibited a notable increase in the transduction of lentivirus in several cell lines. At peak dosing (after which cell toxicity was observed), TPF significantly increased lenti-GFP-associated fluorescence in HepG2 (100 and 67 µM), HT1080 (67 and 44 µM), A549 (100 µM), Jurkat (10–20 µM), while DMF's effect was only statistically significant in HT1080 (~50–120 µM), A549 (~100–150 µM) (Figure 3.5). Remarkably, in Jurkat cells, TPF significantly boosted lentivirus transduction by ~3-fold at a peak concentration of 14 µM, as depicted in (Figure 3.5), while DMF did not exhibit any notable effect under similar conditions.

We used the same cell lines to further assess the impact of TPF and DMF on the transduction efficiency of Ad5-GFP. Here, we observed that both TPF and DMF significantly increased Ad5-GFP transduction in several cell lines 70 h post transduction. TPF increased Ad5-GFP-associated fluorescence in MRC5 (peak ~ 30 µM), A549 (peak ~ 30 µM), HT1080 (peak ~ 50

μM), and HepG2 (peak ~ 50 μM). DMF also increased Ad5-GFP-associated fluorescence in MRC5 (peak ~ 100 μM), A549 (peak ~ 110 μM), HT1080 (peak ~ 100 μM), and HepG2 (peak > 250 μM). Altogether, we observed a significant difference in their peak effective concentrations, with TPF exhibiting better potency for this virus in all the cell lines where there was an increase in transduction observed as illustrated in (Figure 3.6). Lastly, we examined the effects of TPF and DMF on the transduction of AAV2-GFP in HT1080 and HepG2 cell lines. In both cell lines, but most prominently in HT1080 cells, TPF demonstrated a notable increase in AAV2-GFP transduction efficiency achieving >4-fold enhancement at peak concentration (between 22–44 μM, Figure 3.7). In both cell lines, DMF potency was reduced compared to TPF. Altogether, our results suggest that TPF has the potential to be useful more broadly as a potentiator of viral vector-based therapeutics, and demonstrates greater in vitro potency than DMF in enhancing infection, a trend observed across a diverse array of cell lines.

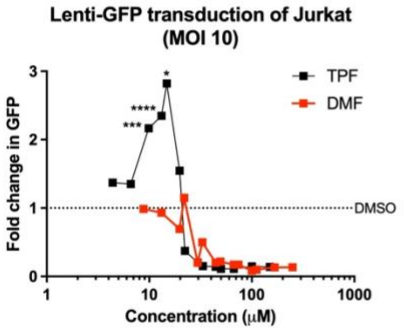
Lenti-GFP transduction of Jurkat
(MOI 10)
TPF
DMF
DMSO
Fold change in GFP
Concentration (μM)

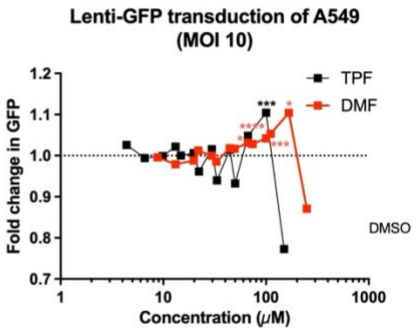
Lenti-GFP transduction of A549
(MOI 10)
TPF
DMF
DMSO
Fold change in GFP
Concentration (μM)

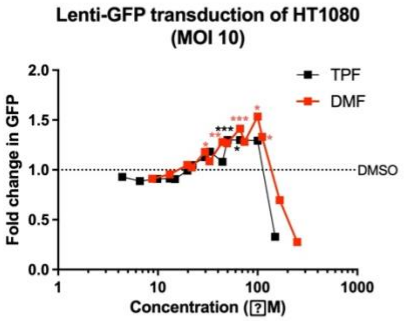
Lenti-GFP transduction of HT1080
(MOI 10)
TPF
DMF
DMSO
Fold change in GFP
Concentration (?M)

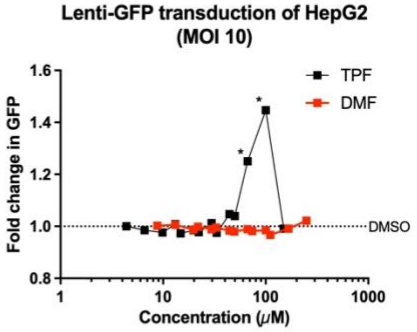
Lenti-GFP transduction of HepG2
(MOI 10)
TPF
DMF
DMSO
Fold change in GFP
Concentration (μM)

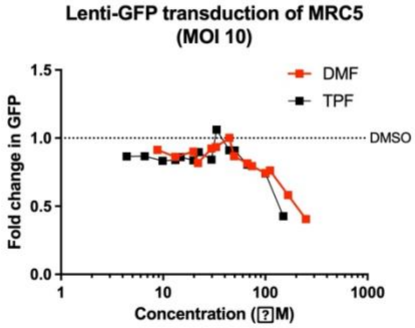
Lenti-GFP transduction of MRC5
(MOI 10)
DMF
TPF
DMSO
Fold change in GFP
Concentration (?M)

Figure 3.5: The impact of TPF in transduction of lentivirus

Jurkat, HT1080, A549, HepG2 or MRC5 cells were seeded in 96well plates and pretreated for 4h with 4-100uM TPF (black lines) or 9-250uM DMF (red lines) in triplicate. Cells were transduced with lentivirus encoding GFP at an MOI of 10. 70 hours post transduction, plates were imaged for GFP and mean fluorescence per well determined using the Agilent Biotek Cytation5. GFP mean intensity was quantified and plotted (n=3, unpaired t-test was performed comparing to the DMSO treated, transduced condition).

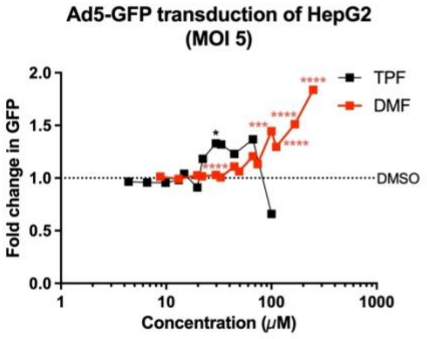
Ad5-GFP transduction of HepG2
(MOI 5)
TPF
DMF
DMSO
Fold change in GFP
Concentration (μM)

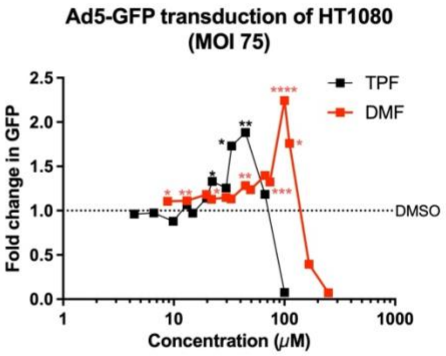
Ad5-GFP transduction of HT1080
(MOI 75)
TPF
DMF
DMSO
Fold change in GFP
Concentration (μM)

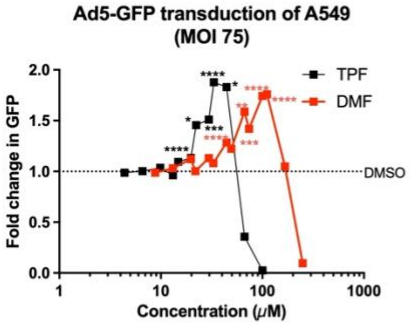
Ad5-GFP transduction of A549
(MOI 75)
TPF
DMF
DMSO
Fold change in GFP
Concentration (μM)

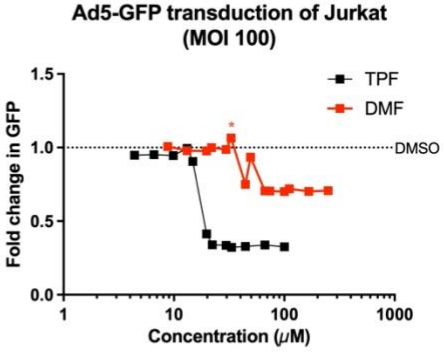
Ad5-GFP transduction of Jurkat
(MOI 100)
TPF
DMF
DMSO
Fold change in GFP
Concentration (μM)

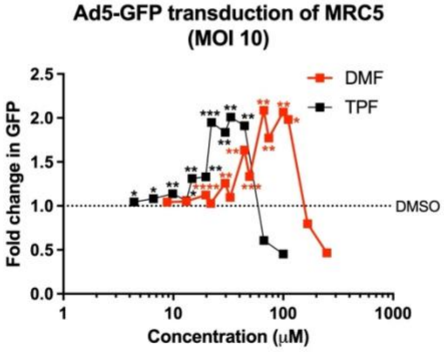
Ad5-GFP transduction of MRC5
(MOI 10)
DMF
TPF
DMSO
Fold change in GFP
Concentration (μM)

Figure 3.6: The impact of TPF in transduction of Ad5-GFP

Jurkat, HT1080, A549, HepG2 or MRC5 cells were seeded in 96well plates and pretreated for 4h with 4-100uM TPF (black lines) or 9-250uM DMF (red lines) in triplicate. Cells were transduced with Ad5 encoding GFP at the indicated MOIs. 70 hours post transduction, plates were imaged for GFP and mean fluorescence per well determined using the Agilent Biotek Cytation5. GFP mean intensity was quantified and plotted (n=3, unpaired t-test was performed comparing to the DMSO treated, transduced condition).

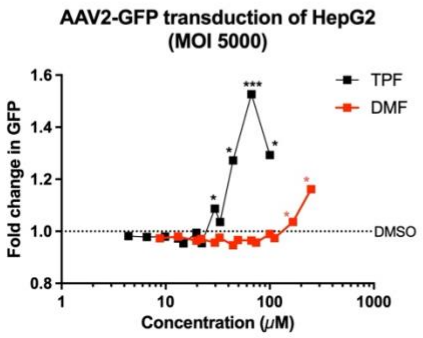
AAV2-GFP transduction of HepG2
(MOI 5000)
Fold change in GFP
1.6
1.4
1.2
1.0
0.8
1
10
100
1000
Concentration (μM)
TPF
DMF
DMSO

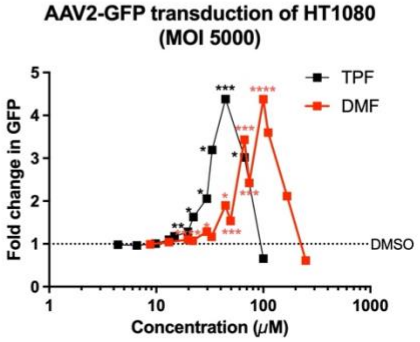
AAV2-GFP transduction of HT1080
(MOI 5000)
Fold change in GFP
5
4
3
2
1
0
1
10
100
1000
Concentration (μM)
TPF
DMF
DMSO

Figure 3.7: The impact of TPF in transduction of AVV-2

HT1080 or HepG2 cells were seeded in 96well plates and pretreated for 4h with 4-100uM TPF (black lines) or 9-250uM DMF (red lines) in triplicate. Cells were transduced with AAV2 encoding GFP at the indicated MOIs. 70 hours post transduction, plates were imaged for GFP and mean fluorescence per well determined using the Agilent Biotek Cytation5. GFP mean intensity was quantified and plotted (n=3, unpaired t-test was performed comparing to the DMSO treated, transduced condition).

3.4. Discussion

Our study shows for the first time that TPF has the potential as a novel pharmacological tool to enhance the activity of oncolytic viruses and other viral vectors. While the value of DMF has been previously explored to this end[45], the current study suggests that TPF has the potential for greater potency for this purpose as shown for a range of viruses in multiple cell lines (Figure 3.2 and Figure 3.4).

Mechanistically, our previous work with multiple maleic and fumaric acid esters, including MMF, the common active metabolite of TPF and DMF, has established the ability of these molecules to downregulate several IFN pathway-related genes via the blocking of NF-κB nuclear translocation [45]. Based on these findings, we hypothesized that TPF might target similar pathways. Our results provide clear evidence that TPF downregulates key antiviral and pro-inflammatory genes, including IFN-β, MX2, and IL6 (Figure 3.4A), thereby enhancing the susceptibility of cancer cells to VSVΔ51 infection. This downregulation, coupled with TPF's inhibition of the NF-κB nuclear translocation induced by TNFα (Figure 3.4C), suggests that much like DMF, TPF modulates innate immune responses, creating a more favorable environment for viral infection and oncolysis in the context of replicating oncolytic viruses. Intriguingly, we also saw that TPF on its own led to an elevation of baseline NF-κB nuclear translocation (Figure 3.3D), which to date has not been observed with DMF[45].

While significant differences in oncolytic (i.e., cytotoxic) potency were observed between TPF and DMF, the difference in enhancement in total viral output comparing TPF and DMF was in contrast relatively limited. The reason this is intriguing is because this difference is seemingly insufficient to explain the comparatively large differences in oncolysis observed, even when looking at each drug's respective peak viral enhancing dose. Given the dual role

of NF-κB in both coordinating the antiviral response as well as cell survival and death, it is tempting to speculate that a shift in baseline NF-κB induced by TPF could contribute to the enhanced impact of TPF on oncolytic activity (Figure 3.4B,D).

While the antiviral response is a well-appreciated tumor resistance barrier in oncolytic virotherapy, our study suggests that this response also impedes the infection efficiency of other viral vectors, even those that do not effectively replicate. The extension of our study to evaluate TPF's influence on different viral vectors provides support for its broader potential application in gene therapy. Engineered replication defective lentiviruses, adenoviruses, and adeno-associated viruses are prominent vectors being evaluated and used clinically in cell therapy (eg., Kymriyah™)[99], gene therapy (e.g. Luxturna™) [100], and even vector-vaccine applications (e.g. COVISHIELD™) [101]. Interestingly, each of these vectors uses distinct mechanisms for cellular attachment, entry, gene delivery, and in some cases integration (i.e., lentivirus). This is perhaps not surprising given that diverse viruses are commonly sensitive to antiviral responses mediated via type I IFN. However, given the viruses are non-replicating, further studies will be required in order to better understand what stage(s) of the infection process is / are most affected by baseline and/or emergent antiviral responses. Evidently, there are also cell-type and virus-type dependencies in relation to the effect of TPF which are not fully understood, since some cell lines were not sensitized to infection by select viruses using TPF (e.g., MRC5 for lentivirus and Jurkat for Ad5, Figure 3.5 and Figure 3.6, respectively). Further, the effects of TPF on oncolytic virus replication and spread, analogously to DMF, were restricted to tumor cells.

Nevertheless, the potential of TPF as a potentiator of oncolytic virus and viral vector-based gene delivery more generally warrants further pre-clinical exploration. TPF-mediated

enhancement could lead to more efficient gene transfer, potentially increasing the therapeutic efficacy of oncolytic virotherapies (as has been demonstrated with DMF previously) as well as gene therapies, supporting their clinical advancement. OVs as standalone treatments in particular have faced many challenges in delivering substantially improved clinical outcomes for cancer patients, with only a handful of approvals globally. Viral vector potentiators including but not limited to TPF could be considered in order to overcome some of these challenges. While our study included only a limited number of patient specimens, the observation of substantial activity of TPF with oncolytic VSVΔ51 in human pancreatic and ovarian cancer tumor explants (Figure 3.3E) offers choice areas for further pre-clinical exploration.

3.5. Materials and Methods

Drugs and Viruses

Dimethyl fumarate (DMF) and Monomethyl fumarate (MMF) were obtained from Sigma-Aldrich (St. Louis, MO, USA) (DMF: Cat#242926; MMF: Cat#651419). Tepilamide fumarate (TPF) was obtained from Dr. Reddy's Laboratories Ltd. (Hyderabad, India). All the drugs were resuspended in 100% DMSO to 100 mM and further diluted at indicated dilutions before use in all in vitro experiments.

Viruses

VSVΔ51 expressing GFP or firefly luciferase (FLuc) was used throughout this study[35][18]. The propagation of all viruses was carried out on Vero cells and subsequently purified using 5–50% OptiPrep (Sigma-Aldrich, St. Louis, MO, USA) gradients. Viral titers were determined using a standard plaque assay on the Vero cells, following a published protocol [19].

HSV.n212 was obtained as a generous gift from Dr. Karen Mossman of McMaster University (Hamilton, Canada). HSV titers were determined by a standard plaque assay on Vero cells according to a previously published protocol [32].

AAV2 expressing GFP was obtained from Virica Biotech.

Lentivirus plasmids were purchased from Thermo Fisher Scientific (Nepean, ON, Canada) (pLenti6.3 GFP expression vector, Cat# V37006, LV MAX Packaging Mix Cat# A43237) and used to transfect HEK293 Viral Production cells (Gibco, Nepean, ON, Canada, Cat#A35347) using the LV MAX kit (Cat# A35348) and quantified by flow cytometry.

Ad5 expressing GFP was purchased from Vector Biolabs (Malvern, PA, USA), amplified on HEK293 cells, purified by CsCl gradient, and quantified using the Adeno-X Rapid Titer Kit from Takara (Palo Alto, CA, USA).

Cell lines

All the cell lines used in this study along with information about their suppliers and the growth media are detailed in (Table S1). The cells were cultured in Dulbecco's Modified Eagle's Medium (DMEM), sourced from either HyClone (Waltham, MA, USA) or Corning (Manassas, VA, USA). This medium was supplemented with 1% penicillin–streptomycin (Gibco) and 10% fetal bovine serum (FBS), obtained from VWR (Mississauga, ON, Canada), to support optimal cell growth and maintenance.

All the cells were incubated at 37 °C in a 5% CO2 humidified incubator and routinely tested for mycoplasma contamination by Hoechst staining and PCR (Diamed, Mississauga, ON, Canada, Cat # ABMG238).

Plaque assay

The Vero cells were initially cultured in 12-well plates at a specific density of 3 × 105 cells per well. The infectious samples underwent a series of dilutions using serum-free DMEM and were subsequently applied (at a volume of 500 µL per well) to the Vero cell monolayers. These cultures were then incubated at 37 °C, 5% CO2 for a duration of 60 min. Following this incubation period, the culture medium was removed and replaced with an overlay. This overlay was prepared by mixing 1% agarose and 2× DMEM supplemented with 20% FBS in a 1:1 ratio. After an additional 24 h incubation, visible plaques were fixed with a mixture of methanol and glacial acetic acid in a 3:1 ratio for a minimum of 1 h, and then stained for 30 min with a Coomassie Blue solution (comprising 4 g of Coomassie Brilliant Blue R (Sigma, Oakville, ON, Canada) (cat. B0149), 800 mL of methanol, 400 mL of acetic acid, and 2800 mL of distilled water) to enable the visualization and counting of plaques.

High-throughput luciferase tittering

Vero cells were cultured in opaque white 96-well plates using 100µl of complete DMEM supplemented with 30 mM HEPES until they reached a confluence of 95–100%. To determine the viral titer of VSVΔ51-Fluc-infected samples, 25µl of each sample was transferred into the wells containing the Vero cells. Additionally, a standard curve was prepared by diluting a purified virus stock with a known titer ranging from 10^8 to 10^{10} PFU/mL. This standard curve was duplicated for each 96-well plate. D'Luciferin (PerkinElmer, Waltham, MA, USA, Cat. # 122799) solution was added to the wells (2 mg/mL) in sterile PBS. Luminescence was read using a Cytation microplate reader at an appropriate sensitivity. Standard curve values allow for the generation of a Hill equation, which was applied to the tittered samples to obtain viral expression units (VEU). For further details can be found in in published protocol [102].

Viral growth curves

Cells were placed in 24-well plates and allowed to grow overnight, reaching full confluency by the following day. Cells were then inoculated with VSVΔ51-Fluc at an MOI of 0.01 (multi-step growth curve) or 1.0 (single-step growth curve). Cells were incubated up to 48 hpi, with 200 µl of supernatant collected and frozen at -80C at the following timepoints: 0, 8, 12, 24, 36, 48 hpi. Viral titer in collected samples were quantified by plaque assay as previously described.

Cell viability assay

Cellular metabolic activity was evaluated using the Resazurin metabolic dye (Millipore Sigma, Oakville, ON, Canada, cat. SI03200) following the manufacturer's instructions. Resazurin solution with a concentration of 10% (v/v, final) was added to the wells containing treated or

untreated and/or infected cells. The cells were then incubated for a duration of 2–4 h, which varied depending on the specific cell line used. Using the BioTek Microplate Reader (BioTek, Winooski, VT, USA) and Gen5 2.07 software, fluorescence was measured at 590 nm upon excitation at 530 nm. The readings were expressed relative to the average of the uninfected, untreated condition.

IFN-β ELISA

The 786-0 cells were plated to confluency in 12-well plates and incubated overnight at 37 °C in a 5% CO_2humidified incubator. Subsequently, the cells were treated with TPF at a concentration of 150 μM. Four hours later, the cells were either infected with VSVΔ51 at a multiplicity of infection (MOI) of 0.05 or underwent a mock infection. Supernatants were collected at 24 h post-infection (hpi). The quantity of human IFN-β in the supernatant was measured using the Human IFN Beta ELISA Kit (PBL Assay Science, Piscataway, NJ, USA, cat. 41410), following the procedure provided by the manufacturer. Absorbance readings were taken using the BioTek Microplate Reader (Agilent, Santa Clara, CA, USA).

Human and Murine Ex Vivo models

BALB/c mice were implanted with CT26.wt 3×10^5 colon cancer cells. Once tumor volumes reached 1500 mm3, the mice were euthanized, and relevant tissues were extracted. For human tissue samples, tumor samples were collected from patients who had given informed consent and followed the Declaration of Helsinki guidelines during surgical resection. The collection of human tissue/fluid for this study was made possible by the Global Tissue Consent and Collection Program at the Ottawa Hospital Research Institute. All the tissues were processed fresh; sliced into 2 mm sections and circular cores of 2 mm diameter were extracted using a punch biopsy tool. These cores were then kept in a humidified incubator at 37 °C and 5% CO2

in DMEM supplemented with 10% serum, 30 mM HEPES, 1% (v/v) penicillin–streptomycin and 0.25 mg/L amphotericin B. The cores were treated with TPF for four hours and then infected with VSVΔ51 at 3 × 104 pfu/core. After 24 h post-infection, fluorescence images were captured using the EVOS Live Cell Imaging System (Thermo Fisher, San Francisco, CA, USA) the supernatant was assessed for viral titer by standard plaque assay.

Quantitative real-time PCR

The extraction of total RNA from both infected and mock-infected 786-0 cells was conducted using the RNeasy Mini Kit, following the instructions provided by the manufacturer. (Qiagen, Toronto, ON, Canada, Cat. 74104). The conversion of one microgram of RNA to complementary DNA (cDNA) was achieved through the use of the RevertAid First Strand cDNA Synthesis Kit. (Thermo Fisher Scientific, Nepean, ON, Canada, Cat. K1621). The real-time polymerase chain reaction (PCR) protocols involved the use of 40 nanograms of complementary DNA (cDNA) and the PowerUp™ SYBR™ Green Master Mix (ThermoFisher Scientific, Cat. A25776) on the 7500 Fast Real-Time PCR system (Applied Biosystems, Thermo Fisher Scientific, Nepean, ON, Canada). Gene expression was normalized to GAPDH, and fold change was calculated relative to the mock-treated samples for each gene using the Pfaffl method[103].

Immunofluorescence staining

The 786-0 cells were seeded on 12 mm glass coverslips (Thomas Scientific, cat. 64-0712), then treated with TNFa $(25\mathrm{ng/mL})$ (Sigma-Aldrich, Oakville, ON, Canada) or TPF (150µM). Next, the adherent cells were washed twice using PBS* containing 1 mM CaCl2 and 500 mM MgCl. The cells were subjected to fixation using a 4% paraformaldehyde solution for a duration of 30 min. Subsequently, permeabilization was achieved by treating the cells with a

0.2% Triton-X 100 solution in 200 mM glycine/PBS for a period of 8 min. The cells were quenched in a 200 mM glycine/PBS solution. Following this, the samples underwent blocking with a 5% BSA/PBS* solution for 1 h at room temperature and were subsequently exposed to the NF-κB/p65 primary antibody (rabbit, cell signaling #8242) overnight in a humidified chamber at 4 °C. Anti-rabbit IgG secondary antibody (cell signaling #4413S) was applied for 60 min, then the samples were mounted onto glass slides and counterstained using Prolong gold antifade with DAPI (Molecular Probes). The slides were imaged using the Zeiss Axiocam HRM Inverted fluorescent microscope (Zeiss, Toronto, Canada) and Axiovision 4.0 software. The images were processed using ImageJ. Nuclear: cytoplasmic signal quantification processes were performed using CellProfiler (Massachusetts Institute of Technology, Cambridge, MA, USA). Each graphed data point represents mean fluorescence from one, individually analyzed nucleus as determined by CellProfiler using the DAPI stain.

Viral vector transduction

Dose–response testing of TPF or DMF followed by transduction with either Lentivirus, AAV-2, or Ad5 was performed in triplicate in the indicated cell lines seeded in 96-well plates to 50% confluency. The cells were treated with a 2 in 3 dilution series of each drug for 4 h followed by transduction with either lentivirus-GFP at MOI 10, AAV2-GFP at MOI 5000, or Ad5-GFP at MOI 5–100. A total of 70 h post transduction, the plates were imaged for GFP using the Cellomics Arrayscan (Thermo Scientific, Waltham, MA, USA), and mean fluorescence per well was determined using the Agilent Biotek Cytation 5 reader (Santa Clara, CA, USA).

Statistics

All the graphs and statistical analyses in our study utilized GraphPad Prism v.10. The specific statistical tests employed for each figure are described in the corresponding figure legends. When comparing the means of two groups, a two-tailed unpaired Student's t-test was applied. For comparisons involving more than two groups, one-way ANOVA with either Dunnett's or Tukey's multiple correction tests was used. The number of biological replicates is denoted by 'n', with the error represented as the standard error of the mean (SD). A p-value less than 0.05 was considered to indicate statistical significance.

Chapter 4: High Throughput Screen Approach Identifies Several Novel Synthetic Compounds with the ability to Potentiate Oncolytic Virus Therapy

Akram Alwithenani[1,2,3], Glib Maznyi[1,2], Marcus M. Spinelli[1] Rozanne Arulanandam*[1,2] Jean-Simon Diallo*[1,2]

[1]Ottawa Hospital Research Institute, Ottawa, Ontario, K1H 8L6;

[2]Biochemistry, Microbiology and Immunology, University of Ottawa, Ottawa, Ontario, K1H 8L1

[3]Department of Clinical Laboratory Science, Faculty of Applied Medical Science, Umm Al-Qura University, Makkah, Saudi Arabia

*Equal contribution

4.1. Abstract

Many different therapeutic strategies are available for cancer patients, from surgical resection to cytotoxic therapy such as chemotherapy and radiation. Recently, immunotherapy and specifically oncolytic virotherapy has emerged as a promising option, with oncolytic HSV-1 being the first OV to be approved by the FDA in 2015. However, not all cancers are sensitive and responsive to OVs. The objective of this study is to discover new types of small molecules that have the potential to enhance the effectiveness of oncolytic viruses. A virus/cell-based method was employed to screen various chemical libraries for the purpose of discovering chemical compounds that could act as sensitizers for OVs to eradicate tumor cells that are otherwise resistant to virus infection. In this high throughput screen, we pre-treated 786-0 (human renal carcinoma) cells with a library of 3200 synthetic small molecules for a duration of 4 hours. Following the pre-treatment, the cells were subsequently infected with oncolytic vesicular stomatitis virus (VSVΔ51) or, in parallel, herpes simplex virus type 1 (HSV-1) both encoding a GFP transgene. Fluorescent imaging and viability assays were subsequently performed and compared to untreated, infected cells. Using this approach, we successfully identified several compounds that exhibit the ability to enhance the replication, and oncolysis of oncolytic VSV and HSV-1 in tumor cells. This promising outcome warrants further investigation into the identified compounds and more in-depth studies to explore their potential applications.

4.2. Introduction

Oncolytic virotherapy represents a promising frontier in cancer treatment, leveraging genetically modified viruses to selectively infect and destroy cancer cells without harming normal tissue [104]. These therapeutic viruses exploit the altered signaling pathways and the immunosuppressive environment of tumors, allowing them to replicate within malignant cells and induce cell death, either through direct lysis or by triggering immune responses against the tumor [105–107]. This approach not only targets the primary tumor but also has the potential to stimulate the body's immune system to recognize and attack metastatic cells, offering a dual mechanism of action against cancer [108].

One of the significant challenges facing oncolytic virotherapy is the resistance of cancer cells to infection and subsequent destruction by oncolytic viruses. This resistance can arise from various factors, including the innate antiviral defenses of cancer cells, the presence of a dense and fibrous tumor microenvironment that impedes viral penetration [109,110], and the heterogeneity of cancer cells, which may include subsets of cells inherently resistant to viral infection [111]. To address these challenges, high-throughput screening methods are increasingly employed to identify drugs or compounds that can sensitize cancer cells to OV. By systematically testing thousands of compounds for their ability to enhance viral entry, replication, and/or oncolysis, researchers can uncover synergistic combinations that overcome resistance mechanisms. This strategy not only broadens the therapeutic potential of OVs but also provides a precision medicine approach to treating various cancers by tailoring treatment strategies to target specific resistance pathways identified in tumor cells.

In the study described, a virus/cell-based assay was employed to screen 3200 chemical compounds. This screen aimed to identify compounds which enhance the activity of oncolytic viruses against tumor cells usually resistant to such infections. The effectiveness of the compounds was determined by measuring two specific indicators: GFP, which marks viral infection, and alamar blue, as a measure of cell viability. DMF was used as a benchmark positive control. Thus, the focus was on discovering compounds that increase both viral infection (as indicated by increased GFP readouts) and cell death (as indicated by changes in alamar blue readouts).

4.3. Results

In our study, we aimed to identify synthetic compounds from a custom-generated library that could sensitize 786-0 cells to oncolytic viruses, specifically VSVΔ51 and HSV.n212. Both viruses were engineered to express Green Fluorescent Protein (GFP), which served as a key indicator of viral spread in our analysis. To assess the efficacy and cytotoxicity of the compounds, we used the Cellomics™ ArrayScan for GFP signal detection and used a metabolic dye, resazurin, as an indicator of cell viability.

Our experimental workflow (see Figure 4.1) began with seeding 96 well plates with 786-0 cells at 95% confluency, followed by a pretreatment phase, where each of the 3200 compounds was administered at a concentration of 5 μM, in 0.5% DMSO final. We included DMF as a positive control due to its known properties of enhancing viral GFP expression and reducing metabolic activity. Cells treated with 0.5% DMSO final without any compound served as the negative control. This pretreatment lasted for 4 hours, after which the cells were infected with either VSVΔ51 at MOI of 0.05 or HSV.n212 at an MOI of 0.1.

For the VSV-infected plates, GFP counts were measured 24 hours post-infection, while metabolic activity was assessed at 48 hours post-infection. In contrast, for the HSV-1 infected plates, both GFP counts, and metabolic activity were analyzed 72 hours post-infection due to the slower kinetics of this virus. To evaluate the direct effects of the compounds on the cell lines, we also included samples treated solely with the compounds, devoid of any viral infection. This allowed us to assess the inherent toxicity of each compound. Each compound was tested in triplicate to ensure reliability and reproducibility of the data.

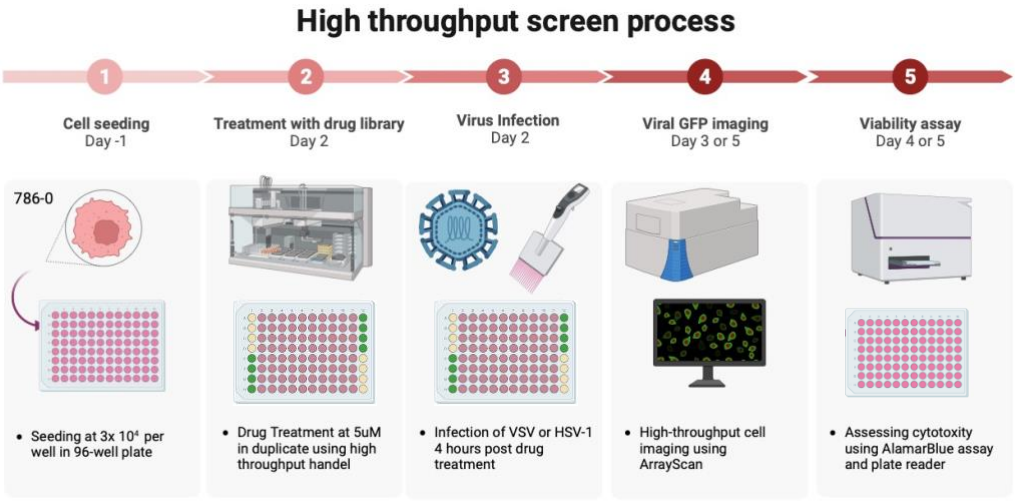
High throughput screen process
1
2
3
4
5
Cell seeding
Day -1
Treatment with drug library
Day 2
Virus Infection
Day 2
Viral GFP imaging
Day 3 or 5
Viability assay
Day 4 or 5
786-0
• Seeding at 3x 10⁴ per well in 96-well plate
• Drug Treatment at 5uM in duplicate using high throughput handel
• Infection of VSV or HSV-1 4 hours post drug treatment
• High-throughput cell imaging using ArrayScan
• Assessing cytotoxity using AlamarBlue assay and plate reader

Figure 4.1: High throughput screening processes diagram

The diagram outlines the step-by-step processes used in this study for screening. The process begins on Day 1 by seeding 786-0 cells into a 96-well plate, with 30,000 cells per well, and allowing them to settle for 24 hours. On Day 2, the cells are treated with a drug library at a concentration of 5 µM for four hours, followed by infection with either HSV-1 or VSVΔ51. On Day 3, plates infected with VSVΔ51 are imaged. Viability is assessed on Day 4 for plates infected with VSVΔ51 and on Day 5 for plates infected with HSV-1, which are also imaged on the same day.

The primary outcome measure was the fold change in GFP expression, normalized to the DMSO-treated control samples. This approach allowed us to assess the impact of the synthetic compounds on the oncolytic viruses expressing GFP, which is indicative of viral activity, and consequently, the potential efficacy in cancer cell killing. The combined use of GFP signal quantification and metabolic viability assays provided a comprehensive overview of the compounds' effects and cytotoxic profiles in the context of oncolytic virotherapy in otherwise refractory 786-0 renal carcinoma cells at starting point. To account for toxicity of the compounds on their own and to identify OV/compound synergies, we also calculated a *viral sensitizer factor*, the logarithm of the viability of drug alone divided by the viability of combination therapy as outlined in method section. The calculated scores for viral sensitization for each compound are displayed in (Figure 4.2D & 4.3D).

We successfully identified several compounds (see table 4.1 and 4.3) that demonstrated an enhanced GFP expression in 786-0 cells compared to those treated with DMSO when using either VSVΔ51 or HSV.n212 as the oncolytic agent, as illustrated in (Figure 4.2 A and 4.3 A). The fold change in GFP for the VSVΔ51 hits ranged from 2 to 31, while the hits for HSV.n212 reached up to a maximum of 2.5-fold increase. We classified any compound with a GFP fold change greater than 3 for (VSVΔ51) and 2 for (HSV.n212) as a potential hit.

Figure 4.2C displays a comparison in the ability of compounds to enhance GFP fluorescence and lead to cytotoxic effects in 786-0 cells wen using VSVΔ51. Among the tested compounds, 19 exceeded a threefold increase in GFP expression (3-fold change), indicating potent enhancement activity (see table 4.1 and 4.3). Within the group of compounds that led to enhanced GFP, notable differences in cytotoxic effects were observed. For example, we can

see differing profiles for compounds AAHTS-V1 and AAHTS-V2 which enhanced GFP by 31.56 and 28.48 fold respectively. At the tested dose, AAHTS-V1 was relatively toxic on its own, killing 83% of the cells independently but achieving 94% cell killing when combined with VSVΔ51. In contrast, AAHTS-V2 showed was relatively non-toxic at the same dose, leading to 7% cell death alone in comparison to 69% when used in conjunction with VSV. Because of differences in toxicity, of the compounds, AAHTS-V2 has a more favourable *viral sensitizer* factor compared to AAHTS-V1 (Fig. 4.2D).

Figure 4.3C presents similar comparative GFP/cell viability data using HSV.n212 as the oncolytic agent. In this screen, only six compounds exceeded the threshold set for enhancement of GFP expression, achieving at least a twofold change (refer to the table 4.3). Notably, the majority of the compounds did not lead to significant enhancement in cell killing within the experimental timeframe. This observation is also reflected in the viral sensitizer scores depicted in Figure 4.3D.

Table 4.1: GPF fold change of VSVΔ51 compounds

Drug name	ID	GFP fold change	p value (GFP)
OICR0307069A01	AAHTS-V1	31.56	0.28
OICR0305430A01	AAHTS-V2	28.48	0.09
OICR0308269A01	AAHTS-V3	24.88	0.02
OICR0305525A01	AAHTS-V4	12.61	0.07
OICR0305501A01	AAHTS-V5	7.61	<0.01
OICR0307286A01	AAHTS-V6	5.89	0.07
OICR0306559A01	AAHTS-V7	4.32	0.03
OICR0307556A01	AAHTS-V8	4.32	0.09
OICR0305926A01	AAHTS-V9	3.61	0.30
OICR0306235A01	AAHTS-V10	3.61	0.13
OICR0307883A01	AAHTS-V11	3.58	0.06
OICR0306539L01	AAHTS-V12	3.57	0.41
OICR0306579L01	AAHTS-V13	3.54	0.26
OICR0308041A01	AAHTS-V14	3.48	<0.01
OICR0307618A01	AAHTS-V15	3.37	0.21
OICR0306131A01	AAHTS-V16	3.33	0.27
OICR0307239A01	AAHTS-V17	3.25	0.37
OICR0306587A01	AAHTS-V18	3.22	0.11
OICR0307997A01	AAHTS-V19	3.15	0.41

Table 4.2: Viability and Viral Sensitizer Score of VSVΔ51 compounds

Drug name	ID	Viability (Drug)	Viability (combo)	p value (Viability of combo)	VSS
OICR0307069A01	AAHTS-V1	17%	6%	0.12	0.47
OICR0305430A01	AAHTS-V2	93%	31%	0.06	0.47
OICR0308269A01	AAHTS-V3	83%	97%	0.53	-0.07
OICR0305525A01	AAHTS-V4	91%	64%	0.12	0.16
OICR0305501A01	AAHTS-V5	114%	91%	0.04	0.10
OICR0307286A01	AAHTS-V6	160%	153%	0.41	0.02
OICR0306559A01	AAHTS-V7	79%	69%	0.17	0.06
OICR0307556A01	AAHTS-V8	43%	23%	0.08	0.26
OICR0305926A01	AAHTS-V9	104%	95%	0.51	0.04
OICR0306235A01	AAHTS-V10	76%	97%	0.20	-0.11
OICR0307883A01	AAHTS-V11	66%	71%	0.11	-0.03
OICR0306539L01	AAHTS-V12	107%	120%	0.40	-0.05
OICR0306579L01	AAHTS-V13	108%	88%	0.71	0.09
OICR0308041A01	AAHTS-V14	109%	103%	0.33	0.03
OICR0307618A01	AAHTS-V15	107%	134%	0.12	-0.10
OICR0306131A01	AAHTS-V16	110%	106%	0.36	0.02
OICR0307239A01	AAHTS-V17	76%	76%	0.49	0.00
OICR0306587A01	AAHTS-V18	84%	87%	0.68	-0.01
OICR0307997A01	AAHTS-V19	111%	120%	0.05	-0.03

Table 4.3: GPF fold change of HSV.n212 compounds

Drug name	ID	GFP fold change	p value (GFP)
OICR0305346A01	AAHTS-H1	2.76	0.005
OICR0305599A01	AAHTS-H2	2.50	0.017
OICR0305926A01	AAHTS-H3	2.49	0.005
OICR0305620A01	AAHTS-H4	2.09	0.157
OICR0306376A01	AAHTS-H5	1.97	0.042
OICR0307576A01	AAHTS-H6	1.95	0.017

Table 4.4: Viability and Viral Sensitizer Score of HSV.n212 compounds

Drug name	ID	Viability (Drug)	Viability (combo)	p value (Viability of combo)	VSS
OICR0305346A01	AAHTS-H1	97%	96%	0.312	0.005
OICR0305599A01	AAHTS-H2	88%	97%	0.537	-0.042
OICR0305926A01	AAHTS-H3	104%	112%	0.004	-0.032
OICR0305620A01	AAHTS-H4	100%	95%	0.241	0.022
OICR0306376A01	AAHTS-H5	133%	131%	0.362	0.007
OICR0307576A01	AAHTS-H6	89%	97%	0.686	-0.037

A

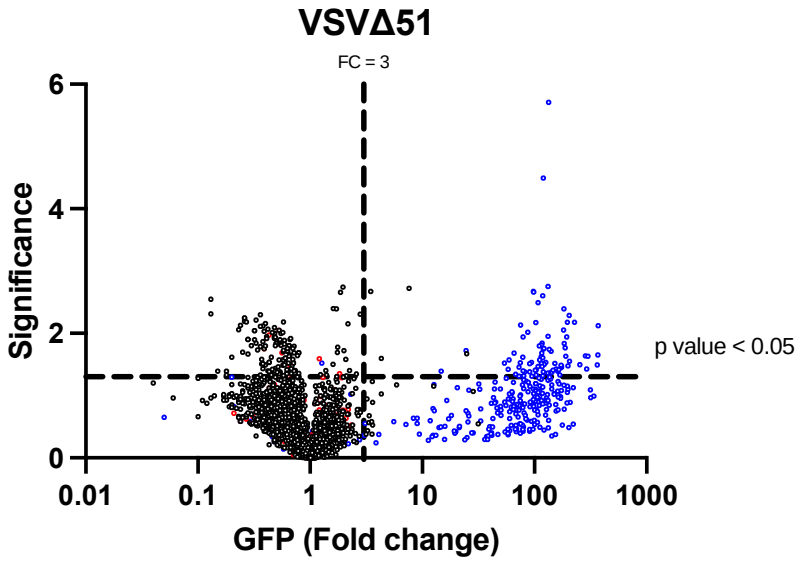
VSVΔ51
FC = 3
p value < 0.05
Significance
GFP (Fold change)
0
2
4
6
0.01
0.1
1
10
100
1000

B

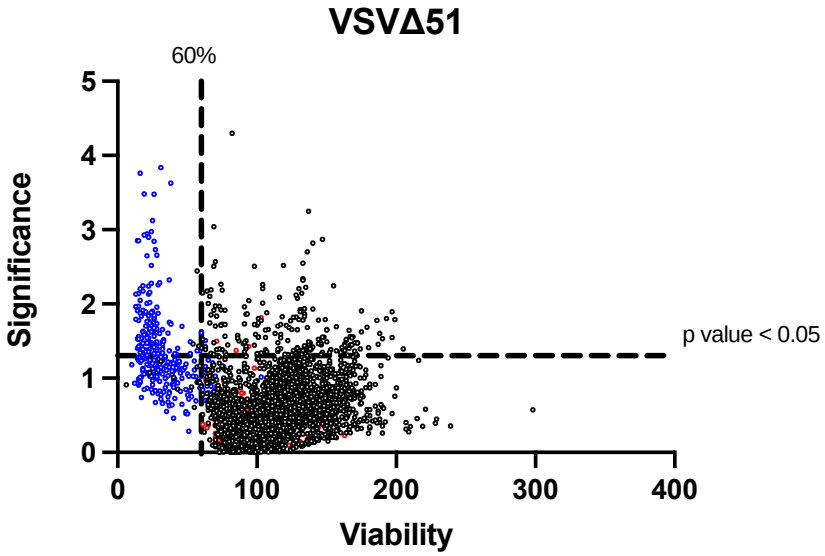
VSVΔ51
60%
p value < 0.05
Significance
Viability
0
1
2
3
4
5
0
100
200
300
400

C

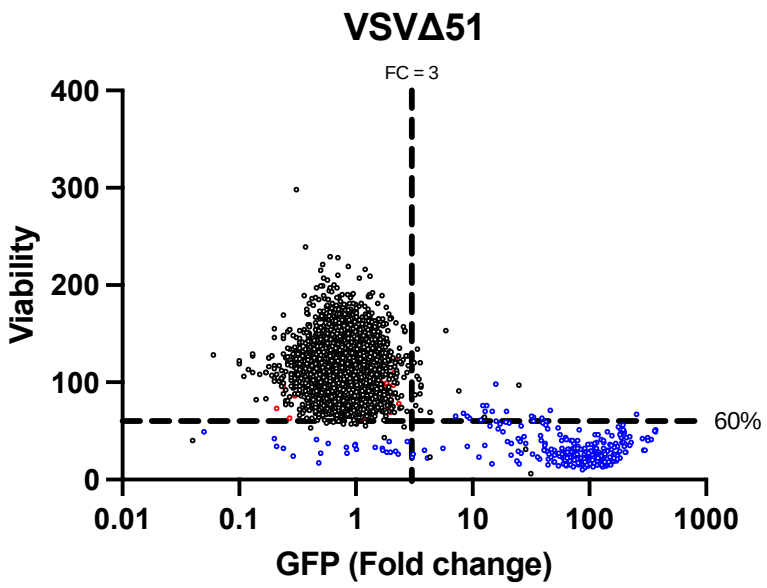
VSVΔ51
FC = 3
400
300
200
100
0
Viability
60%
0.01
0.1
1
10
100
1000
GFP (Fold change)

D

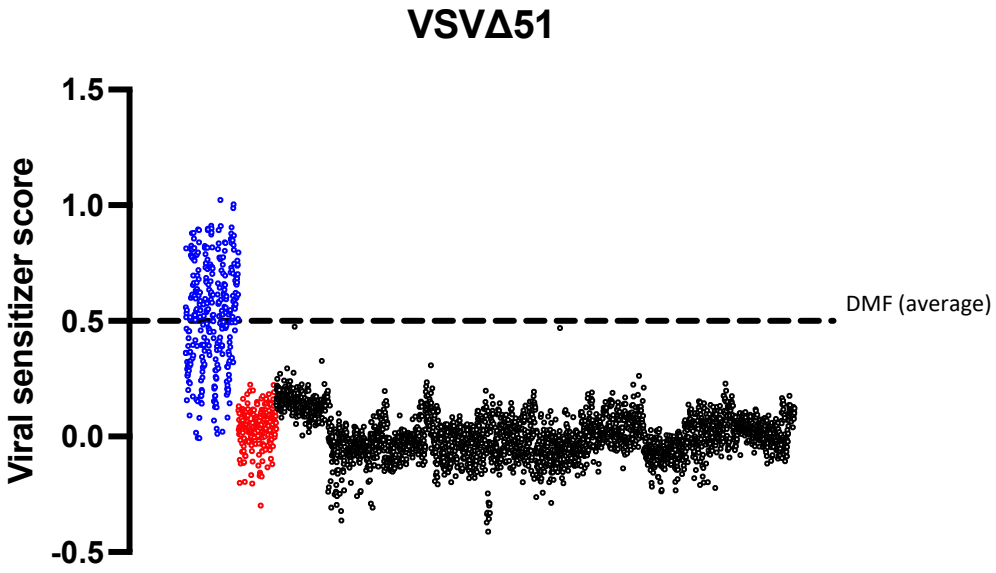
VSVΔ51
1.5
1.0
0.5
0.0
-0.5
Viral sensitizer score
DMF (average)

Figure 4.2: Identification of several synthetic compounds that boost oncolytic VSVΔ51.

Human renal carcinoma (786-0) cells were treated with 3200 compounds for a duration of 4 hours, then infected with VSVΔ51. GFP counts and viability assay were performed. As a positive control, 786-0 cells pre-treated with DMF (150μM) prior to infection are shown in blue. DMSO (red) was used as a negative control. **(A)** 48hpi, high- throughput GFP imaging was conducted. GFP fold change were calculated for each drug tested and values were normalized against infected untreated 786-0 control to obtain fold change **(B)** At 48 hours post-infection (hpi), metabolic activity was quantified utilizing resazurin. The resultant values were adjusted by subtracting the blank controls, and then normalized to the infected but untreated 786-0 control (mock). (**A & B**) To determine statistical significance, an unpaired t-test that assumed unequal variances was conducted. **(D)** The viral sensitizer factor for each drug compound was calculated following Equation method section. As a reference, DMF controls are shown in blue**.**

A

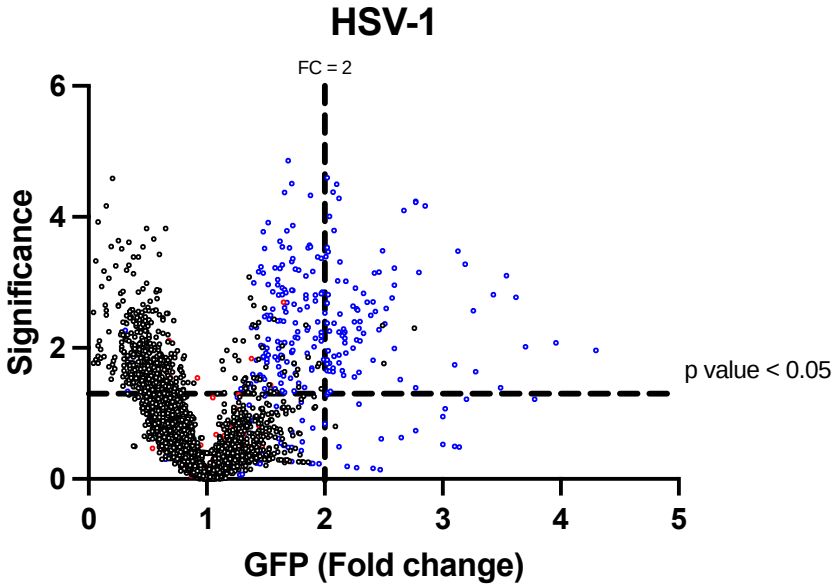
HSV-1
FC = 2
p value < 0.05
Significance
GFP (Fold change)
0
1
2
3
4
5
6

B

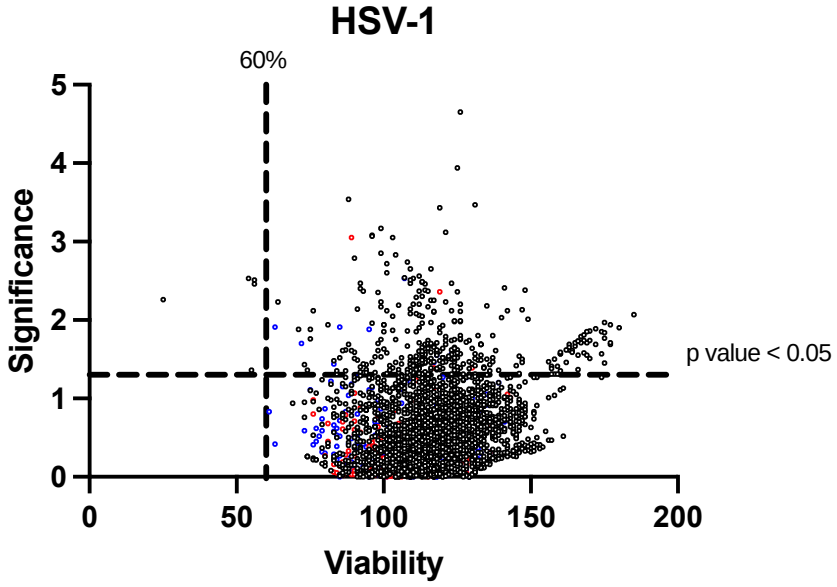
HSV-1
60%
p value < 0.05
Significance
Viability
0
1
2
3
4
5
0
50
100
150
200

C

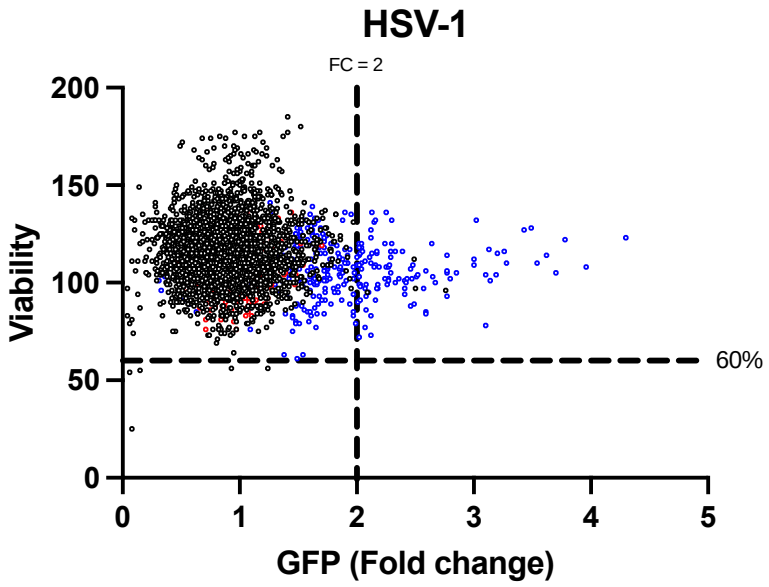
HSV-1
FC = 2
200
150
100
50
0
Viability
60%
0
1
2
3
4
5
GFP (Fold change)

D

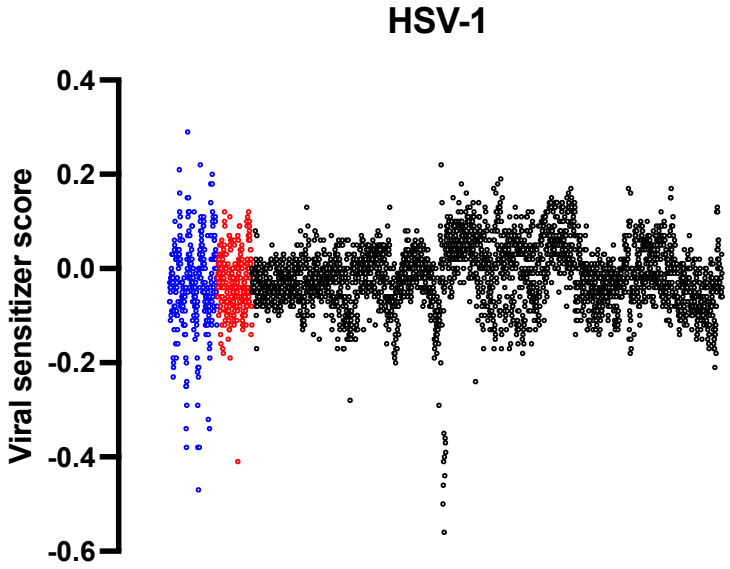
HSV-1
0.4
0.2
0.0
-0.2
-0.4
-0.6
Viral sensitizer score

Figure 4.3: Identification of several synthetic compounds that boost oncolytic HSVn.212.

Human renal carcinoma (786-0) cells were treated with 3200 compounds for a duration of 4 hours, then infected with HSV.n212. GFP counts and viability assay were performed. As a positive control, 786-0 cells pre-treated with DMF (150μM) prior to infection are shown in blue. DMSO (red) was used as a negative control. **(A)** 72hpi, high- throughput GFP imaging was conducted. GFP fold change were calculated for each drug tested and values were normalized against infected untreated 786-0 control to obtain fold change. **(B)** At 72 hours post-infection (hpi), metabolic activity was quantified utilizing resazurin. The resultant values were adjusted by subtracting the blank controls, and then normalized to the infected but untreated 786-0 control (mock). (**A & B**) To determine statistical significance, an unpaired t-test that assumed unequal variances was conducted. **(D)** The viral sensitizer factor for each drug compound was calculated following Equation method section. As a reference, DMF controls are shown in blue**.**

We conducted a clustering analysis using the CDD Vault Visualization tool to assess the structural similarities of drug hits for both VSVΔ51 and HSV.n212, as well as those that are mutual hits. This analysis of similarities was intended to provide deeper insights into the critical components of the molecular structures and may guide us toward the discovery of new compounds that are structurally analogous. We utilized over 30 VSVΔ51 hits for a clustering analysis, as illustrated in Figure 4.4 A. Using the algorithms provided by CDD Vault, the top-performing compounds were organized into several distinct classes. For instance, Figure 4.4 A illustrates two classes of VSVΔ51 hits, each sharing a common sub-structure. Similarly, Figure 4.4 B identifies a common sub-structure in one of the classes of HSV.n212 hits. Examination of the mutual hits shown in Figure 4.4 C reveals that each compound is quite distinct, indicating a diversity among the hits identified for both viruses.

A

VSVΔ51-GFP

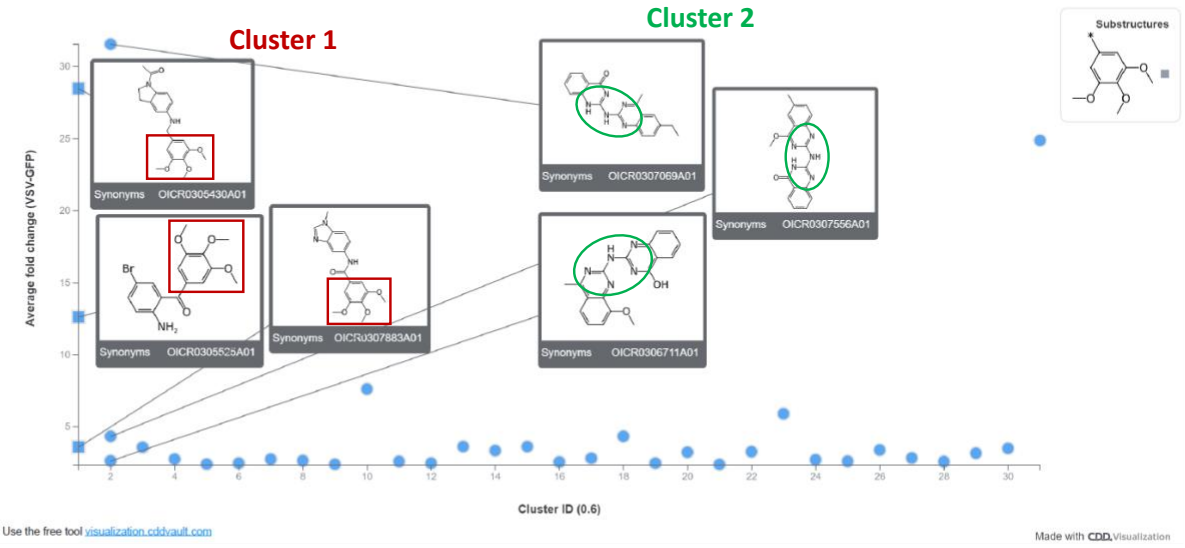
Cluster 1
Cluster 2
Substructures
Synonyms OICR0305430A01
Synonyms OICR0307069A01
Synonyms OICR0307556A01
Synonyms OICR0305525A01
Synonyms OICR0307883A01
Synonyms OICR0306711A01
Average fold change (VSV-GFP)
Cluster ID (0.6)
Use the free tool visualization.cddvault.com
Made with CDD Visualization

B

HSV1-GFP

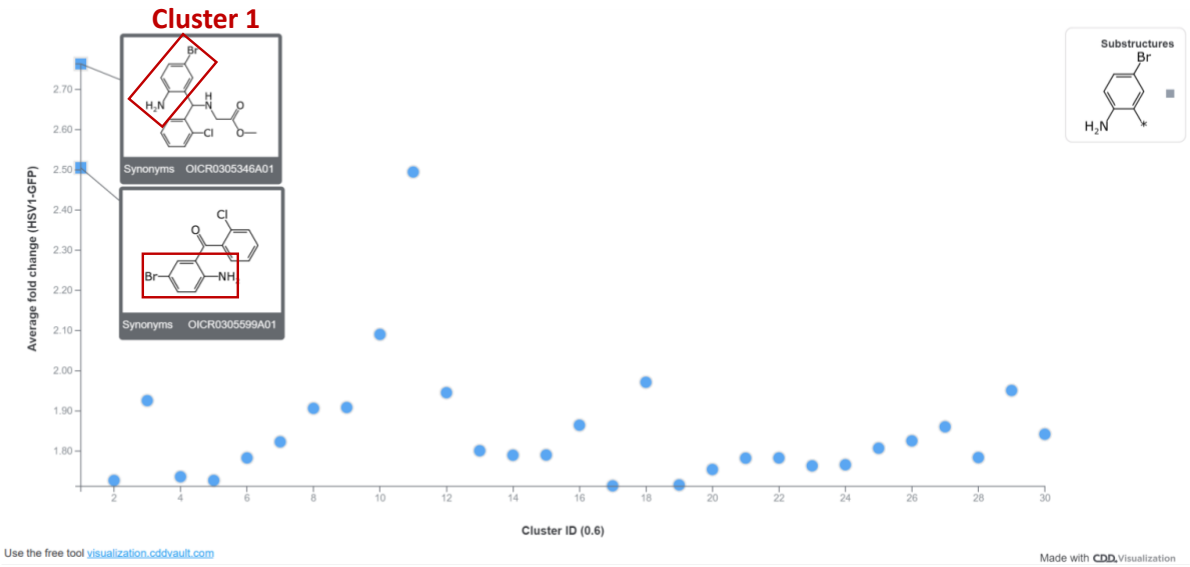
Cluster 1
Synonyms OICR0305346A01
Synonyms OICR0305599A01
Substructures
Average fold change (HSV1-GFP)
Cluster ID (0.6)
Use the free tool visualization.cddvault.com
Made with CDD Visualization

C

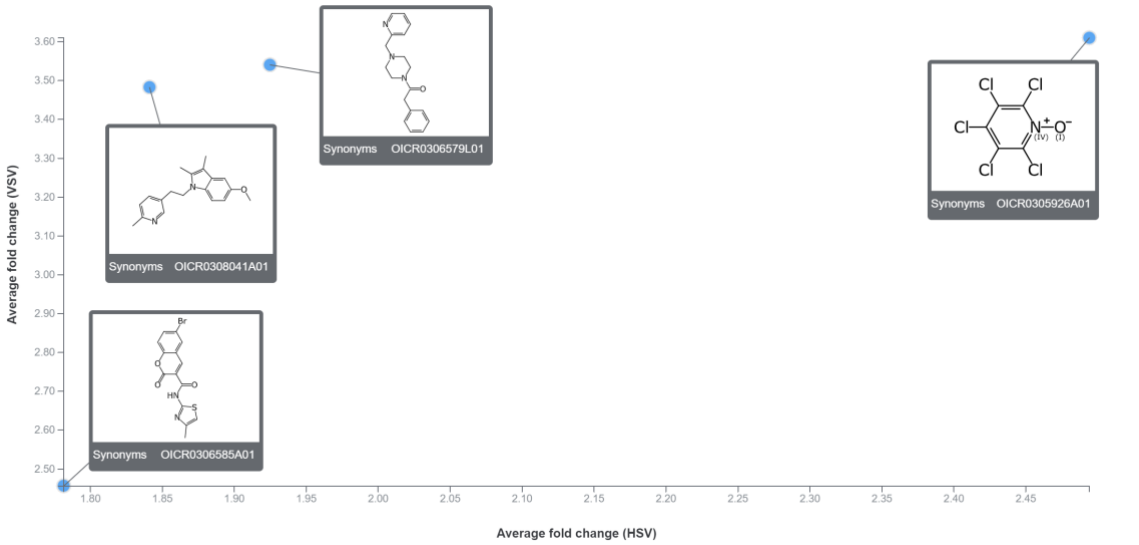
Average fold change (VSV)
3.60
3.50
3.40
3.30
3.20
3.10
3.00
2.90
2.80
2.70
2.60
2.50
1.80
1.85
1.90
1.95
2.00
2.05
2.10
2.15
2.20
2.25
2.30
2.35
2.40
2.45
Average fold change (HSV)
Synonyms OICR0306579L01
Synonyms OICR0308041A01
Synonyms OICR0306585A01
Synonyms OICR0305926A01
Use the free tool visualization.cddvault.com
Made with CDD Visualization

Figure 4.4: Clustering analysis of VSVΔ51, HSV.n212 and mutual hits

Clustering analysis of top hits for the HTS screen were shown. VSVΔ51 hits (A) HSV.n212 hits (B) Mutual hits (C).

Subsequently, top hits for both viruses were requested for re-supply from the manufacturer. AAHTS-V2 and AAHTS-H2 were first obtained and tested as an initial measure of screen validation. Both compounds were validated upon testing with re-supplied material: AAHTS-V2 for VSVΔ51 and AAHTS-H2 for HSV.n212, respectively. We examined the impact of these compounds on 786-0 cells across a wide dosage range. The observed effects across this spectrum are detailed in Figures 4.5 and 4.6. For AAHTS-V2, it exhibits a broad active range from 1 to 100 µM (4.5C-D), which is much more potent than DMF (the positive control used in this study), as DMF has a narrower range of 118 to 266 µM as shown in Figure 4.5A. On the other hand, with AAHTS-H2, we observed a significant GFP increase (8-fold change) with HSV.n212, particularly at 20 µM as shown in Figure 5.6A. In subsequent experiments, we used a murine cancer cell line (CT26wt) to assess the potentially broader impact of AAHTS-V2 in other cell lines and species. AAHTS-V2 treatment led to a significant increase in VSVΔ51-associated GFP fluorescence intensity in CT26wt cells as illustrated in Figure 4.7A. Moreover, a significant augmentation in VSVΔ51 titer was observed at doses as low as 1 µM, as depicted in Figure 4.7B.

A

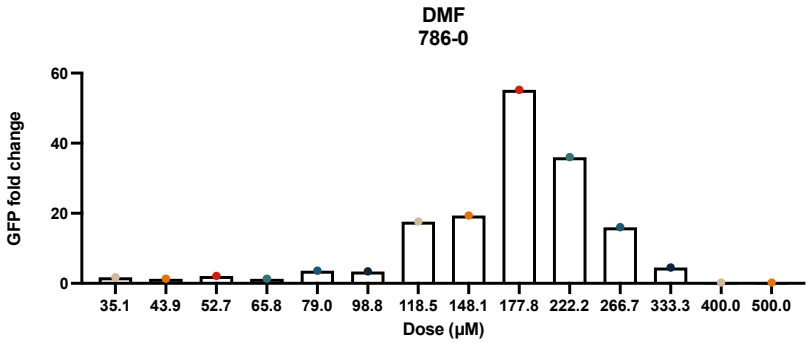
DMF
786-0
GFP fold change
60
40
20
0
35.1
43.9
52.7
65.8
79.0
98.8
118.5
148.1
177.8
222.2
266.7
333.3
400.0
500.0
Dose (μM)

B

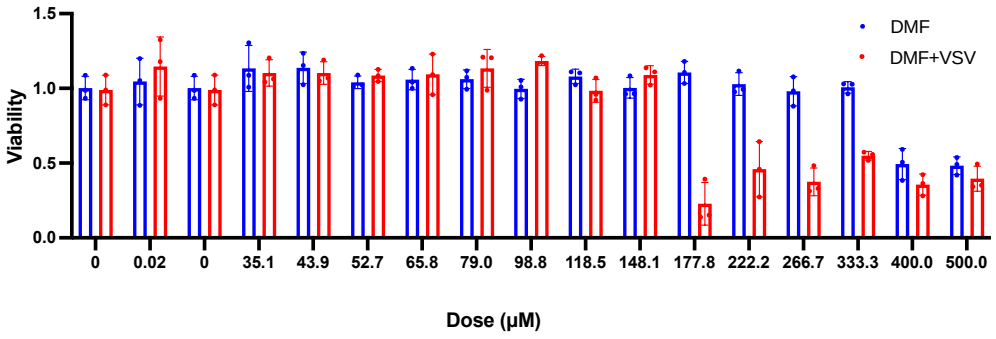
Viability
1.5
1.0
0.5
0.0
DMF
DMF+VSV
0
0.02
0
35.1
43.9
52.7
65.8
79.0
98.8
118.5
148.1
177.8
222.2
266.7
333.3
400.0
500.0
Dose (μM)

C

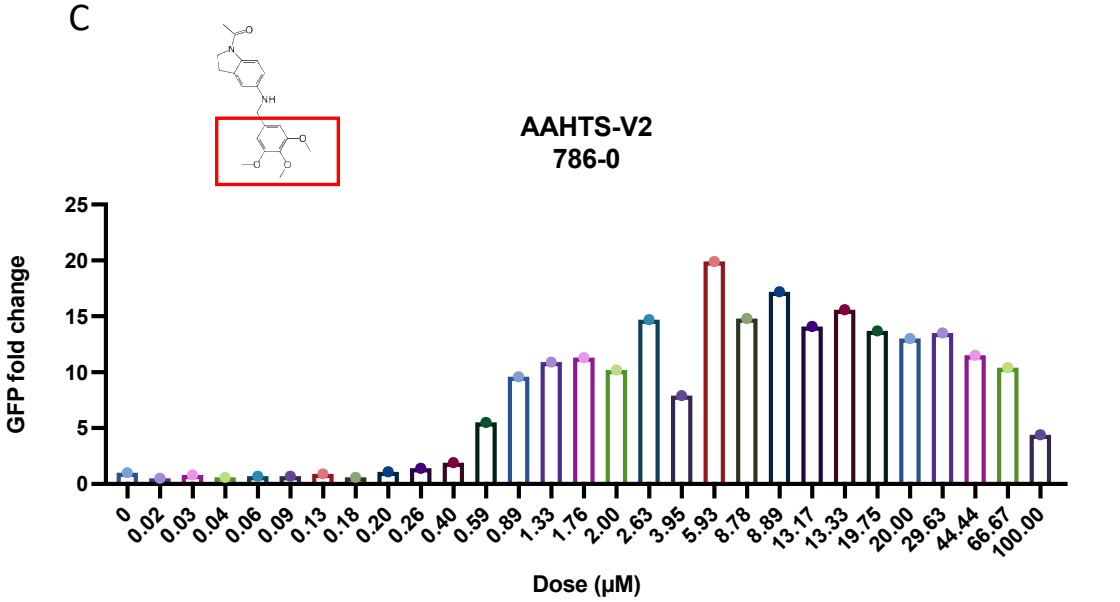
AAHTS-V2
786-0
GFP fold change
25
20
15
10
5
0
0
0.02
0.03
0.04
0.06
0.09
0.13
0.18
0.20
0.26
0.40
0.59
0.89
1.33
1.76
2.00
2.63
3.95
5.93
8.78
8.89
13.17
13.33
19.75
20.00
29.63
44.44
66.67
100.00
Dose (μM)

D

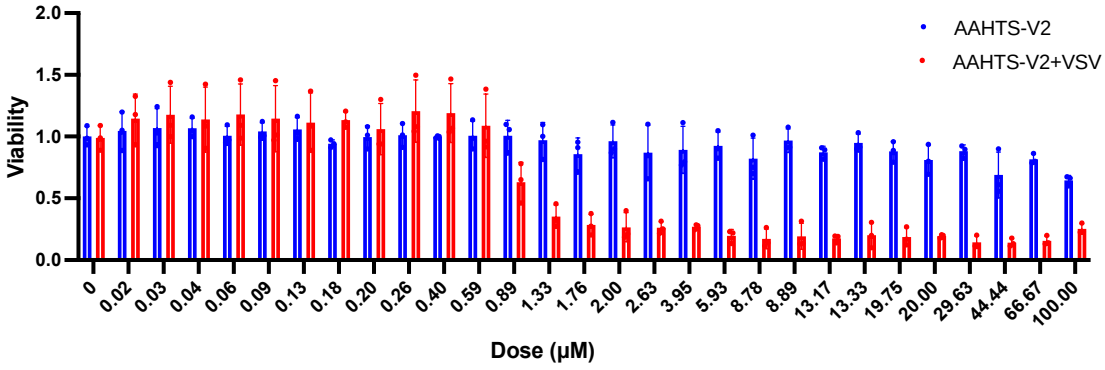
AAHTS-V2
AAHTS-V2+VSV
Viability
2.0
1.5
1.0
0.5
0.0
0
0.02
0.03
0.04
0.06
0.09
0.13
0.18
0.20
0.26
0.40
0.59
0.89
1.33
1.76
2.00
2.63
3.95
5.93
8.78
8.89
13.17
13.33
19.75
20.00
29.63
44.44
66.67
100.00
Dose (μM)

Figure 4.5: Validation of AAHTS-V2 compound on 786-0 cells

Human renal carcinoma (786-0) cells were treated with AAHTSV2 compound or DMF for a duration of 4 hours, then infected with VSVΔ51. GFP counts and viability assay were performed.

A

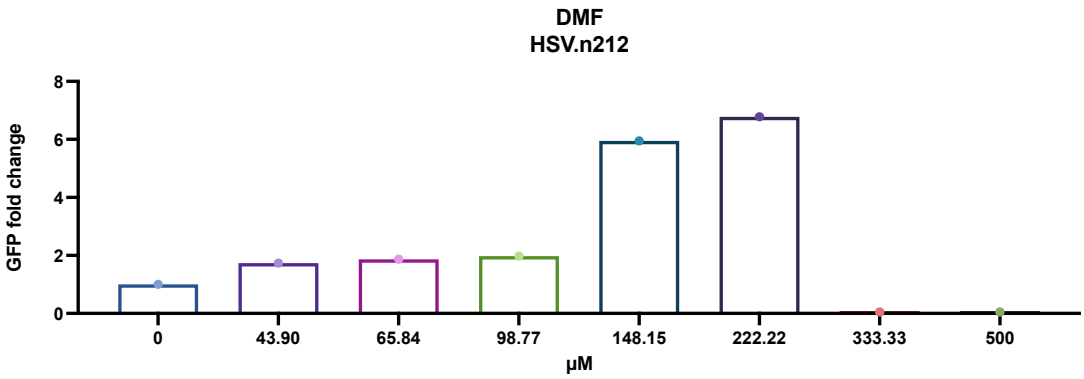
DMF
HSV.n212
GFP fold change
8
6
4
2
0
0
43.90
65.84
98.77
148.15
222.22
333.33
500
μM

B

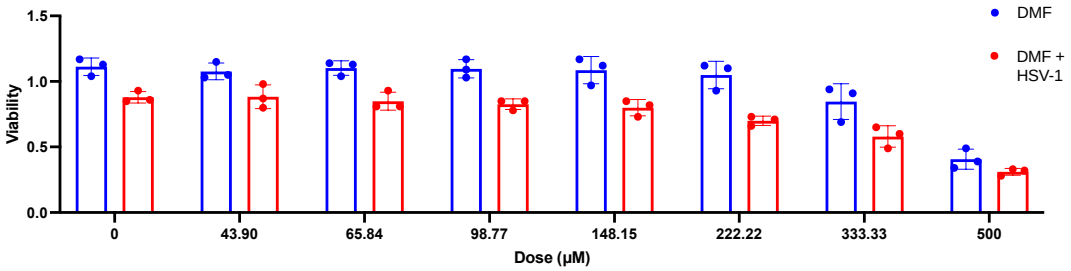
Viability
1.5
1.0
0.5
0.0
0
43.90
65.84
98.77
148.15
222.22
333.33
500
Dose (μM)
DMF
DMF +
HSV-1

C

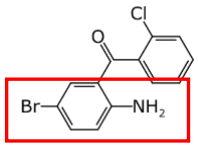
Cl
O
Br
NH2

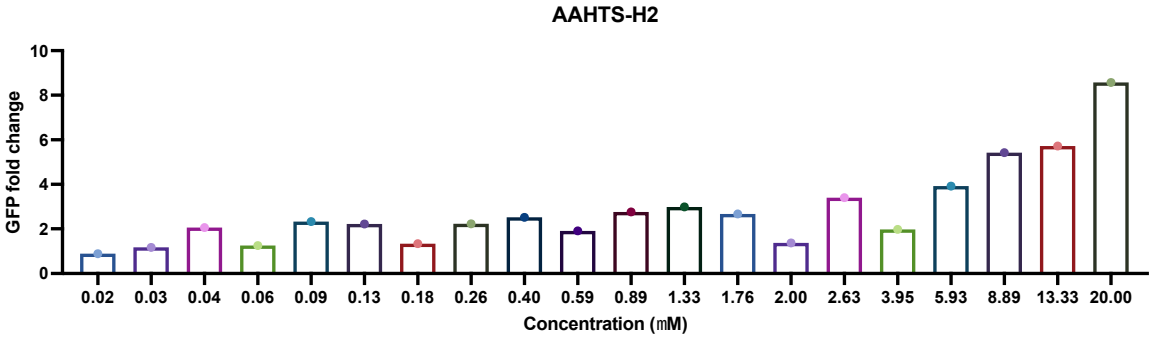
AAHTS-H2
GFP fold change
0
2
4
6
8
10
0.02
0.03
0.04
0.06
0.09
0.13
0.18
0.26
0.40
0.59
0.89
1.33
1.76
2.00
2.63
3.95
5.93
8.89
13.33
20.00
Concentration (mM)

D

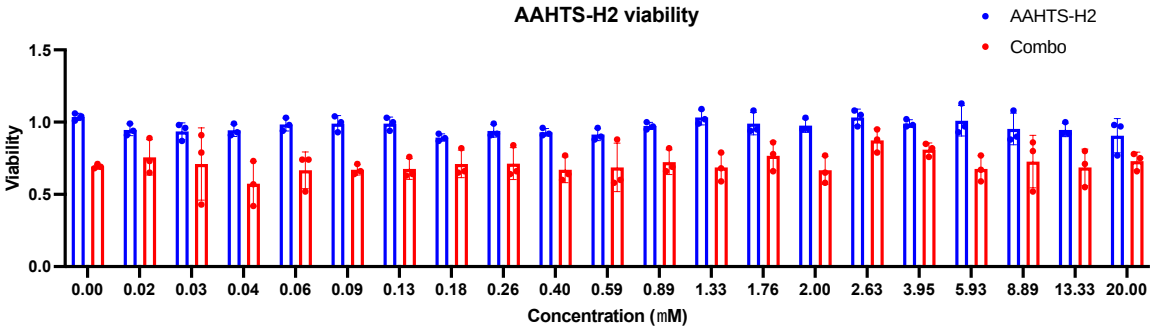
AAHTS-H2 viability
AAHTS-H2
Combo
Viability
0.0
0.5
1.0
1.5
0.00
0.02
0.03
0.04
0.06
0.09
0.13
0.18
0.26
0.40
0.59
0.89
1.33
1.76
2.00
2.63
3.95
5.93
8.89
13.33
20.00
Concentration (mM)

Figure 4.6: Validation of AAHTS-H2 compound on 786-0 cells

Human renal carcinoma (786-0) cells were treated with AAHTS-H2 compound for a duration of 4 hours, then infected with HSV.n212. GFP counts and viability assay were performed.

A

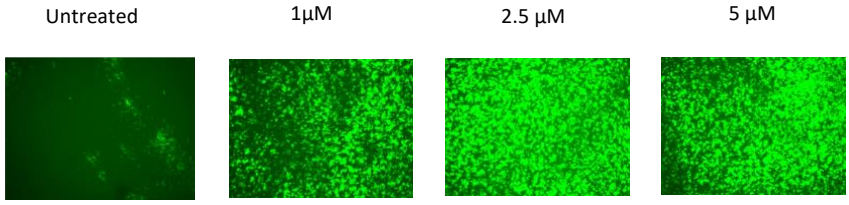
Untreated
1µM
2.5 µM
5 µM

B

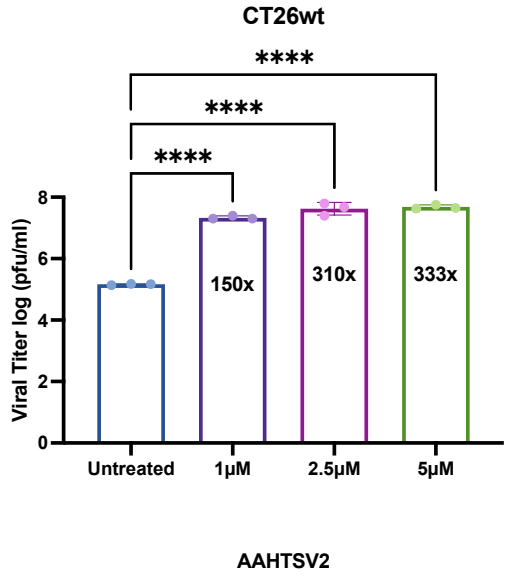
CT26wt
****
****
****
Viral Titer log (pfu/ml)
0
2
4
6
8
150x
310x
333x
Untreated
1µM
2.5µM
5µM
AAHTSV2

Figure 4.7: Assessing the impact of AAHTS-V2 on murine colon carcinoma.

Murine colon carcinoma (CT26.wt) cells were treated with AAHTSV2 compound for a duration of 4 hours, then infected with VSVΔ51. GFP counts **(A)** and viral titer were performed **(B) (**N=3 mean ± SEM; one-way ANOVA with Dunnett's multiple comparisons test compared to Mock)

The selective targeting of cancer tissues by oncolytic virotherapy represents a significant advantage over traditional treatment modalities. To ascertain whether AAHTS-V2 affects the specific infectivity of oncolytic VSVΔ51 in cancer cells without promoting viral replication in healthy tissues, an evaluation in ex vivo cultured tissues was undertaken. Mice were inoculated with murine colon carcinoma CT26.wt subcutaneously until tumours reached 1500mm^3 then tumour and healthy muscle tissues were harvested, cored and cultured. These cores were then infected with VSVΔ51, either with or without prior treatment with AAHTS-V2. Fluorescence microscopy images presented in Figure 4.8A depict the cores treated with AAHTS-V2 before infection with VSVΔ51. The fluorescent images, alongside the viral titration data shown in Figure 4.8B, reveals a pronounced increase in VSVΔ51 infectivity in the cancerous CT26.wt cores post-AAHTS-V2 treatment. Conversely, there was no enhancement in cores from healthy muscle, underscoring the preservation of the virus's cancer-selectivity even after AAHTS-V2 pre-treatment.

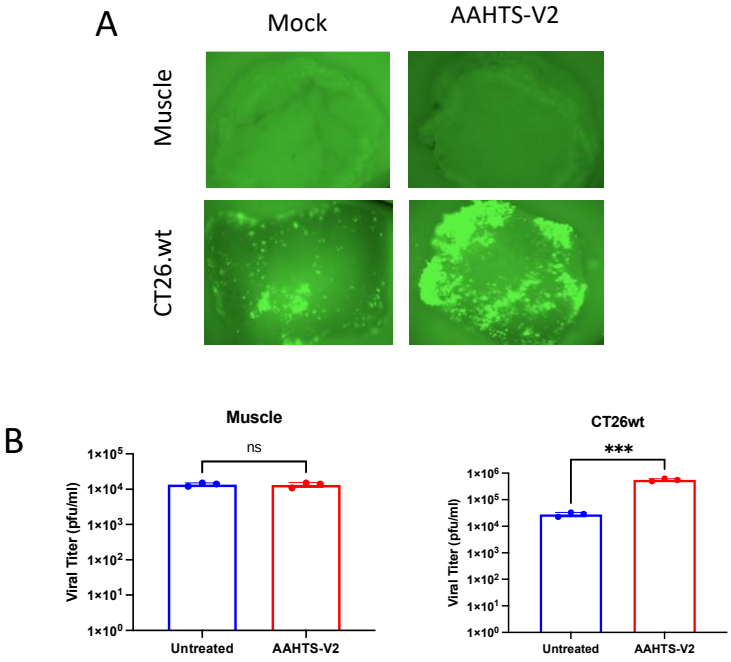
A
Mock
AAHTS-V2
Muscle
CT26.wt
B
Muscle
ns
Viral Titer (pfu/ml)
1×10^5
1×10^4
1×10^3
1×10^2
1×10^1
1×10^0
Untreated
AAHTS-V2
CT26wt
***
Viral Titer (pfu/ml)
1×10^6
1×10^5
1×10^4
1×10^3
1×10^2
1×10^1
1×10^0
Untreated
AAHTS-V2

Figure 4.8: AAHTS-V2 promotes VSVΔ51 infection in ex vivo models.

CT26.wt colon tumors were grown in BALB/c mice, once reaching a volume of 1500mm^3. Tissues were collected, cored. Clinical specimens were obtained and cored. Cores were treated with AAHTS-V2 then infected with VSVΔ51 3x10^4 (pfu/core). Fluorescent images were taken 24h post infection, and supernatants were collected at 24 hpi for viral titer quantification by plaque assay (n>5, mean ± SD; ***P<0.001 by two-tailed t-test).

4.4. Discussion

This study aimed to uncover novel synthetic compounds capable of sensitizing 786-0 renal carcinoma cells to oncolytic virotherapy, specifically employing VSVΔ51 and HSV-1 viruses engineered to express GFP. The rationale was grounded in the promise of oncolytic virotherapy as a selective and potent anticancer strategy, offering a potential complementary approach to conventional cancer therapies due to its dual capacity for direct oncolysis and induction of systemic anti-tumor immune responses. Our findings underscore the significant potential of leveraging chemical libraries to identify compounds that enhance the efficacy of oncolytic viruses, thereby amplifying their therapeutic index against cancer cells.

AAHTS-V2 emerged as a compound of particular interest, demonstrating a pronounced capacity to enhance VSVΔ51 infectivity in cancerous cells while sparing healthy tissue (Figure 4.8). This selective potentiation of oncolytic activity aligns with the core objectives of oncolytic virotherapy—maximizing tumoral virulence without compromising safety. The findings from our murine model experiments, particularly the retention of virus selectivity towards cancer cells even in the presence of AAHTS-V2, bolster the argument for further exploring this compound's mechanism and potential in oncolytic virotherapy enhancement.

AAHTS-H2 is another promising compound identified for HSV-1. Given the complex biology of HSV-1 and recent clinical advancements, finding novel compounds that play a role in enhancing replication or boosting the therapeutic efficacy of HSV-1 is of great interest in the oncolytic virotherapy field. It would be particularly interesting to delve deeper into

understanding the broader applicability, cancer selectivity, and potential mechanism of action of this compound analogously to AAHTS-V2.

While we successfully identified many potential lead molecules through the described screens, the study has several limitations affecting the outcomes. Although there were enhancements in GFP expression compared to DMSO-treated samples in the high-throughput screen, not all compounds achieving a GFP fold increase greater than 3 for VSVΔ51 or 2 for HSV.n212 reached statistical significance. This may be due to several factors in our screening setup. For example, control wells on the edges of the 96-well plate experienced media evaporation, introducing variability in viral infection and GFP expression. Additionally, using alamar blue (resazurin) to assess cell viability in HSV-infected samples was hindered by the longer incubation times needed for significant effects, which we did not extend due to concerns over cell health at high seeding densities of 30,000 cells per well. Lower densities led to variable GFP signals, impacting the reliability of measurements. Despite these issues, we validated one hit for each virus (AAHTS-V2 and AAHTS-H2), with more candidates currently undergoing validation. While not all hits are expected to validate due to assay limitations, the initial successes suggest a potential for a high validation rate.

Looking ahead, several avenues of investigation remain. The mechanism by which AAHTS-V2 and AAHTS-H2 enhances viral infectivity warrants detailed investigation, potentially involving genomic, proteomic, and metabolomic studies to elucidate the pathways modulated by the compounds. Finally, expanding the study to include other cancer cell lines and models

will be essential to validate the generality of the observed effects and to fine-tune the application of those compounds in oncolytic virotherapy.

One way to uncover the mechanisms of synthetic small molecules with unknown molecular targets is by a focused approach involving structural analysis and database searches. By employing cheminformatics tools like RDKit, we can analyze molecular structures and compare them against databases such as PubChem and DrugBank to identify similar structures with known targets. This strategy is geared towards pinpointing clinically approved compounds with structural similarities, offering insights into potential safety and efficacy profiles. Such comparative studies are pivotal for hypothesizing the biological targets of new compounds and guiding experimental validations, thereby accelerating their clinical applicability in enhancing oncolytic virotherapy.

In conclusion, our study represents a significant stride towards identifying new molecules that can lead to harnessing the full potential of oncolytic virotherapy in cancer treatment. By identifying and characterizing compounds that sensitize cancer cells to viral infection, we pave the way for novel therapeutic strategies that could significantly enhance patient outcomes in the fight against cancer.

4.5. Materials and Methods

Drugs

Throughout this study, we used a selected subset of molecules from a collection of synthetic compounds obtained from ChemDiv, totaling 3,200 compounds. Stock concentrations for these compounds were prepared at 1 mM in 100% DMSO, and we treated samples at a final concentration of 5 µM with 0.5% DMSO.

Cell lines

All cells in this study were obtained from ATCC. The cell cultures were maintained in Dulbecco's Modified Eagle's Medium (DMEM), obtained from HyClone (Waltham, Massachusetts) or Corning (Manassas, Virginia). To ensure ideal conditions for cell growth and sustainability, the medium was enriched with 10% fetal bovine serum (FBS) from VWR (Mississauga, Ontario) and 1% penicillin-streptomycin from Gibco. The cells were kept at a constant temperature of 37°C within a humidified incubator containing 5% CO2 and were regularly screened for mycoplasma infections using Hoechst staining and PCR techniques, with the PCR reagents sourced from Diamed (Mississauga, Ontario, Catalog # ABMG238).

Viruses

VSVΔ51 expressing GFP was used throughout this study. The propagation of all viruses was carried out on Vero cells and subsequently purified using 5%–50% OptiPrep (Sigma-Aldrich, St. Louis, MO) gradients. Viral titers were assessed using a standard plaque assay on Vero cells, following a published protocol [92].

HSV.n212 was obtained as a generous gift from Dr. Karen Mossman of McMaster University (Hamilton, Canada). HSV.n212 titers were determined by a standard plaque assay on Vero cells according to a previously published protocol [29]

Plaque assay

Vero cells were seeded in 12-well plates at a density of 3x10^5 cells per well and exposed to diluted infectious samples in serum-free DMEM (500 µL per well). After incubating for 60 minutes at 37°C in 5% CO2, the medium was replaced with a 1:1 mix of 1% agarose and 2× DMEM with 20% FBS overlay. Post a 24-hour incubation, plaques were fixed with methanol:acetic acid (3:1) for over an hour, stained with Coomassie Blue for 30 minutes, and then counted.

Cell viability assay

The assessment of cellular metabolic function was conducted using the Resazurin metabolic dye (Millipore Sigma, cat. SI03200), in accordance with the provided guidelines. A Resazurin solution, prepared to a 10% (v/v) final concentration, was introduced into the wells containing either treated or infected cell populations. Following this, a 2-4 hour incubation period was allowed, the duration of which was adjusted based on the particular cell line under investigation. Fluorescence readings were taken at an emission wavelength of 590 nm after excitation at 530 nm, utilizing a BioTek Microplate Reader (BioTek, Winooski, VT, USA) equipped with Gen5 2.07 software. The results were normalized to the average fluorescence of control wells that were neither infected nor treated.

Viral sensitizer score was calculated based on the following equation.

$$Log10\ \frac{Viability\ of\ drug\ alone}{Viability\ of\ drug + Virus}$$

Ex vivo models

CT26.wt colon cancer cells (3x 10^5) were injected into BALB/c mice. When the tumors grew to 1500 mm^3, the animals were humanely sacrificed to collect the necessary tissues. These tissues were then sectioned into 2 mm slices, and circular 2 mm diameter samples were obtained using a biopsy punch. These samples were incubated at 37°C with 5% CO2 in DMEM enriched with 10% serum, 30mM HEPES, 1% penicillin-streptomycin (v/v), and 0.25 mg/L amphotericin B. The tissue cores received AAHTS-V2 treatment for four hours before being exposed to VSVΔ51 at a concentration of 3 x 10^4 pfu/core. Fluorescence imaging was conducted 24 hours after infection using the EVOS Live Cell Imaging System (Thermo Fisher), and the supernatant's viral load was determined through a standard plaque assay.

Statistics

GraphPad Prism was the tool of choice for both graph creation and statistical analysis throughout our research. The statistical methods used for each data set are detailed in the legends accompanying the respective figures. To compare the averages between two distinct groups, we employed the two-tailed unpaired Student's t-test. When the analysis involved multiple groups, we resorted to one-way ANOVA, followed by Dunnett's or Tukey's post-

hoc tests for multiple comparisons. The symbol 'n' represents the count of biological replicates, and we report variability as the standard error of the mean (SEM). Statistical significance was attributed to p values below 0.05.

Chapter 5: Concluding Remarks

The challenge of tumor resistance significantly hampers the clinical efficacy of oncolytic virotherapy, a promising cancer treatment strategy that leverages oncolytic viruses to target and destroy cancer cells selectively [112]. Recognizing the urgent need to overcome this obstacle, our research introduces novel strategies aimed at sensitizing tumors to OV infection through the use of small molecules. We specifically explored the efficacy of DMF and TPF in enhancing the oncolytic potential of HSV-1 and VSVΔ51. DMF, known for its anti-tumor, immunomodulatory properties, and FDA approval for other indications [81], was shown to significantly increase HSV-1 propagation across various cancer cell lines, leading to enhanced viral oncolysis (Figure 2.1). Similarly, TPF emerged as a potent pharmacological tool, potentially outperforming DMF by downregulating key antiviral and pro-inflammatory genes, thus creating a more conducive environment for viral infection and oncolysis. Our work delves into the mechanisms by which these molecules modulate the immune response, including DMF's inhibition of the cellular response to type I interferon and TPF's inhibition of NF-κB nuclear translocation, offering mechanistic insights into their roles in overcoming tumor resistance to OV therapy. This thesis not only addresses a critical barrier to the success of oncolytic virotherapy but also opens new avenues for the development of more effective cancer treatments, underscoring the potential of combining OVs with small molecules to enhance therapeutic outcomes.

In Chapter 2 of the thesis, the role of DMF in enhancing the propagation of HSV-1 in cancer cells was thoroughly investigated, revealing significant implications for the field of oncolytic virotherapy. DMF, a small molecule with potent anti-tumor properties, immunomodulatory capabilities, and an FDA-approved status for the treatment of multiple sclerosis, demonstrates a versatile therapeutic potential in oncology. Our study showcases DMF's ability to notably augment HSV-1 propagation, evidenced by increased expression of virally encoded green fluorescent protein across various HSV-1 mutant strains (Figure S2.3). This leads to enhanced viral output and significantly improved oncolytic effects within multiple human and murine cancer cell lines, underscoring DMF's role in facilitating viral spread and cytotoxicity against cancer cells.

Beyond its direct effects on viral propagation, DMF exerts profound immunomodulatory effects that are pivotal in the context of oncolytic virotherapy. Specifically, DMF inhibits the cellular response to type I interferon, partly by reducing IFN production through the modulation of NF-κB pathways. This inhibition is crucial as it leads to a decreased expression of interferon-stimulated genes, which are often upregulated in OV-resistant tumors as a defense mechanism against viral infection. By dampening the antiviral response, DMF creates a more permissive environment for HSV-1 infection and replication in tumor cells, thereby enhancing the efficacy of oncolytic virotherapy.

In Chapter 3 of the thesis, the exploration shifts towards TPF, presenting it as a novel and potentially more potent pharmacological tool than DMF for enhancing the activity of oncolytic viruses. TPF's mechanism of action is particularly intriguing, as it demonstrates the ability to downregulate antiviral and pro-inflammatory genes, thereby creating a more conducive environment for viral oncolysis. This ability is crucial in the context of oncolytic virotherapy, where the innate immune response of cancer cells often acts as a barrier to effective viral infection and spread.

TPF's efficacy is rooted in its impact on the NF-κB pathway, a critical regulator of the immune response, including the expression of antiviral and pro-inflammatory genes. By inhibiting NF-κB nuclear translocation, TPF effectively reduces the expression of key antiviral genes such as IFN-β, MX2, and pro-inflammatory cytokines like IL6. This reduction in antiviral and inflammatory signaling is pivotal, as it diminishes the cancer cells' ability to mount an effective defense against oncolytic viruses, thereby enhancing viral spread, and oncolytic efficacy.

Furthermore, the study provides evidence that TPF, unlike DMF, may induce a shift in baseline NF-κB activity, leading to an elevated state of NF-κB nuclear translocation even in the absence of external stimuli. This paradoxical elevation of NF-κB activity could potentially contribute to the enhanced oncolytic activity observed with TPF, suggesting a complex interplay between NF-κB signaling and viral oncolysis.

The findings from Chapter 3 underscore the broader implications of TPF in the realm of gene therapy. Our research highlights the significant role of antiviral responses in impeding the efficiency of not only oncolytic virotherapy but also the infection capabilities of various non-replicating viral vectors, a crucial aspect for advancements in gene therapy. By expanding our investigation to include the impact of TPF on diverse viral vectors, we've laid groundwork indicating its potential wide-ranging benefits across gene therapy applications. This includes its use with engineered viruses such as replication-defective lentiviruses, adenoviruses, and adeno-associated viruses, which are integral to current clinical practices in cell therapy (e.g., Kymriah™), gene therapy (e.g., Luxturna™), and vector-vaccine development (e.g., COVISHIELD™). Notably, these vectors engage different methods for cell entry, gene delivery, and, in some cases, genomic integration, like lentiviruses. Our findings underscore the sensitivity of these diverse viral mechanisms to the antiviral effects triggered by type I interferon, suggesting a common vulnerability. However, the specific stages of the viral life cycle most affected by antiviral defenses, particularly in non-replicating viruses, warrant further investigation to deepen our understanding. Additionally, our results reveal a variable sensitivity to TPF among different cell and virus types, indicating complex interactions that affect TPF's ability to enhance viral infection efficiency in certain contexts (e.g., MRC5 cells with Lentivirus and Jurkat cells with Ad5). Moreover, akin to DMF, TPF's facilitation of oncolytic virus replication and spread was observed to be selective for tumor cells, suggesting a targeted approach in cancer treatment.

In chapter 4, the study explored the use of synthetic compounds to increase the sensitivity of 786-0 renal carcinoma cells to oncolytic viruses, VSVΔ51 and HSV-1, which are genetically engineered to express GFP. Highlighting oncolytic virotherapy's capacity for targeted cancer cell destruction and systemic immune response activation, the research identified compounds from chemical libraries that could boost the therapeutic efficacy of oncolytic viruses. Among these, AAHTS-V2 and AAHTS-H2 were notable for their ability to enhance VSVΔ51 and HSV.n212 infectivity in cancer cells respectively, suggesting a promising avenue to improve oncolytic virotherapy's effectiveness.

The study underscores the practicality of using chemical libraries to find sensitizers for oncolytic viruses, indicating a potential to expand cancer treatment options. Future directions include expanding validation, including other hits identified for VSVΔ51 and HSV-1. Additionally, investigating AAHTS-V2 and AAHTS-H2 mechanism of action, exploring combinations with other OVs, and testing on different cancer models as well as in an expanded array of normal tissues, and basic toxicological and pharmacokinetic assessment to pave the way for clinical application. This aspect is critical given other previously discovered synthetic compounds using high-throughput screening suffered from inadequate pharmacological properties, which could be overcome through medicinal chemistry and structure activity relationship studies [113]. This is notably an advantage of exploring clinically more advanced drugs such as DMF and TPF. Conversely, challenges relating to commercialization can create barriers in the context of known drugs repurposed for a new application such as what was described here in the context of OV therapy. Ultimately, the study contributes to the advancement of oncolytic virotherapy as a novel cancer treatment method, offering the potential to improve outcomes for cancer patients significantly.

In summary this thesis pushes the frontier of enhancing oncolytic virotherapy through innovative pharmacological agents and synthetic compounds, highlighting the potential utility of DMF and TPF, alongside the identification of novel compounds like AAHTS-V2 and AAHTS-H2 identified from chemical libraries. Together, these insights underscore a multi-faceted approach to refining oncolytic virotherapy, offering hope for more effective, targeted cancer treatments.

Contribution of collaborators

Chapter 2: Unlocking the Potential of Dimethyl Fumarate: Enhancing Oncolytic HSV-1 Efficacy for Wider Cancer Applications

Contribution: Conceptualization, A.A., and J.S.D.; Methodology, A.A., and J.S.D.; Investigation, A.A., M.T., R.A., Z.T. and A.C.; Writing – Original Draft, A.A.; Writing – Review & Editing, A.A., R.A. and J.S.D.; Funding Acquisition, J.S.D.; Supervision, R.A. and J.S.D.

Figure 2.1: AA was responsible for all figures.

Figure 2.2: AA was responsible for all figures. MT assisted with Fig. 2.2C and D

Figure 2.3: AA was responsible for all figures.

Figure 2.4: AA was responsible for all figures.

Figure 2.5: AA was responsible for all figures. MT and AC assisted with Fig. 2.5A and B

Figure 2.6: AA was responsible for all figures. MT, AC and ZT assisted with Fig. 2.6A, B and C.

AA wrote majority (over 90%) of the original manuscript.

Chapter 3: Tepilamide Fumarate as a Novel Potentiator of Virus-Based Therapy

Contribution: Conceptualization, A.A., and J.S.D.; Methodology, A.A., and J.S.D.; Investigation, A.A., M.S., R.A., B.W. and V.G.; Writing – Original Draft, A.A.; Writing –

Review & Editing, A.A., R.A. T.A. and J.S.D.; Funding Acquisition, J.S.D.; Supervision, R.A. and J.S.D.

Figure 3.1: AA was responsible for all figures.

Figure 3.2: AA was responsible for all figures.

Figure 2.3: AA was responsible for all figures. MS assisted with Fig. 2.3E

Figure 2.4: AA was responsible for all figures. BW assisted with Fig. 2.4C and D

Figure 2.6-8: RA was responsible for all figures.

Figure S3.4: AA & V.G. were responsible for all figures.

AA wrote majority (over 90%) of the original manuscript.

Chapter 4: High Throughput Screen Approach Identifies Several Novel Synthetic Compounds with the ability to Potentiate Oncolytic Virus Therapy

Contribution: Conceptualization, A.A., R.A, and J.S.D.; Methodology, A.A., and R.A.; Investigation, A.A., G.M., R.A., M.S.; Writing – Original Draft, A.A.; Writing – Review & Editing, A.A., R.A. and J.S.D.; Funding Acquisition, J.S.D.; Supervision, R.A. and J.S.D.

Figure 4.2-3 : AA was responsible for the visualization with the assistance of RA and GM.

Figure 4.4 : RA was responsible for the visualization with the assistance of MS.

Figure 4.45-6: AA was responsible for the visualization with the assistance of RA

Figure 4.7-8: AA was responsible for the figures.

Chapter 6: References

1. Cancer Statistics 2023. Canadian Cancer Statistics Advisory Committee in collaboration with the Canadian Cancer Society, Statistics Canada and the Public Health Agency of Canada. Toronto, ON: Canadian Cancer Society; 2023.;

2. Tian T, Olson S, Whitacre JM, Harding A. The origins of cancer robustness and evolvability. Integr Biol Quant Biosci Nano Macro. 2011 Jan;3(1):17–30.

3. Hanahan D. Hallmarks of Cancer: New Dimensions. Cancer Discov. 2022 Jan 1;12(1):31–46.

4. Chen DS, Mellman I. Oncology Meets Immunology: The Cancer-Immunity Cycle. Immunity. 2013 Jul 25;39(1):1–10.

5. Hanahan D, Weinberg RA. Hallmarks of Cancer: The Next Generation. Cell. 2011 Mar;144(5):646–74.

6. Postow MA, Sidlow R, Hellmann MD. Immune-Related Adverse Events Associated with Immune Checkpoint Blockade. N Engl J Med. 2018 Jan 11;378(2):158–68.

7. Morad G, Helmink BA, Sharma P, Wargo JA. Hallmarks of response, resistance, and toxicity to immune checkpoint blockade. Cell. 2021 Oct 14;184(21):5309–37.

8. Dobosz P, Dzieciątkowski T. The Intriguing History of Cancer Immunotherapy. Front Immunol [Internet]. 2019 Dec 17 [cited 2024 Apr 27];10. Available from: https://www.frontiersin.org/journals/immunology/articles/10.3389/fimmu.2019.02965/full

9. Fu LQ, Wang SB, Cai MH, Wang XJ, Chen JY, Tong XM, et al. Recent advances in oncolytic virus-based cancer therapy. Virus Res. 2019 Sep;270:197675.

10. Kelly E, Russell SJ. History of oncolytic viruses: genesis to genetic engineering. Mol Ther J Am Soc Gene Ther. 2007 Apr;15(4):651–9.

11. Malfitano AM, Di Somma S, Iannuzzi CA, Pentimalli F, Portella G. Virotherapy: From single agents to combinatorial treatments. Biochem Pharmacol. 2020 Jul;177:113986.

12. Russell SJ, Barber GN. Oncolytic Viruses as Antigen-Agnostic Cancer Vaccines. Cancer Cell. 2018 Apr 9;33(4):599–605.

13. Szpara ML, Van Doorslaer K. Mechanisms of DNA Virus Evolution. Encycl Virol. 2021;71–8.

14. Li K, Zhao Y, Hu X, Jiao J, Wang W, Yao H. Advances in the clinical development of oncolytic viruses. Am J Transl Res. 2022;14(6):4192–206.

15. Haseley A, Alvarez-Breckenridge C, Chaudhury AR, Kaur B. Advances in oncolytic virus therapy for glioma. Recent Patents CNS Drug Discov. 2009 Jan;4(1):1–13.

16. Poltronieri P, Sun B, Mallardo M. RNA Viruses: RNA Roles in Pathogenesis, Coreplication and Viral Load. Curr Genomics. 2015 Oct;16(5):327–35.

17. Smith S, Reuven N, Mohni KN, Schumacher AJ, Weller SK. Structure of the Herpes Simplex Virus 1 Genome: Manipulation of Nicks and Gaps Can Abrogate Infectivity and Alter the Cellular DNA Damage Response. J Virol. 2014 Sep;88(17):10146–56.

18. Shen Y, Nemunaitis J. Herpes simplex virus 1 (HSV-1) for cancer treatment. Cancer Gene Ther. 2006 Nov;13(11):975–92.

19. Martuza RL, Malick A, Markert JM, Ruffner KL, Coen DM. Experimental therapy of human glioma by means of a genetically engineered virus mutant. Science. 1991 May 10;252(5007):854–6.

20. Mineta T, Rabkin SD, Martuza RL. Treatment of malignant gliomas using ganciclovir-hypersensitive, ribonucleotide reductase-deficient herpes simplex viral mutant. Cancer Res. 1994 Aug 1;54(15):3963–6.

21. Yamada Y, Kimura H, Morishima T, Daikoku T, Maeno K, Nishiyama Y. The pathogenicity of ribonucleotide reductase-null mutants of herpes simplex virus type 1 in mice. J Infect Dis. 1991 Dec;164(6):1091–7.

22. Mineta T, Rabkin SD, Yazaki T, Hunter WD, Martuza RL. Attenuated multi-mutated herpes simplex virus-1 for the treatment of malignant gliomas. Nat Med. 1995 Sep;1(9):938–43.

23. Markert JM, Medlock MD, Rabkin SD, Gillespie GY, Todo T, Hunter WD, et al. Conditionally replicating herpes simplex virus mutant, G207 for the treatment of malignant glioma: results of a phase I trial. Gene Ther. 2000 May;7(10):867–74.

24. Todo T, Martuza RL, Rabkin SD, Johnson PA. Oncolytic herpes simplex virus vector with enhanced MHC class I presentation and tumor cell killing. Proc Natl Acad Sci U S A. 2001 May 22;98(11):6396–401.

25. Todo T, Ito H, Ino Y, Ohtsu H, Ota Y, Shibahara J, et al. Intratumoral oncolytic herpes virus G47Δ for residual or recurrent glioblastoma: a phase 2 trial. Nat Med. 2022 Aug;28(8):1630–9.

26. Andtbacka RHI, Kaufman HL, Collichio F, Amatruda T, Senzer N, Chesney J, et al. Talimogene Laherparepvec Improves Durable Response Rate in Patients With Advanced Melanoma. J Clin Oncol Off J Am Soc Clin Oncol. 2015 Sep 1;33(25):2780–8.

27. Kaufman HL, Shalhout SZ, Iodice G. Talimogene Laherparepvec: Moving From First-In-Class to Best-In-Class. Front Mol Biosci. 2022;9:834841.

28. Liu BL, Robinson M, Han ZQ, Branston RH, English C, Reay P, et al. ICP34.5 deleted herpes simplex virus with enhanced oncolytic, immune stimulating, and anti-tumour properties. Gene Ther. 2003 Feb;10(4):292–303.

29. Hummel JL, Safroneeva E, Mossman KL. The role of ICP0-Null HSV-1 and interferon signaling defects in the effective treatment of breast adenocarcinoma. Mol Ther J Am Soc Gene Ther. 2005 Dec;12(6):1101–10.

30. Mossman KL, Saffran HA, Smiley JR. Herpes simplex virus ICP0 mutants are hypersensitive to interferon. J Virol. 2000 Feb;74(4):2052–6.

31. Vesicular Stomatitis Virus - an overview | ScienceDirect Topics [Internet]. [cited 2024 Mar 28]. Available from: https://www.sciencedirect.com/topics/veterinary-science-and-veterinary-medicine/vesicular-stomatitis-virus

32. Sobol PT, Boudreau JE, Stephenson K, Wan Y, Lichty BD, Mossman KL. Adaptive antiviral immunity is a determinant of the therapeutic success of oncolytic virotherapy. Mol Ther J Am Soc Gene Ther. 2011 Feb;19(2):335–44.

33. Workenhe ST, Simmons G, Pol JG, Lichty BD, Halford WP, Mossman KL. Immunogenic HSV-mediated Oncolysis Shapes the Antitumor Immune Response and Contributes to Therapeutic Efficacy. Mol Ther. 2014 Jan;22(1):123–31.

34. Bishnoi S, Tiwari R, Gupta S, Byrareddy SN, Nayak D. Oncotargeting by Vesicular Stomatitis Virus (VSV): Advances in Cancer Therapy. Viruses. 2018 Feb 23;10(2):90.

35. Stojdl DF, Lichty BD, tenOever BR, Paterson JM, Power AT, Knowles S, et al. VSV strains with defects in their ability to shutdown innate immunity are potent systemic anti-cancer agents. Cancer Cell. 2003 Oct;4(4):263–75.

36. Bommareddy PK, Shettigar M, Kaufman HL. Integrating oncolytic viruses in combination cancer immunotherapy. Nat Rev Immunol. 2018 Aug;18(8):498–513.

37. Haralambieva I, Iankov I, Hasegawa K, Harvey M, Russell SJ, Peng KW. Engineering oncolytic measles virus to circumvent the intracellular innate immune response. Mol Ther J Am Soc Gene Ther. 2007 Mar;15(3):588–97.

38. Wong B, Bergeron A, Maznyi G, Ng K, Jirovec A, Birdi HK, et al. Pevonedistat, a First in-class NEDD8-activating Enzyme Inhibitor, sensitizes cancer cells to VSVΔ51 Oncolytic Virotherapy. Mol Ther J Am Soc Gene Ther. 2023 Sep 27;S1525-0016(23)00504-X.

39. Errington F, Steele L, Prestwich R, Harrington KJ, Pandha HS, Vidal L, et al. Reovirus activates human dendritic cells to promote innate antitumor immunity. J Immunol Baltim Md 1950. 2008 May 1;180(9):6018–26.

40. Fulci G, Dmitrieva N, Gianni D, Fontana EJ, Pan X, Lu Y, et al. Depletion of peripheral macrophages and brain microglia increases brain tumor titers of oncolytic viruses. Cancer Res. 2007 Oct 1;67(19):9398–406.

41. Altomonte J, Wu L, Chen L, Meseck M, Ebert O, García-Sastre A, et al. Exponential enhancement of oncolytic vesicular stomatitis virus potency by vector-mediated suppression of inflammatory responses in vivo. Mol Ther J Am Soc Gene Ther. 2008 Jan;16(1):146–53.

42. Lichty BD, Power AT, Stojdl DF, Bell JC. Vesicular stomatitis virus: re-inventing the bullet. Trends Mol Med. 2004 May;10(5):210–6.

43. Alain T, Lun X, Martineau Y, Sean P, Pulendran B, Petroulakis E, et al. Vesicular stomatitis virus oncolysis is potentiated by impairing mTORC1-dependent type I IFN production. Proc Natl Acad Sci U S A. 2010 Jan 26;107(4):1576–81.

44. Arulanandam R, Batenchuk C, Varette O, Zakaria C, Garcia V, Forbes NE, et al. Microtubule disruption synergizes with oncolytic virotherapy by inhibiting interferon translation and potentiating bystander killing. Nat Commun. 2015 Mar 30;6:6410.

45. Selman M, Ou P, Rousso C, Bergeron A, Krishnan R, Pikor L, et al. Dimethyl fumarate potentiates oncolytic virotherapy through NF-κB inhibition. Sci Transl Med. 2018 Jan 24;10(425):eaao1613.

46. Alwithenani A, Taha Z, Thomson M, Chen A, Wong B, Arulanandam R, et al. Unlocking the potential of dimethyl fumarate: enhancing oncolytic HSV-1 efficacy for wider cancer applications. Front Immunol. 2023;14:1332929.

47. Nguyên TLA, Abdelbary H, Arguello M, Breitbach C, Leveille S, Diallo JS, et al. Chemical targeting of the innate antiviral response by histone deacetylase inhibitors renders refractory cancers sensitive to viral oncolysis. Proc Natl Acad Sci. 2008 Sep 30;105(39):14981–6.

48. Panne D, Maniatis T, Harrison SC. An atomic model of the interferon-beta enhanceosome. Cell. 2007 Jun 15;129(6):1111–23.

49. Honda K, Takaoka A, Taniguchi T. Type I interferon [corrected] gene induction by the interferon regulatory factor family of transcription factors. Immunity. 2006 Sep;25(3):349–60.

50. Takaoka A, Yanai H. Interferon signalling network in innate defence. Cell Microbiol. 2006 Jun;8(6):907–22.

51. Kurokawa C, Iankov ID, Anderson SK, Aderca I, Leontovich AA, Maurer MJ, et al. Constitutive Interferon Pathway Activation in Tumors as an Efficacy Determinant Following Oncolytic Virotherapy. J Natl Cancer Inst. 2018 Oct 1;110(10):1123–32.

52. Escobar-Zarate D, Liu YP, Suksanpaisan L, Russell SJ, Peng KW. Overcoming cancer cell resistance to VSV oncolysis with JAK1/2 inhibitors. Cancer Gene Ther. 2013 Oct;20(10):582–9.

53. Du Z, Wei L, Murti A, Pfeffer SR, Fan M, Yang CH, et al. Non-conventional signal transduction by type 1 interferons: the NF-kappaB pathway. J Cell Biochem. 2007 Dec 1;102(5):1087–94.

54. Cataldi M, Shah NR, Felt SA, Grdzelishvili VZ. Breaking resistance of pancreatic cancer cells to an attenuated vesicular stomatitis virus through a novel activity of IKK inhibitor TPCA-1. Virology. 2015 Nov;485:340–54.

55. Du Z, Whitt MA, Baumann J, Garner JM, Morton CL, Davidoff AM, et al. Inhibition of type I interferon-mediated antiviral action in human glioma cells by the IKK inhibitors BMS-345541 and TPCA-1. J Interferon Cytokine Res Off J Int Soc Interferon Cytokine Res. 2012 Aug;32(8):368–77.

56. Gilmore TD, Herscovitch M. Inhibitors of NF-kappaB signaling: 785 and counting. Oncogene. 2006 Oct 30;25(51):6887–99.

57. Ben Yebdri F, Van Grevenynghe J, Tang VA, Goulet ML, Wu JH, Stojdl DF, et al. Triptolide-mediated inhibition of interferon signaling enhances vesicular stomatitis virus-based oncolysis. Mol Ther J Am Soc Gene Ther. 2013 Nov;21(11):2043–53.

58. Burness CB, Deeks ED. Dimethyl fumarate: a review of its use in patients with relapsing-remitting multiple sclerosis. CNS Drugs. 2014 Apr;28(4):373–87.

59. Litjens NHR, van Strijen E, van Gulpen C, Mattie H, van Dissel JT, Thio HB, et al. In vitro pharmacokinetics of anti-psoriatic fumaric acid esters. BMC Pharmacol. 2004 Oct 12;4:22.

60. Peng H, Guerau-de-Arellano M, Mehta VB, Yang Y, Huss DJ, Papenfuss TL, et al. Dimethyl fumarate inhibits dendritic cell maturation via nuclear factor κB (NF-κB) and extracellular signal-regulated kinase 1 and 2 (ERK1/2) and mitogen stress-activated kinase 1 (MSK1) signaling. J Biol Chem. 2012 Aug 10;287(33):28017–26.

61. McGuire VA, Ruiz-Zorrilla Diez T, Emmerich CH, Strickson S, Ritorto MS, Sutavani RV, et al. Dimethyl fumarate blocks pro-inflammatory cytokine production via inhibition of TLR induced M1 and K63 ubiquitin chain formation. Sci Rep. 2016 Aug 8;6:31159.

62. Kastrati I, Siklos MI, Calderon-Gierszal EL, El-Shennawy L, Georgieva G, Thayer EN, et al. Dimethyl Fumarate Inhibits the Nuclear Factor κB Pathway in Breast Cancer Cells by Covalent Modification of p65 Protein. J Biol Chem. 2016 Feb 12;291(7):3639–47.

63. Takaya K, Suzuki T, Motohashi H, Onodera K, Satomi S, Kensler TW, et al. Validation of the multiple sensor mechanism of the Keap1-Nrf2 system. Free Radic Biol Med. 2012 Aug 15;53(4):817–27.

64. Kansanen E, Kuosmanen SM, Leinonen H, Levonen AL. The Keap1-Nrf2 pathway: Mechanisms of activation and dysregulation in cancer. Redox Biol. 2013 Jan 18;1(1):45–9.

65. Saidu NEB, Noé G, Cerles O, Cabel L, Kavian-Tessler N, Chouzenoux S, et al. Dimethyl Fumarate Controls the NRF2/DJ-1 Axis in Cancer Cells: Therapeutic Applications. Mol Cancer Ther. 2017 Mar 1;16(3):529–39.

66. Dibbert S, Clement B, Skak-Nielsen T, Mrowietz U, Rostami-Yazdi M. Detection of fumarate-glutathione adducts in the portal vein blood of rats: evidence for rapid dimethylfumarate metabolism. Arch Dermatol Res. 2013 Jul;305(5):447–51.

67. Loewe R, Valero T, Kremling S, Pratscher B, Kunstfeld R, Pehamberger H, et al. Dimethylfumarate impairs melanoma growth and metastasis. Cancer Res. 2006 Dec 15;66(24):11888–96.

68. Yamazoe Y, Tsubaki M, Matsuoka H, Satou T, Itoh T, Kusunoki T, et al. Dimethylfumarate inhibits tumor cell invasion and metastasis by suppressing the expression and activities of matrix metalloproteinases in melanoma cells. Cell Biol Int. 2009 Oct;33(10):1087–94.

69. Han G, Zhou Q. Dimethylfumarate induces cell cycle arrest and apoptosis via regulating intracellular redox systems in HeLa cells. In Vitro Cell Dev Biol Anim. 2016 Dec;52(10):1034–41.

70. X X, Y Z, Cy M, Xm X, Yq Z, Cg W, et al. Dimethyl fumarate induces necroptosis in colon cancer cells through GSH depletion/ROS increase/MAPKs activation pathway. Br J Pharmacol [Internet]. 2015 Aug [cited 2023 Aug 31];172(15). Available from: https://pubmed.ncbi.nlm.nih.gov/25953698/

71. Mrowietz U, Kircik L, Reich K, Munjal S, Shenoy S, Lebwohl M. Tepilamide Fumarate (PPC-06) Extended Release Tablets in Patients with Moderate-to-Severe Plaque Psoriasis: Safety and Efficacy Results from the Randomized, Double-blind, Placebo-controlled AFFIRM Study. J Clin Aesthetic Dermatol. 2022 Jan;15(1):53–8.

72. Mahoney DJ, Lefebvre C, Allan K, Brun J, Sanaei CA, Baird S, et al. Virus-tumor interactome screen reveals ER stress response can reprogram resistant cancers for oncolytic virus-triggered caspase-2 cell death. Cancer Cell. 2011 Oct 18;20(4):443–56.

73. Diallo JS, Boeuf FL, Lai F, Cox J, Vaha-Koskela M, Abdelbary H, et al. A High-throughput Pharmacoviral Approach Identifies Novel Oncolytic Virus Sensitizers. Mol Ther. 2010 Jun;18(6):1123–9.

74. Ilkow CS, Swift SL, Bell JC, Diallo JS. From Scourge to Cure: Tumour-Selective Viral Pathogenesis as a New Strategy against Cancer. PLoS Pathog. 2014 Jan 16;10(1):e1003836.

75. Russell SJ, Peng KW, Bell JC. Oncolytic virotherapy. Nat Biotechnol. 2012 Jul;30(7):658–70.

76. Lichty BD, Breitbach CJ, Stojdl DF, Bell JC. Going viral with cancer immunotherapy. Nat Rev Cancer. 2014 Aug;14(8):559–67.

77. Randazzo BP, Bhat MG, Kesari S, Fraser NW, Moira Brown S. Treatment of Experimental Subcutaneous Human Melanoma with a Replication-Restricted Herpes Simplex Virus Mutant. J Invest Dermatol. 1997 Jun 1;108(6):933–7.

78. Saha D, Martuza RL, Rabkin SD. Macrophage Polarization Contributes to Glioblastoma Eradication by Combination Immunovirotherapy and Immune Checkpoint Blockade. Cancer Cell. 2017 Aug 14;32(2):253-267.e5.

79. Liu YP, Suksanpaisan L, Steele MB, Russell SJ, Peng KW. Induction of antiviral genes by the tumor microenvironment confers resistance to virotherapy. Sci Rep. 2013 Aug 7;3(1):2375.

80. Selman M, Rousso C, Bergeron A, Son HH, Krishnan R, El-Sayes NA, et al. Multi-modal Potentiation of Oncolytic Virotherapy by Vanadium Compounds. Mol Ther. 2018 Jan 3;26(1):56–69.

81. Al-Jaderi Z, Maghazachi AA. Utilization of Dimethyl Fumarate and Related Molecules for Treatment of Multiple Sclerosis, Cancer, and Other Diseases. Front Immunol [Internet]. 2016 [cited 2023 Aug 31];7. Available from: https://www.frontiersin.org/articles/10.3389/fimmu.2016.00278

82. Nicolay JP, Müller-Decker K, Schroeder A, Brechmann M, Möbs M, Géraud C, et al. Dimethyl fumarate restores apoptosis sensitivity and inhibits tumor growth and metastasis in CTCL by targeting NF-κB. Blood. 2016 Aug 11;128(6):805–15.

83. Kaluzki I, Hrgovic I, Hailemariam-Jahn T, Doll M, Kleemann J, Valesky EM, et al. Dimethylfumarate inhibits melanoma cell proliferation via p21 and p53 induction and bcl-2 and cyclin B1 downregulation. Tumour Biol J Int Soc Oncodevelopmental Biol Med. 2016 Oct;37(10):13627–35.

84. Gillard GO, Collette B, Anderson J, Chao J, Scannevin RH, Huss DJ, et al. DMF, but not other fumarates, inhibits NF-κB activity in vitro in an Nrf2-independent manner. J Neuroimmunol. 2015 Jun 15;283:74–85.

85. Gu B, DeAngelis LM. Enhanced cytotoxicity of bioreductive antitumor agents with dimethyl fumarate in human glioblastoma cells. Anticancer Drugs. 2005 Feb;16(2):167–74.

86. Bomprezzi R. Dimethyl fumarate in the treatment of relapsing-remitting multiple sclerosis: an overview. Ther Adv Neurol Disord. 2015 Jan;8(1):20–30.

87. Ghoreschi K, Brück J, Kellerer C, Deng C, Peng H, Rothfuss O, et al. Fumarates improve psoriasis and multiple sclerosis by inducing type II dendritic cells. J Exp Med. 2011 Oct 24;208(11):2291–303.

88. Valero T, Steele S, Neumüller K, Bracher A, Niederleithner H, Pehamberger H, et al. Combination of Dacarbazine and Dimethylfumarate Efficiently Reduces Melanoma Lymph Node Metastasis. J Invest Dermatol. 2010 Apr;130(4):1087–94.

89. Wu Z, Zheng Y, Sheng J, Han Y, Yang Y, Pan H, et al. CD3+CD4-CD8- (Double-Negative) T Cells in Inflammation, Immune Disorders and Cancer. Front Immunol [Internet]. 2022 [cited 2023 Oct 2];13. Available from: https://www.frontiersin.org/articles/10.3389/fimmu.2022.816005

90. Wu Q, Wang Q, Mao G, Dowling CA, Lundy SK, Mao-Draayer Y. Dimethyl Fumarate Selectively Reduces Memory T Cells and Shifts the Balance between Th1/Th17 and Th2 in Multiple Sclerosis Patients. J Immunol. 2017 Apr 15;198(8):3069–80.

91. Keller BA, Laight BJ, Varette O, Broom A, Wedge MÈ, McSweeney B, et al. Personalized oncology and BRAFK601N melanoma: model development, drug discovery, and clinical correlation. J Cancer Res Clin Oncol. 2021 May;147(5):1365–78.

92. Diallo JS, Vähä-Koskela M, Le Boeuf F, Bell J. Propagation, purification, and in vivo testing of oncolytic vesicular stomatitis virus strains. Methods Mol Biol Clifton NJ. 2012;797:127–40.

93. Kaufman HL, Kohlhapp FJ, Zloza A. Oncolytic viruses: a new class of immunotherapy drugs. Nat Rev Drug Discov. 2015 Sep;14(9):642–62.

94. Arulanandam R, Batenchuk C, Angarita FA, Ottolino-Perry K, Cousineau S, Mottashed A, et al. VEGF-Mediated Induction of PRD1-BF1/Blimp1 Expression Sensitizes Tumor Vasculature to Oncolytic Virus Infection. Cancer Cell. 2015 Aug 10;28(2):210–24.

95. Alsharifi M, Müllbacher A, Regner M. Interferon type I responses in primary and secondary infections. Immunol Cell Biol. 2008;86(3):239–45.

96. Matveeva OV, Chumakov PM. Defects in interferon pathways as potential biomarkers of sensitivity to oncolytic viruses. Rev Med Virol. 2018 Nov;28(6):e2008.

97. Active-site mTOR inhibitors augment HSV1-dICP0 infection in cancer cells via dysregulated eIF4E/4E-BP axis | PLOS Pathogens [Internet]. [cited 2023 Dec 16]. Available from: https://journals.plos.org/plospathogens/article?id=10.1371/journal.ppat.1007264

98. Diallo JS, Roy D, Abdelbary H, De Silva N, Bell JC. Ex vivo infection of live tissue with oncolytic viruses. J Vis Exp JoVE. 2011 Jun 25;(52):2854.

99. Ali S, Kjeken R, Niederlaender C, Markey G, Saunders TS, Opsata M, et al. The European Medicines Agency Review of Kymriah (Tisagenlecleucel) for the Treatment of Acute Lymphoblastic Leukemia and Diffuse Large B-Cell Lymphoma. The Oncologist. 2020 Feb;25(2):e321–7.

100. Keeler AM, Flotte TR. Recombinant Adeno-Associated Virus Gene Therapy in Light of Luxturna (and Zolgensma and Glybera): Where Are We, and How Did We Get Here? Annu Rev Virol. 2019 Sep 29;6(1):601–21.

101. Knoll MD, Wonodi C. Oxford-AstraZeneca COVID-19 vaccine efficacy. Lancet Lond Engl. 2021 Jan 9;397(10269):72–4.

102. Garcia V, Krishnan R, Davis C, Batenchuk C, Le Boeuf F, Abdelbary H, et al. High-throughput Titration of Luciferase-expressing Recombinant Viruses. J Vis Exp JoVE. 2014 Sep 19;(91):51890.

103. Pfaffl MW. A new mathematical model for relative quantification in real-time RT-PCR. Nucleic Acids Res. 2001 May 1;29(9):e45.

104. Fukuhara H, Ino Y, Todo T. Oncolytic virus therapy: A new era of cancer treatment at dawn. Cancer Sci. 2016 Oct;107(10):1373–9.

105. Wilcox ME, Yang W, Senger D, Rewcastle NB, Morris DG, Brasher PM, et al. Reovirus as an oncolytic agent against experimental human malignant gliomas. J Natl Cancer Inst. 2001 Jun 20;93(12):903–12.

106. Mansour M, Palese P, Zamarin D. Oncolytic specificity of Newcastle disease virus is mediated by selectivity for apoptosis-resistant cells. J Virol. 2011 Jun;85(12):6015–23.

107. Zitvogel L, Galluzzi L, Kepp O, Smyth MJ, Kroemer G. Type I interferons in anticancer immunity. Nat Rev Immunol. 2015 Jul;15(7):405–14.

108. Raja J, Ludwig JM, Gettinger SN, Schalper KA, Kim HS. Oncolytic virus immunotherapy: future prospects for oncology. J Immunother Cancer. 2018 Dec 4;6(1):140.

109. Larrieux A, Sanjuán R. Cellular resistance to an oncolytic virus is driven by chronic activation of innate immunity. iScience. 2023 Jan 20;26(1):105749.

110. Liang M, Wang J, Wu C, Wu M, Hu J, Dai J, et al. Targeting matrix metalloproteinase MMP3 greatly enhances oncolytic virus mediated tumor therapy. Transl Oncol. 2021 Dec;14(12):101221.

111. Shalhout SZ, Miller DM, Emerick KS, Kaufman HL. Therapy with oncolytic viruses: progress and challenges. Nat Rev Clin Oncol. 2023 Mar;20(3):160–77.

112. Gujar S, Bell J, Diallo JS. SnapShot: Cancer Immunotherapy with Oncolytic Viruses. Cell. 2019 Feb 21;176(5):1240-1240.e1.

113. First-in-class small molecule potentiators of cancer virotherapy - Google Search [Internet]. [cited 2024 Apr 9]. Available from: https://www.google.com/search?client=safari&rls=en&q=First-in-class+small+molecule+potentiators+of+cancer+virotherapy&ie=UTF-8&oe=UTF-8

Appendix A Chapter 2: Supplemental information

Unlocking the Potential of Dimethyl Fumarate: Enhancing Oncolytic HSV-1 Efficacy for Wider Cancer Applications

Akram Alwithenani[1,2,3], Zaid Taha[1,2], Max Thomson[1], Andrew Chen[1], Boaz Wong[1,2], Rozanne Arulanandam[1], Jean-Simon Diallo[1,2]

[1]Centre for Cancer Therapeutics, Ottawa Hospital Research Institute, Ottawa, Ontario, K1H 8L6, Canada.

[2]Department of Biochemistry, Microbiology, and Immunology, Faculty of Medicine, University of Ottawa, Ontario, K1H 8M5, Canada

[3]Department of Clinical Laboratory Science, Faculty of Applied Medical Science, Umm Al-Qura University, Makkah, Saudi Arabia

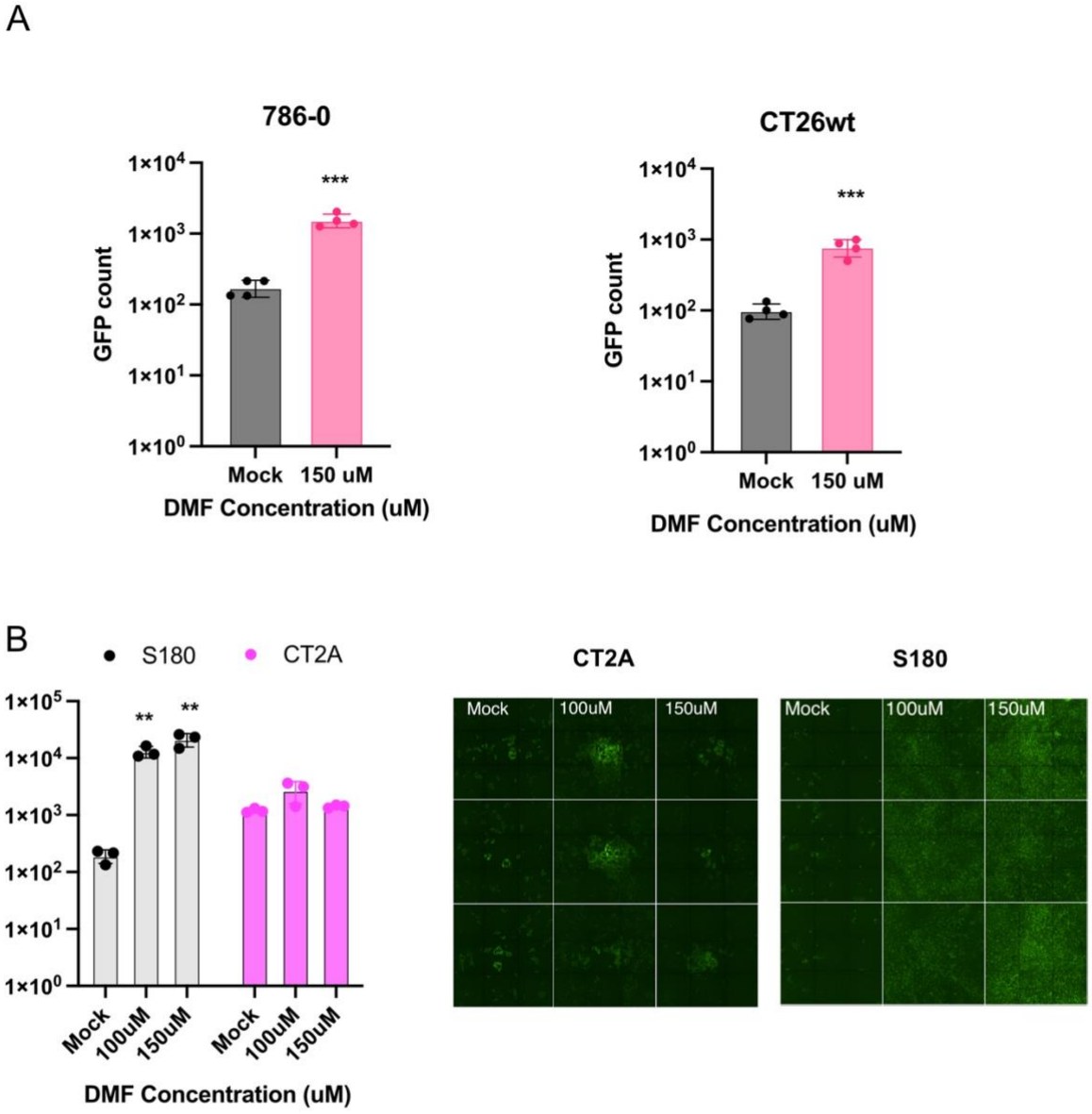
A
786-0
GFP count
1×10^4
1×10^3
1×10^2
1×10^1
1×10^0
***
Mock
150 uM
DMF Concentration (uM)
CT26wt
GFP count
1×10^4
1×10^3
1×10^2
1×10^1
1×10^0
***
Mock
150 uM
DMF Concentration (uM)
B
S180
CT2A
GFP count
1×10^5
1×10^4
1×10^3
1×10^2
1×10^1
1×10^0
**
**
Mock
100uM
150uM
Mock
100uM
150uM
DMF Concentration (uM)
CT2A
Mock
100uM
150uM
S180
Mock
100uM
150uM

Figure S2.1: DMF enhances GFP of HSV.n212 in Several cancer cell lines.

(A) representative GFP counts and images of 786-0 and CT26.wt cells upon treatment as described in Figure 1. (n = 3; mean ± SD; two-tailed t-test; *P < 0.05, ***P < 0.001). **(B)** GFP count and florescent images of CT2A and S180 Cells upon treatment as described in Figure 1. [n = 3; mean ± SD; *P < 0.05, ***P < 0.001, one-way analysis of variance (ANOVA), as compared to the untreated condition].

Table S2.1: Synergistic Effect of DMF + HSV.n212 in CT26.wt Model. This table presents the Combination Index Score (CSI) for the combined treatment of DMF and HSV.n212, specifically in their capacity to induce cell death. The data was analyzed utilizing the Compusyn software. The computation of the combination index was executed through a predictive algorithm. Notably, a score below 1 within this framework signifies a synergistic effect under the specified condition.

Dose DMF (uM)	**Dose HSV.n212 (MOI)**	**Effect**	**CI**
50	0.01	0.85	0.72
100	0.01	0.66	0.71
150	0.01	0.48	0.77
222	0.01	0.2	0.72

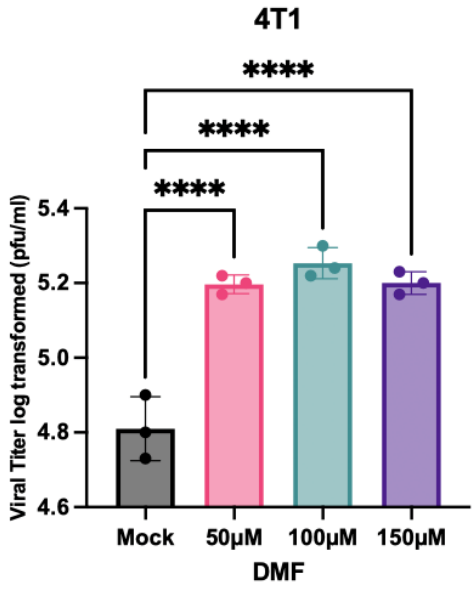
4T1
****
****
****
Viral Titer log transformed (pfu/ml)
5.4
5.2
5.0
4.8
4.6
Mock
50μM
100μM
150μM
DMF

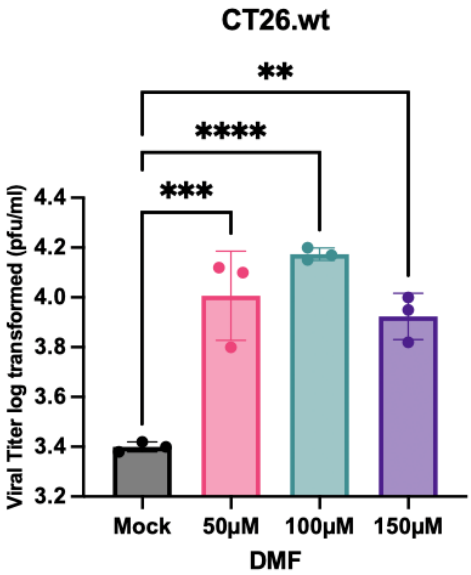
CT26.wt
**
****
***
Viral Titer log transformed (pfu/ml)
4.4
4.2
4.0
3.8
3.6
3.4
3.2
Mock
50μM
100μM
150μM
DMF

Figure S2.2: DMF enhances HSVd810.

Murine mammary carcinoma (4T1) and murine colon carcinoma (CT26.wt) cell lines were pretreated with DMF at various concentrations (0uM, 50uM, 100uM, 150uM) and four hour later infected with HSV.d810 at MOI of (0.1). Corresponding viral titers were determined 48 hours after infection from pellets. Florescence images were taken from all conditions. [n = 3; mean ± SD; *P < 0.05, ***P < 0.001, one-way analysis of variance (ANOVA), as compared to the untreated condition].

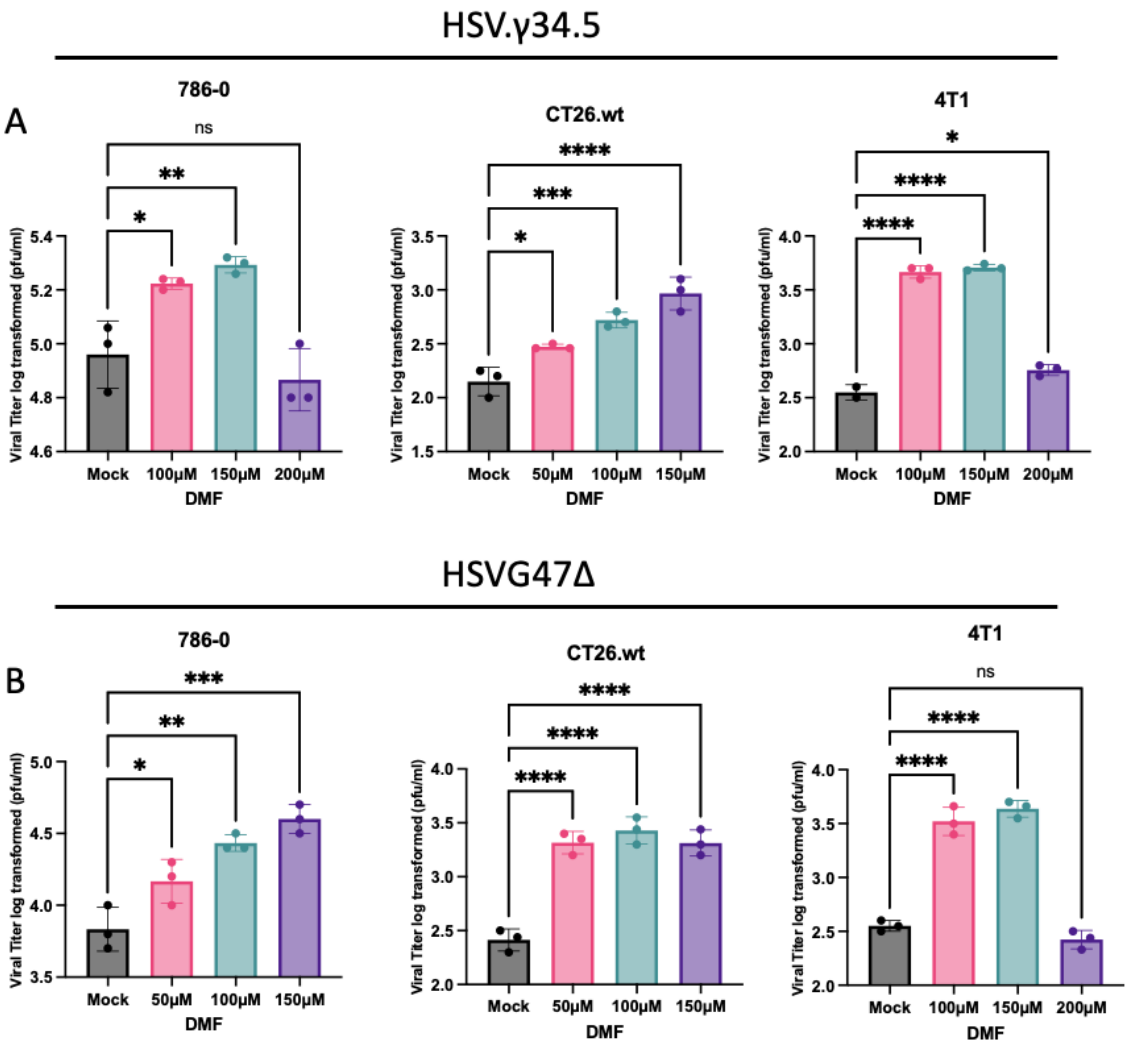
HSV.γ34.5
A
786-0
ns
**
*
Viral Titer log transformed (pfu/ml)
5.4
5.2
5.0
4.8
4.6
Mock
100μM
150μM
200μM
DMF
CT26.wt
****
***
*
3.5
3.0
2.5
2.0
1.5
Mock
50μM
100μM
150μM
DMF
4T1
*
****
****
4.0
3.5
3.0
2.5
2.0
Mock
100μM
150μM
200μM
DMF
HSVG47Δ
B
786-0
***
**
*
5.0
4.5
4.0
3.5
Mock
50μM
100μM
150μM
DMF
CT26.wt
****
****
****
4.0
3.5
3.0
2.5
2.0
Mock
50μM
100μM
150μM
DMF
4T1
ns
****
****
4.0
3.5
3.0
2.5
2.0
Mock
100μM
150μM
200μM
DMF

Figure S2.3: DMF enhances HSVγ34.5 and HSVG47Δ.

Murine mammary carcinoma (4T1) and other murine and human cell lines were pretreated with DMF at various concentrations (0uM, 50uM, 100uM, 150uM) and four hour later infected with HSV.γ34.5 at MO of (0.01) as shown in (A) or HSVG47Δ at MOI of (0.01) as shown in (B). Corresponding viral titers were determined 48 hours after infection from pellets. Florescence images were taken from all conditions. [n = 3; mean ± SD; *P < 0.05, ***P < 0.001, one-way analysis of variance (ANOVA), as compared to the untreated condition].

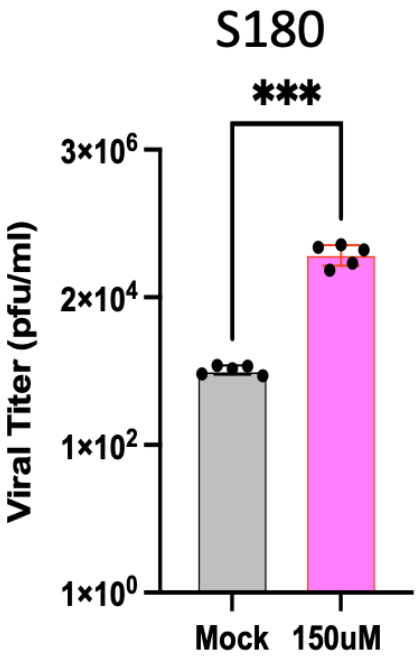
S180
***
3×10^6
2×10^4
1×10^2
1×10^0
Viral Titer (pfu/ml)
Mock
150uM

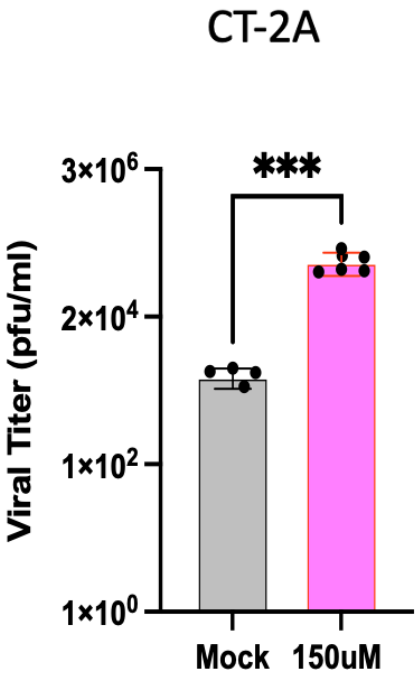
CT-2A
***
3×10^6
2×10^4
1×10^2
1×10^0
Viral Titer (pfu/ml)
Mock
150uM

Figure S2.4: DMF promotes HSV.n212 infection in S180 and CT2A tumour cores.

Infectious viral particles were quantified from S180 and CT2A tumour cores upon treatment as described in Figure 2 by standard plaque assay. (n = 5; mean ± SD; two-tailed t-test).

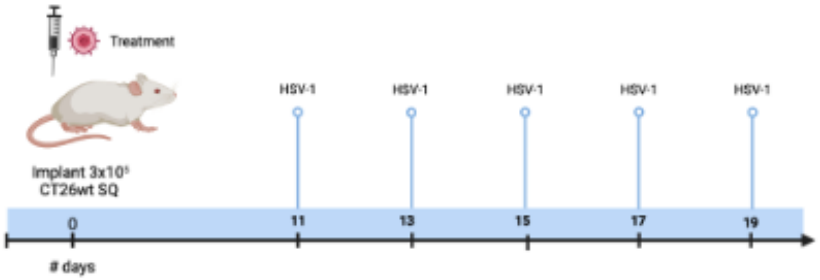
Treatment
HSV-1
HSV-1
HSV-1
HSV-1
HSV-1
Implant 3x10⁵
CT26wt SQ
0
11
13
15
17
19
days

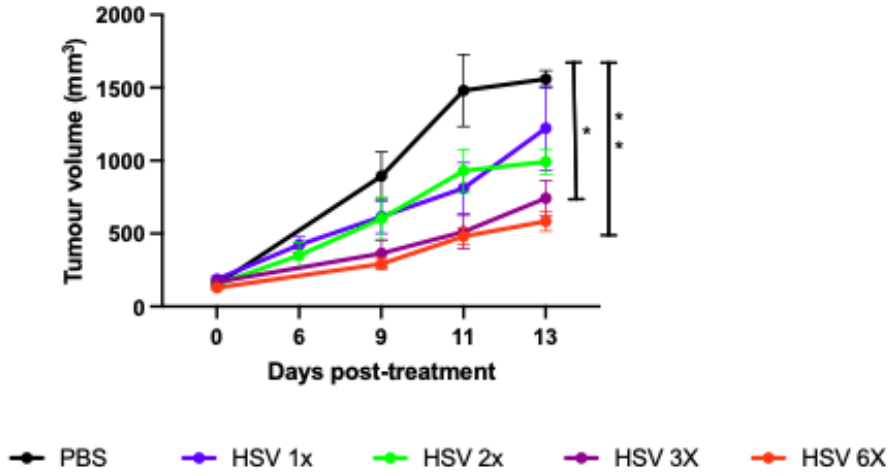
Tumour volume (mm³)
2000
1500
1000
500
0
0
6
9
11
13
Days post-treatment
*
*
*
PBS
HSV 1x
HSV 2x
HSV 3X
HSV 6X

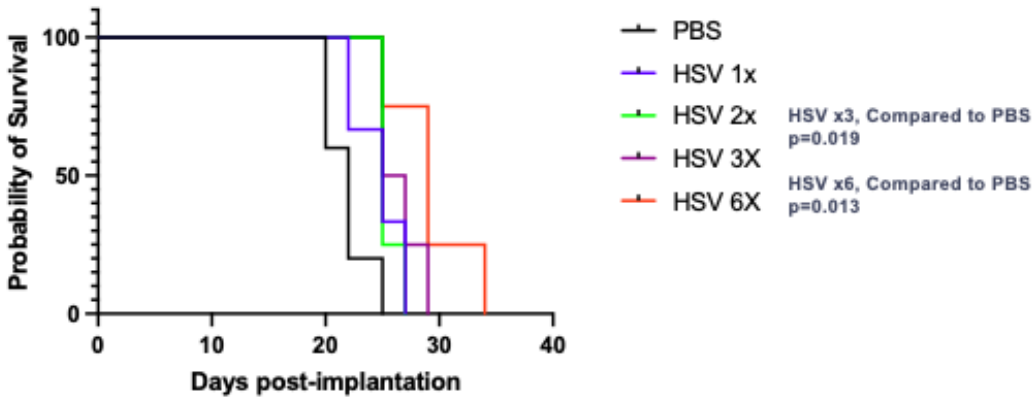
Probability of Survival
100
50
0
0
10
20
30
40
Days post-implantation
PBS
HSV 1x
HSV 2x
HSV 3X
HSV 6X
HSV x3, Compared to PBS
p=0.019
HSV x6, Compared to PBS
p=0.013

Figure S2.5: HSV.n212 dose optimization in vivo.

BALB/c mice were implanted with 3×10^5 CT26.wt cells. Once tumors were ~100 mm^3, mice were treated with several doses as indicated in the diagram with the regimen of HSV.n212 (1 x 10^8 pfu) or PBS (intratumorally). Tumor growth and survival (endpoint tumor size of 1500 mm^3) was monitored over time.

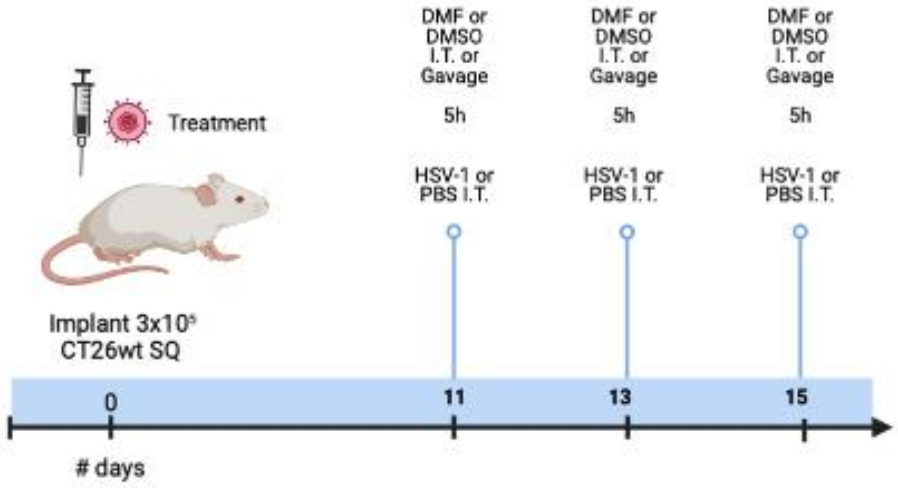
DMF or DMSO I.T. or Gavage
5h
HSV-1 or PBS I.T.
Treatment
Implant 3x10⁵ CT26wt SQ
0
11
13
15
days

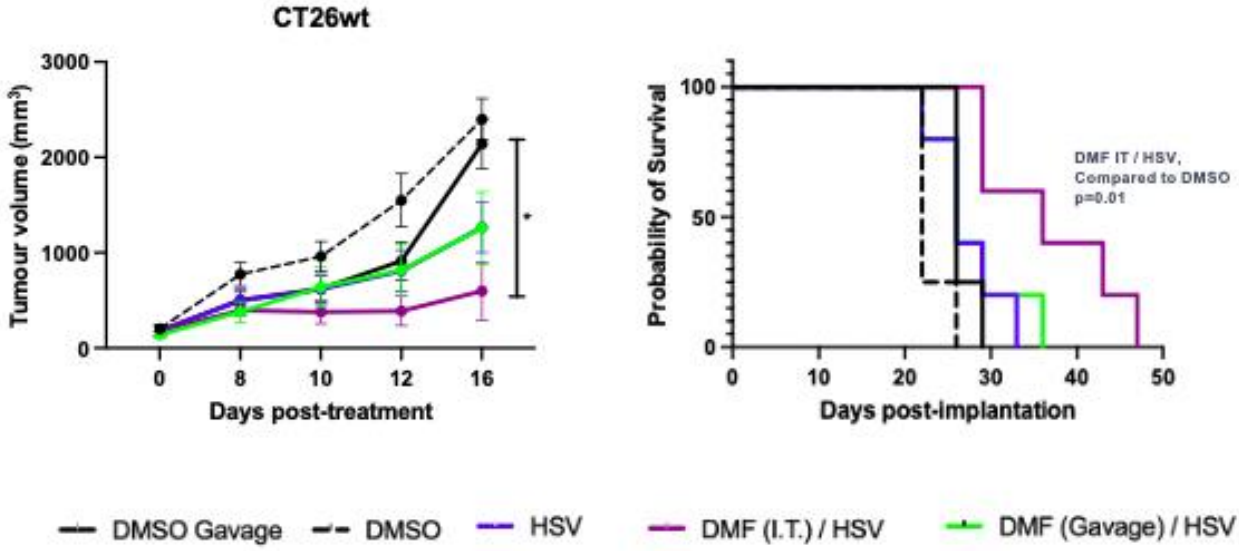
CT26wt
Tumour volume (mm³)
3000
2000
1000
0
0
8
10
12
16
Days post-treatment
*
Probability of Survival
100
50
0
0
10
20
30
40
50
Days post-implantation
DMF IT / HSV, Compared to DMSO p=0.01
DMSO Gavage
DMSO
HSV
DMF (I.T.) / HSV
DMF (Gavage) / HSV

Figure S2.6: DMF Administered intratumorally improved survival compared to gavage.

Colon CT26.wt tumors were implanted with 3×10^5 into the right flank of BALB/c mice. Upon reaching ~100 mm^3, tumors were injected intratumorally with HSV.n212 or with either dimethyl sulfoxide (DMSO) or DMF (200mg/kg, either i.t. or gavage). Tumor volumes were monitored every 2-3 days. Mice were culled when tumor volumes reached 1500 mm^3 for survival analysis. Kaplan-Meier curves were plotted and compared using the log-rank (Mantel-Cox) test.

Appendix B: Chapter 3 Supplemental Information
Tepilamide Fumarate as a Novel Potentiator of Virus-Based Therapy

Akram Alwithenani[1, 2, 3], Rozanne Arulanandam[1], Boaz Wong[1, 2], Marcus M. Spinelli[1], Victoria H. Gilchrist[1,4], Tommy Alain[1,4], Jean-Simon Diallo[1,2]

[1]Centre for Cancer Therapeutics, Ottawa Hospital Research Institute, Ottawa, Ontario, K1H 8L6, Canada.

[2]Department of Biochemistry, Microbiology, and Immunology, Faculty of Medicine, University of Ottawa, Ontario, K1H 8M5, Canada

[3]Department of Clinical Laboratory Science, Faculty of Applied Medical Science, Umm Al-Qura University, Makkah, Saudi Arabia

[4]Children's Hospital of Eastern Ontario Research Institute, Apoptosis Research Center, Ottawa, ON, Canada

A

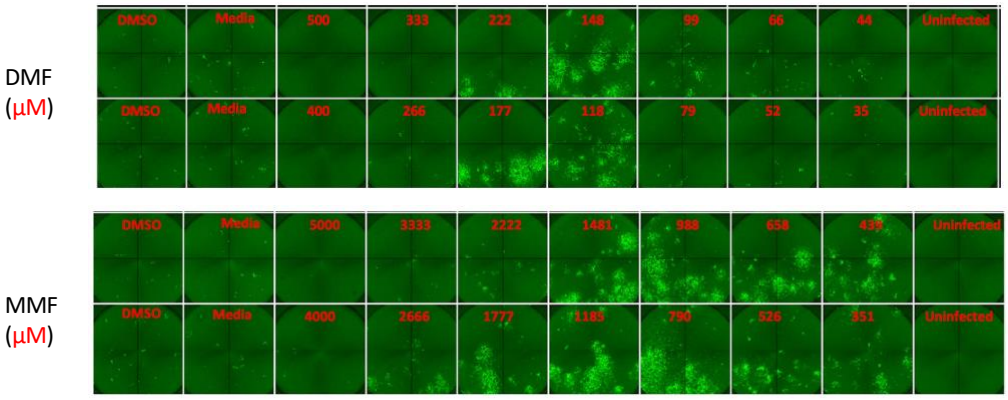
DMF
(μM)
DMSO
Media
500
333
222
148
99
66
44
Uninfected
DMSO
Media
400
266
177
118
79
52
35
Uninfected
MMF
(μM)
DMSO
Media
5000
3333
2222
1481
988
658
439
Uninfected
DMSO
Media
4000
2666
1777
1185
790
526
351
Uninfected

B

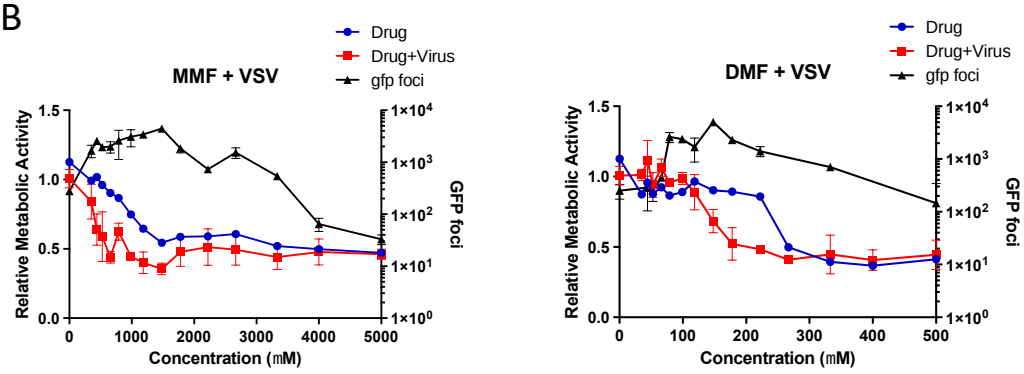
MMF + VSV
Drug
Drug+Virus
gfp foci
Relative Metabolic Activity
GFP foci
Concentration (mM)
DMF + VSV
Drug
Drug+Virus
gfp foci
Relative Metabolic Activity
GFP foci
Concentration (mM)

Figure S3.1: The impact of DMF, MMF on 786-0 cells.

786-0 cells were treated with indicated drugs with a range of concentrations then infected with VSVΔ51 expressing GFP (MOI 0.05). Corresponding fluorescent images were taken 24 hours post infection as shown in (A). GFP was quantified with a Cellomics ArrayScan® VTI HCS Reader (Thermo Fisher Scientific). Cell viability was assessed in all cells tested 48 hours after infection. The results were adjusted relative to the average values recorded for the respective uninfected and untreated cells as shown in (B).

A

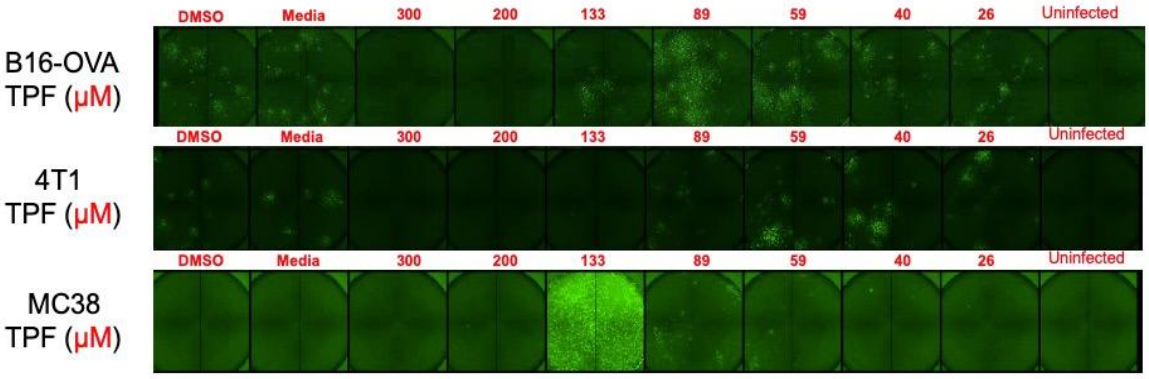
DMSO
Media
300
200
133
89
59
40
26
Uninfected
B16-OVA
TPF (μM)
4T1
TPF (μM)
MC38
TPF (μM)

B

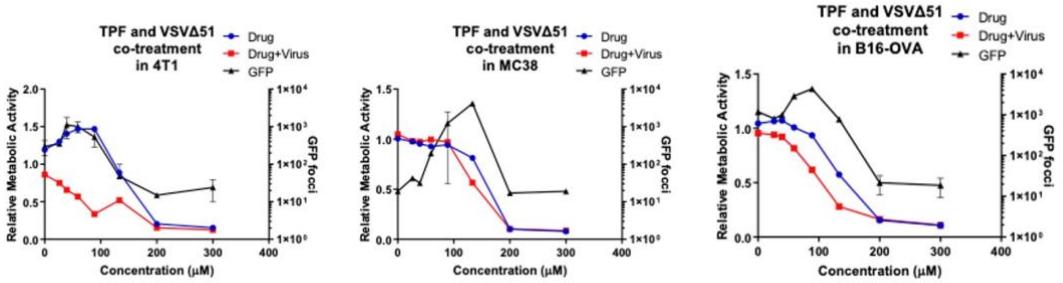
TPF and VSVΔ51
co-treatment
in 4T1
Drug
Drug+Virus
GFP
Relative Metabolic Activity
GFP foci
Concentration (μM)
TPF and VSVΔ51
co-treatment
in MC38
TPF and VSVΔ51
co-treatment
in B16-OVA

Figure S3.2: TPF promotes VSVΔ51 infection in several murine cancer cells.

A panel of murine cell lines were treated with TPF with a range of concentrations then infected with VSVΔ51 expressing GFP (MOI 0.05). Corresponding fluorescent images were taken 24-48 hours post infection as shown in (A). GFP was quantified with a Cellomics ArrayScan® VTI HCS Reader (Thermo Fisher Scientific). Cell viability was assessed in all cells tested 48 hours after infection. The results were adjusted relative to the average values recorded for the respective uninfected and untreated cells as shown in (B).

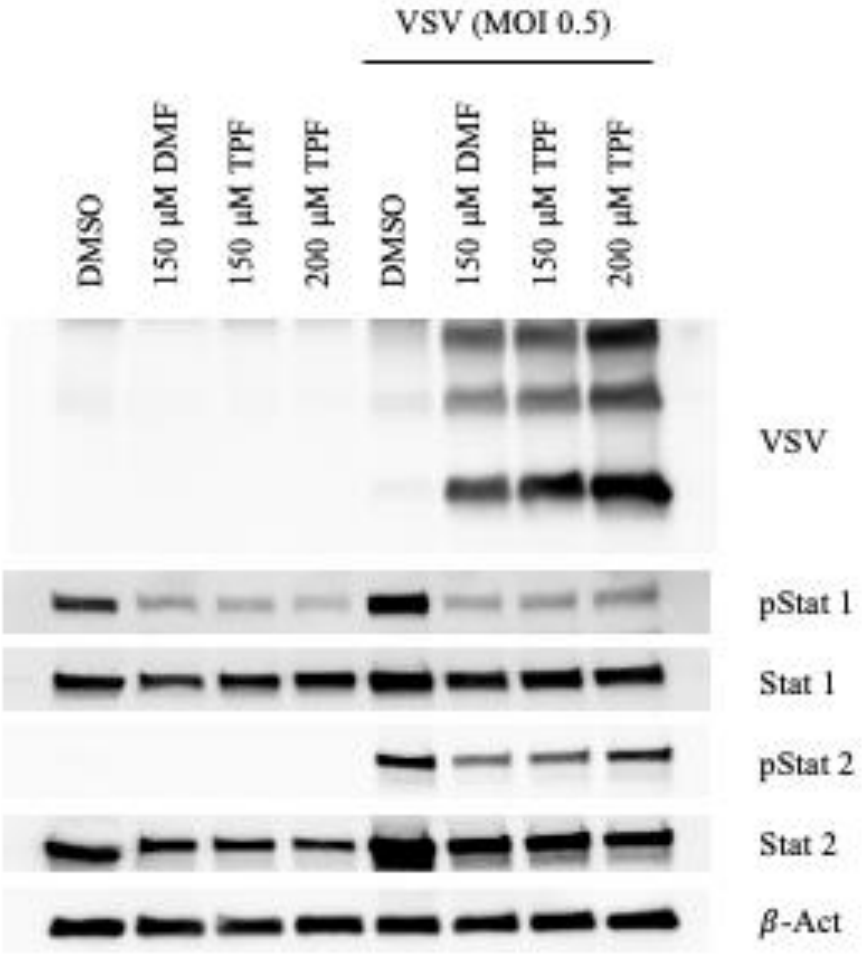
VSV (MOI 0.5)
DMSO
150 μM DMF
150 μM TPF
200 μM TPF
DMSO
150 μM DMF
150 μM TPF
200 μM TPF
VSV
pStat 1
Stat 1
pStat 2
Stat 2
β-Act

Figure S3.3: TPF decrease activation of STAT1 and STAT2.

STAT1 and STAT2 phosphorylation status was analyzed by western blot using whole cell lysates from 786-0 cells treated with TPF or DMF with indicated concentration then infected with VSVΔ51 for 24 hours.

Table S3.1: Clinical characteristics of patients-derived tumor specimens used in the study.

Specimen	ID	Age	Biological Sex	Pathology Report
Lung	GTC 565	61	Female	Invasive mucinous adenocarcinoma
Lung	GTC 564	73	Male	Squamous cell carcinoma
Pancreas	GTC 569	65	Female	Ductal adenocarcinoma
Ovarian	GTC 567	51	Female	High grade serous carcinoma
Pancreas	GTC 572	82	Female	Well differentiated neuroendocrine tumour
Colon	GTC 586	76	Male	Moderately differentiated invasive colonic adenocarcinoma

Table S3.2 : List of cell lines used in this study.

Cell lines	Organism	Tissue	Cell type	Growth media	Vendor	Catalog number
Vero	African green monkey	Kidney		DMEM	ATCC	CCL-81
786-0	Human	Kidney	Renal cell adenocarcinoma	DMEM	ATCC	CRL-1932
CT26.wt	Mouse	Colon	Carcinoma	DMEM	ATCC	CRL-2638
JIMT-1	Human	Breast	Carcinoma	DMEM	DSMZ	ACC-589
HT1080	Human		Fibrosarcoma	DMEM	ATCC	CCL-121
A549	Human	Lung	Carcinoma	RPMI	ATCC	CCL-185
HepG2	Human	Liver	Carcinoma	DMEM	ATCC	HB-8065
MRC5	Human	Lung	Fibroblast	DMEM	ATCC	CCL-171
Jurkat	Human	Blood	Lymphocyte	RPMI		
B16-OVA	Mouse	Skin	Melanoma	RPMI	**	

** Provided by Dr. Yonghong Wan (McMaster University, Hamilton, Ontario, Canada)

Table S3.3: List of primers used in this study.

Model	Gene	Forward primer (5' to 3')	Reverse primer (5' to 3')
VSV	M	ATACTCAGATGTGGCAGCCG	GATCTGCCAATACCGCTGGA
	N	GATAGTACCGGAGGATTGACG	TCAAACCATCCGAGCCATTC
Human	GAPDH	ACAGTCAGCCGCATCTTCTT	GTTAAAAGCAGCCCTGGTGA
	IFN-β	CATTACCTGAAGGCCAAGGA	CAGCATCTGCTGGTTGAAGA
	MX2	GAACGTGCAGCGAGCTTGTC	AAGGCTTGTGGGCCTTAGAC
	CCL5	GCAGTCGTCCACAGGTCAAG	TCTTCTCTGGGTTGGCACAC
	IL-6	ACCCCCAATAAATATAGGACTGGA	GAAGGCGCTTGTGGAGAAGG
	IFITM1	CCGTGAAGTCTAGGGACAGG	GGTAGACTGTCACAGAGCCG

Appendix C: Curriculum Vitae

AKRAM ALWITHENANI

PROFESSIONAL SUMMARY

I am a dedicated and accomplished professional, soon to complete my PhD in Oncolytic Virotherapy. My research has contributed to understanding the mechanisms of oncolytic virotherapy and its potential clinical applications. My commitment to advancing oncological treatment options is driven by my academic background and a passion for developing innovative solutions in the fight against cancer.

WORK HISTORY

PhD student, 09/2019 – 06/2024
Ottawa Hospital Research Institute – Ottawa, Canada
I worked in several projects during my PhD.

- Investigating the impact of two FDA approved drugs on oncolytic viruses such as HSV-1 and VSV. Assessing their efficacy in cancer cells and in several animals' models
- Design and develop recombinant Viruses. I made several HSV-1 expressing therapeutic genes using different methods.
- Design and develop High throughput screen to identify novel compounds that sensitizes oncolytic viruses.

Master's student, 05/2016 – 04/2018
Dalhousie University – Halifax, Canada
My thesis was about investigating lung cancer biomarkers in human lung cancer patients. I did screen for common gene mutations and PD-L1 expression and assess their correlation with clinical pathological data.

SKILLS

- Virology skills: Cloning, viral RNA/DNA generation, virus production
- Molecular techniques: DNA/RNA extraction, PCR, qPCR, qRT-PCR
- High throughput screening
- Animal studies: Animal handling and experimentation
- Protein analysis: IHC, ELISA, WB

- Immunological assays: Flow cytometry, staining, ELISPOT.
- Cell culture expertise: Tissue culture, viral titration
- Localization assays: Immunofluorescence techniques

EDUCATION

Doctor of Philosophy: Pathology and Experimental Medicine, 09/2019 – 04/2024
University of Ottawa - Ottawa, Canada

Master of Science: Pathology, 01/2016 – 04/2018
Dalhousie University - Halifax, Canada

Bachelor of Science: Laboratory Medicine, 09/2009 – 04/2014
Umm AlQura University – Makkah, Saudi Arabia

RESEARCH ACTIVITIES

1. High Throughput Screen Approach Identifies Several Novel Synthetic Compounds with the ability to Potentiate Oncolytic Virus Therapy**. In preparation**. (**Original Paper**).
   Role: First Author

2. Antibiotics and Viruses: From Antiviral Applications to Random Mutagenesis and Engineering Cytokine-Expressing Oncolytic Viruses. *Nature biomedical engineering*. (**Original Paper**).
   Role: Co-author
3. Tepilamide Fumarate as an Adjuvant in Oncolytic Virus Therapy: Unveiling Its Anticancer Potential. *Viruses.* (**Original Paper**).
   Role: First Author

4. Tailoring the tumour to the therapy: Complementary dual-virus strategy drives expression of synthetic target and cognate T-cell engager for endogenous-antigen agnostic immunotherapy. *Nature communication*. (**Original Paper**).
   Role: Co-author

5. Unlocking the potential of dimethyl fumarate: enhancing oncolytic HSV-1 efficacy for wider cancer applications. *Frontiers in Immunology* (2023). (**Original Paper**)
   Role: First Author

6. Pevonedistat, a first-in-class NEDD8-activating enzyme inhibitor, sensitizes cancer cells to VSVΔ51 oncolytic virotherapy. *Molecular Therapy* (2023). (**Original Paper**)

Role: Co-author

7. Profiling non-small cell lung cancer reveals that PD-L1 is associated with wild type EGFR and vascular invasion, and immunohistochemistry quantification of PD-L1 correlates weakly with RT-qPCR. *Plos one* (2021)
   (**Original Paper**)
   Role: First Author
8. Nanomaterials for antiangiogenic therapies for cancer: a promising tool for personalized medicine. *International journal of molecular sciences* (2021)
   (**Review Paper**)
   Role: Co-author
9. Molecular profiling of non-small cell lung cancer. *PLoS One* 15.8 (2020)
   (**Original Paper**)
   Role: Co-author

10. Alwithenani A, Althubiti M. Systematic analysis of spleen tyrosine kinase expression and its clinical outcomes in various cancers. *Saudi Journal of Medicine & Medical Sciences*. (2020)
    (**Original Paper**)
    Role: First Author